Departament d'Enginyeria Electrònica

UNIVERSITAT POLITÈCNICA DE CATALUNYA

Enabling the Internet of Things through Energy Harvesting: A circuit-aware system synthesis-oriented analysis approach

A thesis submitted for the fulfillment of the degree of Doctor of Philosophy in Electrical Engineering

Raül Gómez Cid-Fuentes

Advisors: *Eduard Alarcón and Albert Cabellos-Aparicio*

July 2016

Acknowledgments

Right before writing the last lines of this thesis, It is now time to thanks the people who have been there along these years. Even though it I find it impossible to thank everyone who has accompanied me throughout this journey, I would like to show my express gratitude to all of them.

First and foremost, I am deeply indebted with my extraordinary advisors, Dr. Eduard Alarcón and Albert Cabellos-Aparicio. Their tireless dedication and enthusiasm have served me as source of inspiration at every step along these years. Thank you for betting on my work even when I felt lost, and to always find a workaround for those moments.

Among all the highlights of this thesis, I would definitely choose my research stay at Northeastern University as one of the best memories. I am grateful to Dr. Kaushik R. Chowdhury, not only for having hosted me in his research group GENESYS and treated just like any other member, but also for his support, ideas and enthusiasm before, during and after my stay. I would like to say thanks to my kind colleagues at the GENSYS Lab, they made me feel welcome from the first day. I owe a special thanks to Dr. Stefano Basagni. Stefano helped shaping my ideas into real work. Special thanks to Yousof M. Naderi and Rahman Doost-Mohammady for their inspiring discussions and patience.

Here I would also like to acknowledge the members who kindly agreed to participate in my thesis examination panel. Thanks to Dr. Tommaso Melodia, Dr. Jesús Alonso-Zárate and Dr. Francesc Moll. Also I need to thanks again Dr. Kaushik R. Chowhury and Dr. Tommaso Melodia for their additional effort to review my work.

At the same level of importance there are the colleagues with whom I have had the pleasure to share this part of my life. Thanks to Ignacio Llatser, Sergi Abadal and Albert Mestres. I am in deep gratitude to your invaluable contributions. Albert Mestres has been more than a colleague and his contributions to this work

are also found in the personal side. I would also like to thank all those members from D6-008. Thanks to Albert López for being both an excellent manager and person. Thanks to Alberto Rodrídguez and Florin Coras, who have made this journey much more enjoyable. Special thanks to Simon S. Assaf and Shirin Salehi, two exceptional students, who I have no doubt will have much to contribute to the research community. Finally, thanks all those colleagues who spend their day in the neighboring buildings. Thanks to Sergi Gorreta, Joan Capdevila, Eric Calle, Jordi Querol and Mario Iannazzo.

There are four additional people, which have constituted the two fundamental pillars of the most personal side of this work. First, thanks to my parents and brother who have become an undemolishable pillar. They have always been there to make everything easy and smooth. Finally, thanks to Zoraida Marquès. Even though she is the last person in this acknowledgments, she really is the first elsewhere. She has become the strongest pillar, which has permitted to build the entire thesis on top.

Abstract

Powering wireless sensors has become a key challenge to enable the Internet of Things vision. A common approach to achieve this is to use Energy Harvesting. By means of this technology, sensors have access to an unlimited source of energy, which can extend their operation lifetime.

Unfortunately, typically the energy that is available surrounding the sensors is neither controllable nor predictable, showing significant variations in the expected harvested energy in terms of both space and time. This can cause the temporal disconnection of parts of the wireless network.

The objective of this thesis is to mitigate the undesirable effects of the spatio-temporal variations of the surrounding energy, by following a two-fold approach: first, to provide a high level understanding of the involved trade-offs in the design of a wireless sensor and the interconnecting network. Then, to synthesize an energy field to guarantee the required amount of ambient energy at the surrounding of the considered nodes.

The first part of the thesis starts by presenting a formal description of the environment. The derived energy model is first used to answer fundamental questions on throughput scaling and, then, to provide design guidelines for energy harvesting sensors. It is found that energy harvesting is a scalable solution to power and recharge IoT sensors, which require additional circuit design to guarantee their operation in energy scarce scenarios.

On the second part of this work, wireless RF power transmission from controllable Energy Transmitters (ETs) is considered as a feasible approach to synthesize an energy field to power sensors at-a-distance, hence tackling the lack of available ambient energy in spatial regions, at the cost of occupying the available wireless spectrum. Due to the limited transmission range of this approach, the use of multiple ETs to cover entire areas is required. We first discuss on the feasibility of synthesizing energy fields with multiple ETs. We show that powering those sensors with multiple ETs stands as a scalable approach, which presents a trade-off between the channel conditions and the energy multiplexing design complexity. We, then, present an opportunistic scheme to leverage the generated interferences of multiple ETs. Finally, we propose a joint energy and communi-

cation method to circumvent the imposed trade-offs of in-band multi-ET wireless RF power transmission.

Overall, we find that the analysis and design of wireless networked sensing systems, enabled by energy harvesting, and the development of novel wireless RF power transmissions schemes will play a key role in the future development of autonomous IoT deployments.

Contents

List of Figures

List of Tables

Chapter 1

Introduction

Wireless networked sensing systems are the "invisible" enablers of pervasive communications, remote monitoring and surveillance, the Internet of Things, and of all those systems that are an increasingly essential part of our everyday life. Powering these systems is becoming the crucial challenge, as key requirements such as cost effectiveness, very small form factors and decade-long lifetimes are difficult to meet by using nodes that are battery-less or with low-capacity batteries. Hence, alternative sources of energy must be considered to tackle this problem.

A promising approach to perpetually operate the sensor systems is by acquiring the energy that is found in the close environment of the sensor. Physical phenomena, such as solar energy, vibration, human movement or electromagnetic RF waves have demonstrated potential as sources of energy, where sensors can rely on to autonomously run unattended tasks without the need of manual replacement of batteries. This has been generally referred as *Energy Harvesting* and it is defined as a process by which the ambient energy located at the close environment of the considered device is captured, converted into electrical current and stored for later use in powering the desired tasks of the device.

Energy Harvesting is being considered as the key-enabling-technology of the Internet of Things and promises to change the way the considered devices make use of the energy. Through this technique, the considered sensors have a time-unlimited access to a scarce source of energy, which relaxes the need for large energy storage units and manual re-charging or replacement, to guarantee a sufficient operation lifetime. Accordingly, a proper design of the electrical device, which aims at handling the temporal variations in access and demand of energy,

brings several benefits in the considered IoT deployment scenarios, such as size reduction, node placement in inaccessible locations, reduction of maintenance costs and an increase on the network operation lifetime.

Unfortunately, the energy that is available at the close environment of the sensing system is not controllable, and often not even predictable, hence showing significant variations in the expected harvested energy in terms of both space and time. In this sense, spatial energy shadowing causes that certain areas of the network may render disconnected from normal operation, whereas temporal fadings may temporarily inhibit sensing operations, temporarily interrupt the network operation or to cause excessive traffic delays.

For this reason, two alternatives raise as a measure to guarantee an uninterrupted operation. On the one hand, defining models to analyze and proper design both sensing systems and IoT networks are required. The aim of these models needs to cover, among others, battery dimensioning to mitigate temporal variations in the energy access and optimal routing and traffic balancing to mitigate spatial variations of the available energy. On the other hand, wireless RF power transmission from controllable *Energy Transmitters* (ETs) stands as a feasible, artificially generated source of energy to power sensors at-a-distance and to tackle the lack of available ambient energy in spatial regions. Given that RF propagation is affected by severe path-loss, the transmission distance of a wireless RF power transmission link is rather limited to just a few meters of distance, hence, multiple deployments of ETs that coordinately transfer energy towards the sensing systems are usually considered to cover entire networking areas.

The analysis and design of energy-harvesting-enabled wireless networked sensing systems and the development of novel highly-efficient wireless RF power transmissions schemes have significantly attracted the attention of the research community at many design layers. The topics that have been mostly set to tackle range from the design of energy harvesting transceivers and circuits, the impact of these in the sensor performance and the eventual network operation, the design of energy harvesting alternatives specifically suited for wireless RF energy transmission, coordination among multiple ET entities and the coexistence of simultaneous transmission of energy and data.

1.1 Motivation and Objectives

Energy harvesting and Wireless RF power transmission are research fields that have been treated as separated problems, where each has presented their own research challenges and associated trade-offs.

However, the fact that both approaches pursue a common objective, that is to autonomously recharge the networked systems, along with the conceptual difference based on acquiring energy which is either exogenous or endogenous of the system under study, brings the following open question: *Can we leverage the acquired knowledge in the study of physical energy harvesting phenomena to design Wireless RF power transmission schemes?* To answer this question this thesis is separated into two parts. The former refers to energy harvesting and aims at *analyzing* existing ambient energy in the form of an energy field. The latter refers to wireless RF power transmission and aims at *synthesizing* arbitrary energy fields with the help of multiple ETs that are deployed over the networking area.

1.1.1 Energy Harvesting

Interrelating the separated layers in the design of a complete energy harvesting enabled communication system throughout a vertical approach is still a pending challenge. As a result, several works analyze particular use-cases and provide quantitative results, which are hard to extrapolate when the conditions of the problem differ. The lack of qualitative trade-offs hinders the mutual understanding between both network and circuit communities and, hence, hindering design guidelines of critical circuit and system components.

Accordingly, generic feasibility studies that aim at relating the trend between tangible magnitudes are missing, such as the relating available input power at the node locations or number of deployed systems in a IoT to metrics for network and communication evaluation, such as the throughput of a network. In these lines, answering simple questions, such as: *How does the throughput of a network varies when the deployed nodes start failing?* need to be addressed, regardless of the non-triviality of its answer.

Objectives

The scarce nature and poor predictability of the energy sources requires additional efforts during the design stage. In this direction, the objectives of this thesis are:

- To provide a formal description of the energy harvesting process by proposing a general-purpose energy model. This model needs to capture the spatio-temporal variations of the ambient energy, as well as the node sensor system implications.
- To study the scaling laws on the capacity of the network throughput. This study assesses the viability using energy harvesting as the unique source of energy of the deployed nodes. It provides a high-level understanding of the energy harvesting process, its implications on the network performance and the imposed design trade-offs.
- To study the implications of the spatio-temporal variations of the surrounding energy, and to analyze the performance of mulit-EH and self-tunable EH as feasible solutions to circumvent their associated challenges.

1.1.2 Wireless RF Power Transmission

In a many-to-many wireless RF power transmission set-up for the IoT, where more than one ET delivers power to multiple sensors, RF waves radiated from these systems may interfere with each other at the receiver end if these are transmitted in the same frequency band. Devising energy multiplexing methods to avoid the destructive interference is still a pending challenge. However, despite these methods, the use of multiple ETs to cover an entire area of interest leads to concerns of scalability [144].

In order to design cost-effective communicating systems, the RF spectrum must be shared for both power and data transmissions. This reduces the need of duplicated antennas and hardware. Unfortunately, alternating between tasks may seriously affect network operation and performance. In fact, Time multiplexing between both tasks reduces, not only the eventual transmitted power, but also the idle time for data communications. As such, scheduling data transmissions in constrained time-slots increases the protocol complexity. For this reason, devising methods for energy provisioning without affecting data communications

appears to be the challenge that the research community has most recently set to tackle [48].

Objectives

The deployment of multiple ETs to cover entire networking areas imposes several research challenges. In this direction, the objectives of this thesis are:

- To study the scaling laws of the cumulative power that is injected in the network. This study assesses the viability of using wireless RF power transmission from multiple ETs. It provides high-level understanding of the wireless RF power transmission process, as well as the design considerations of the energy multiplexing approaches, depending on the physical environment and the channel quality.
- To propose an energy multiplexing method that constrains the protocol complexity, while it improves the transmission of energy.
- To design a method to concurrently enable reception of power (from an ET) and information (from neighboring nodes) in an in-band fashion. This pursues an improvement of the network performance, without incurring into additional hardware and protocol complexity.

1.2 Thesis overview and contributions

Along this work, several tasks are placed in order to interrelate the multiple layer design of energy harvesting systems and to enhance the transmission of energy. The realized tasks and contributions are shown in Fig. 1.1. Accordingly, the overall content is divided into two parts, namely energy harvesting (analysis) and wireless RF power transmission (synthesis). In the former, first an energy model is derived that is necessary to derive the remainder contributions. Then, an analytical expression to bound the per node throughput capacity in a wireless network, when this is powered by energy harvesting is derived. Finally, design space exploration of energy harvesting sensors is proposed, tackling, spatio-temporal correlation of the energy and both multi-source and self-tunable energy harvesters. In the latter, an analytical expression to justify the use a

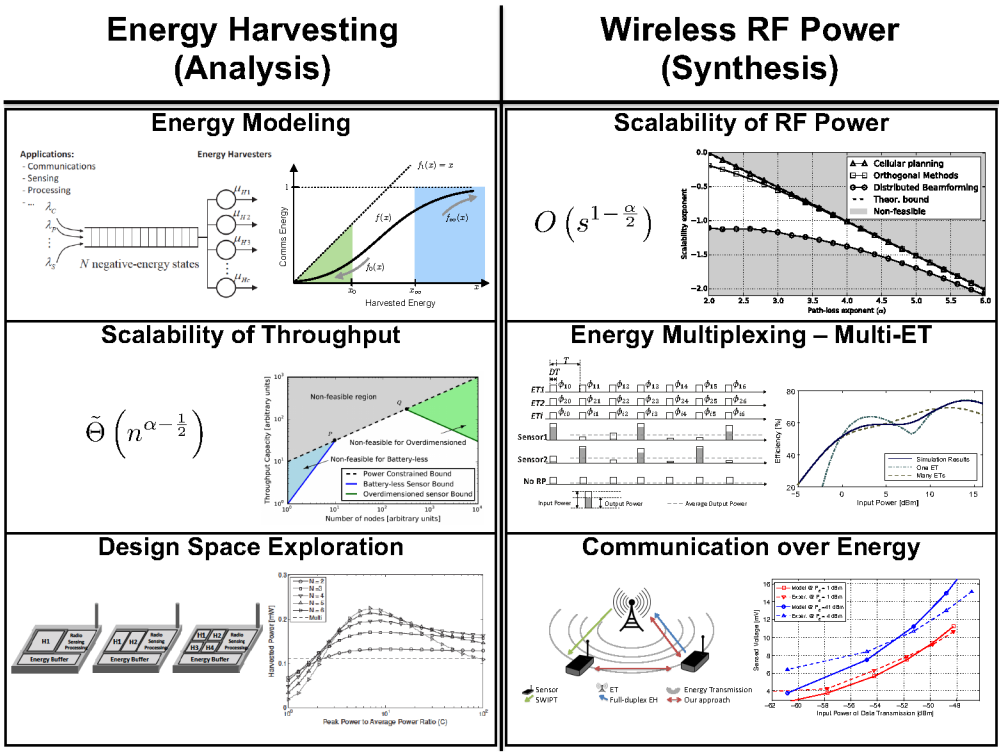

Figure 1.1: Overview of the proposed contributions in this thesis.

multi-ETs as a scalable solution to extend the coverage of deployed IoT. Then, an energy multiplexing method to leverage multi-ET interference is presented. Finally, a method to permit simultaneous wireless charging and in-band data communication is presented.

The aforementioned contributions are described in more detail next.

1.2.1 Energy Harvesting Tehniques for WSN

The first part of this work aims to develop a generic theory to model and characterize nodes and networks powered by a generic energy harvesting source. The topics that are covered here are:

Energy Model

Because energy harvesting and wireless RF power transmission are usually considered as separated scenarios, it is needed to develop a generic, energy-source agnostic model to characterize the access of energy at the eventual sensor devices. Hence, this model needs to cover two separated aspects. On the one hand, a generic model for the ambient energy is required, such that it simplifies the notation and helps the understanding of the energy harvesting process. On the other hand, a model to characterize the management of this energy, once the energy is harvested, needs to be further investigated. As such, this model needs to also consider the transmission patterns, statistics of the energy at the reception and internal efficiencies of the sensor.

By considering this model, we are able to define important metrics and concepts that will stand as the basis of the remaining work presented in this thesis. Among other important concepts, this model defines: the spatio-temporal correlation between the energy that is harvested at the node locations; the energy path function of a node device that bridges the communication requirements to the available energy in the environment, and the Energy-Erlang (E2), a statistical unit to handle energy resources. It is noteworthy that the proposed model also has multi-source energy harveting capabilities, such that modeling the operation of complex sensors, powered by a set of different energy harvesters is simplified.

Scalability of Throughput Capacity

The scalability of the per node throughput capacity of a wireless network was first bounded by Gupta and Kumar [50] showing that the throughput of a wireless network in bandwidth limited conditions *decreases* with the number of deployed nodes, n, as $\Theta(1/\sqrt{n \log n})$. At a high level, this bound showed that wireless networks are not scalable with the number of nodes, therefore constraining the deployment of nodes to just a few devices. More recently, a more closely related bound, was found for power constrained, free-space conditions, showing that the througphut *increases* with the number of deployed nodes, n, as $\tilde{\Theta}(\sqrt{n})$, where $\tilde{\Theta}$ refers to the soft-order bound [98]. Given that the available resources in an energy harvesting enabled WSN are very limited, reaching a non-scalable bound would signify that a IoT network powered by energy harvesting cannot leverage node

cooperation to enhance their performance, hence rendering impractical. Therefore, a scalabiltiy analysis to evaluate the throughput scaling with the number of nodes is required.

For this, a scalability analysis of the throughput capacity of an IoT powered by energy harvesting has been addressed. Throughout this analysis, we are able to derive a closed-form expression that relates the channel conditions, energy management at the sensors and the bounds in throughput scaling of the given network. By identifying the limits in the functionality of the nodes, we are able to understand at a high level the main trade-offs between the energy-communication conversion process, channel properties and eventual throughput.

Design space exploration of EH-powered nodes

As it is shown in the scalability analysis, the design of the energy management units of a sensor node has a decisive impact upon, not only of the sensor performance itself, but also on the overall network operation. Among other parameters, it has been shown that the capabilities of the energy harvester and the capacity of the energy storage unit play a very important role to ensure ideal throughput. In particular, it is shown that the quantity of harvested power directly impact on the throughput, whereas relatively small energy buffers can yield to non-resilient to node failure network operations.

For this, a study of the dimensioning of the energy harvester and energy buffer is provided. First, the impact upon the performance of the node, in terms of energy outage probability, with the size of the energy buffer is discussed. To derive these first results, a single energy harvester that optimally operates is assumed. Then, the joint energy harvesting - energy storage unit design is studied in a multi-source energy harvesting configuration. Finally, the idea of self-tunable energy harvesters is discussed and its performance and trade-offs are compared to multi-source energy harvesters.

1.2.2 Wireless RF Power Transmission

The obtained knowledge along the devoted chapters to energy harvesting aims at orienting the design of the energy network, defined as a set of deployed Energy Transmitters over the networking area. In addition, to leverage the properties of

energy harvesting to implement sustainable IoT.

We describe next the primary contributions in the field of wireless RF power transmission:

Scalability of the Energy Field and Throughput Capacity

Extensive experimentation has shown a relatively short charging range of a single energy transmitter [36]. This has motivated the deployment of multiple ETs over large deployment areas [97] in WSN. Indeed, the presence of multiple ETs reduces the average propagation distance to the energy harvesting sensors, and thus decreases the attenuation level of the energy waves. However, it is still unclear that the combination of multiple transmissions can help reducing the overall transmitted power.

A first step towards the design of integrated energy networks and WSN refers to analyzing the scalability of the required energy in terms of the number of deployed ETs. At a high level, it is investigated whether the combination of multiple ETs can help reducing the overall transmitted energy or, if on the contrary, the deploying multiple ETs brings additional trade-offs and research problems that may preclude an eventual operation. As the main results show, increasing the number of deployed ETs for a given deployment is shown favorable in most daily environments. However, the design of multiple access methods for multi-ET transmissions i desired to achieve the best performance.

A Multiple Access Method for Multiple Energy Transmitters

Wireless RF power transmission from multiple ETs brings several trade-offs in the design, since simultaneous transmissions that may overlap over the medium can destroy each other. In particular, the constructive and destructive combination of RF waves generate very large peaks and drops of power in a non-controllable spatial-dependent manner. As a result, the underlying nodes, cannot guarantee a minimum of harvested power, hence interrupting their normal operation. The aim of existing MAC protocols for RF energy harvesting sensor networks with multiple ETs is to mitigate the impact of interferences.

For this, we introduce an energy multiplexing method, which aims at handling the simultaneous transmissions of power from the multiple ETs. This method

relies on the fundamental assumption that efficiency is maximized when the input power varies in time as much as possible, since the energy harvesters operate with increasing efficiency as a function of the input power [105, 33, 100, 14].

Communications over Wireless Energy

The last step of this work is to effectively combine the wireless RF power transmission with the inter-node communication. Existing approaches devote separated access times for both operations when data communication and RF energy recharging occur in-band, raising architectural and protocol level challenges.

Accordingly, we propose a novel method to permit the concurrent transmission of data and energy that solves this problem. This allows ETs to transmit energy and sensors to transmit data in the same band synchronously. By considering this approach, nodes are able to avoid system duplicity at many design levels, hence potentially reducing manufacturing costs, power consumption and overall size.

1.3 Thesis Outline

The remainder of this thesis is structured as follows. The next chapter presents the necessary background that is required to understand and justify the main contributions of this thesis. Accordingly, it first overviews the main applications of energy harvesting and wireless RF power transmission for the Internet of Things. Then, it revises the current state-of-the-art of the proposed technologies. The following chapters, divided in two parts, namely energy harvesting and wireless RF power transmission, present the main contributions of this work. Chapter 3 introduces the developed models that have been considered to analyze and characterize the energy access and utilization. Chapter 4 addresses the scalability of wireless sensor networks powered by the use of energy harvesting. Chapter 5 studies the impact of non-uniform energy fields in terms of both temporal and spatial dimensions. These three chapters are based on the work published in [21, 23, 29, 31] and refer to the first part of this work referred as energy harvesting. The following chapters conform the wireless RF power transmission part of this work. Accordingly, Chapter 6 performs a feasibility analysis

of multi-ET wireless RF power transmission and compares the ideal performance of the different energy multiplexing methods. This chapter has been submitted for publication in [26]. Chapter 7 presents an opportunistic method for energy multiplexing in a many (ETs)-to-many (sensors) scenario that leverages the circuital properties of existing energy harvesters to optimize their input-to-output power conversion efficiency. This chapter has been presented in [27, 28]. Chapter 8 proposes a method to permit simultaneous wireless RF power transmission and node-to-node communications in an in-band manner. The results of this chapter have been presented in [24, 25]. Finally, Chapter 9 concludes the thesis and presents ideas for future work.

Chapter 2

Related Work and Background

This chapter aims at contextualizing the contributions of this thesis. Accordingly, it first overviews the main applications and benefits of using energy harvesting and wireless RF power transmission for the Internet of Things. Then, it revises the current state-of-the-art of the proposed technologies.

2.1 Applications and Benefits

Energy harvesting and wireless RF power transmission are usually referred as key-enabling technologies for the Internet of Things. By leveraging the delivered power of such approaches, sensors will offer an unattended operation, reduce maintenance costs, reduce their size and enable applications that are considered unfeasible due to lack of practical accessibility.

Among the numerous applications of the Internet of Things, we find that energy harvesting and wireless RF power transmission techniques will have a determining impact in the following fields:

2.1.1 Perpetual Operation

The major benefit of energy harvesting and wireless RF power transmission in the field of the Internet of Things is provided by the fact that the communicating nodes are able to continuously harvest energy and to recharge their internal energy buffers.

To enable an almost uninterrupted operation of the deployed nodes, it is required to properly design the energy buffer capacity [23], transmission policies [7], scheduling [57] and communication protocols [6]. If any interruption occurs, the operating nodes must re-adapt the network operation until the failing nodes harvest sufficient energy and restart their operation [9].

2.1.2 Size Downscaling

As a consequence of the perpetual operation of the sensors, these no longer require large batteries to store energy for a few months of continuous operation [9]. On the contrary, these need to store just a small portion of the overall required energy, such that it powers the node while the ambient energy is shadowed.

A clear example of size downscaling is observed in solar powered sensors. By implementing a solar panel, sensors move from storing energy for a few months to just a few days, i.e., these just need to accumulate a portion of this energy to power the devices at night and days without much sunlight.

2.1.3 Safety and Security

Sensors that implement energy harvesting and wireless RF power transmission technologies enable fully-wireless approaches, such that these do not require to implement accessible wires or physical ports. Accordingly, these sensors can be hermetically sealed to separate the electrical circuitry and the system environment, bringing several benefits in terms of both security and safety.

On the one hand, such a closed system can only communicate through the wireless communication unit. This avoids any type of malicious attack that needs a physical or wired connection to capture internal signaling. On the other hand, the actual physical separation permits a sensor deployment in highly-inflammable environments, since any possible electrical spark will not ignite the flammable fluid.

2.1.4 Flexibility and Ubiquitousness

In addition to the benefits in terms of safety and security. Enabling fully wireless sensors also changes the way in that IoT is conceived since the communicating

systems can be placed nearly anywhere. On the one hand, communicating systems can be deployed in locations that rendered unfeasible due to lack of accessibility to realize human maintenance. In addition to this, nodes do not need to be placed in known locations, as well as these can be dynamically displaced due to either environmental conditions or opportunism.

2.1.5 Economic and Environmental Impact

Energy harvesting and wireless RF power transmission permits the development of unattended wireless sensor networks that offer real-time monitoring of the nearby environment. This facilitates fast emergency control actions, plus an efficient use of the supplies, along with the associated cost reductions. Provided that this approach aims at suppressing the use of batteries and to perpetually recharge the sensors by means of the ambient energy, the IoT maintenance costs are assumed negligible and so its ecological footprint.

In addition to this, the ubiquitousness property of this approach will also open a whole set of new applications, broadening the existing IoT market. Accordingly, the economic impact of energy harvesting for IoT does not only lay on maintenance cost reductions, but also in the creation of new end applications.

2.2 Ambient Energy Sources

In an energy-harvesting-enabled wireless sensor node, the energy which is used to enable the sensing, processing and communications is fully obtained from its close environment by means of ambient energy harvesters [128]. In a real context, the energy that is used to power the sensors can be derived from a diverse set of physical phenomena, such as solar, thermal, acoustic, vibrational or RF energy. Unfortunately the available energy which can be harvested from each source of energy is usually limited and presents an unpredictable pattern in both temporal and spatial domains [128, 23]. For this, energy harvesting has become, on the one hand the key enabling technology for the IoT, whereas on the other hand, one of the largest constraints in capabilities and future performance of the networked systems.

In a general sense, it is found that some of the most important parame-

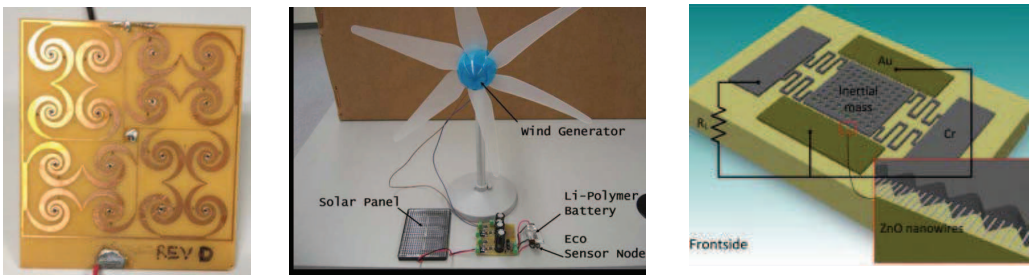

Figure 2.1: Examples of energy transducers: a rectenna [51](left), wind generator [107] (center) and a ZnO energy harvester [95](right).

ters to characterize a given source of energy are controllability, predictability, power availability or density and conversion efficiency of state-of-the-art transducers [128]. Controllability denotes the ability to modify the properties or power density of the source of energy. As an example, human movement stands as a controllable source of energy since. Predictability refers to the degree of prediction on the characteristics of the source of energy. For instance, solar energy is a predictable source of energy [46, 44]. Power availability or density is the expectable quantity of power that a sensor can harvest from the given source. This is size or area dependent, so it is usually expressed in terms of power over area units. Due to the unpredictable nature of the energy sources, the power density is illustrative and may vary over two orders of magnitude [128]. In Table 2.1 we show some results on the most relevant energy sources.

Table 2.1: Listing and characterization of the energy sources

Energy Source	Properties	Available Energy	Efficiency
Solar [132, 65, 8]	Uncontrollable, predictable	100 mW/cm^2	15% to 20%
Wind [142, 107, 81]	Uncontrollable, predictable	2 mW/cm^2	70%
Human Movement [124]	Controllable, predictable	1 mW to 1 W	7.5% to 40%
RF ambient Energy[15]	Uncontrollable, Unpredictable	1nW to 100 mW	40% to 50%
Vibration [116, 52]	Uncontrollable, Unpredictable	2 μW/cm^2	-

Fig. 2.1 shows examples of energy harvesting for RF ambient energy (left), wind (center) and Vibration (right). We describe next the most commonly considered sources of energy to power Internet of Things sensing systems and provide examples of implemented prototypes.

2.2.1 Solar Energy

Powering systems from solar energy is a widely considered approach, not only in the context of IoT, but in all nowadays applications. Even though, light is a time-dependent, time-varying source of power, it follows a predictable pattern [46]. This makes solar energy, one of the most stable and desired sources of energy for the considered sensors.

To scavenge the energy, sensors integrate photovoltaic cells that convert the incident light into an electrical current [73]. This generates an output DC current that can be leveraged to power the entire sensing system. the harvested power is in the order of 100 mW/cm^2. The pattern of the received power is uncontrollable and it is very affected by the geographical placement of the entire network and the particular location of the nodes. Hence, the actual received power varies over a large range. This shows a maximum power generation in outdoors locations with the photovoltaic cell facing the light source.

Solar energy shows a daily trend that is largely predictable. It has been shown that by considering accurate modeling and transmission policies, it is possible to achieve an energy neutral operation [73]. Thanks to this, solar energy has been widely considered to power WSN sensors as a mechanism to power and to re-charge the internal batteries. Among others, we find the following existing sensing platforms: [65, 64, 114, 73, 108].

2.2.2 Mechanical Vibration

Daily activities generate large amounts of residual energy that is expressed in the form of vibrations and mechanical movement. Plausible examples range from the subtle vibration of a floor or wall of a building when someone walks nearby, to severe excitation caused by industrial machinery. In all, mechanical vibrations are present in a wide variety of both frequency and amplitude ranges, which require application-specific hardware to optimize the energy scavenging [19].

To harvest energy from mechanical movement, an inertial mass can be used to generate electricity [5]. In particular, the acceleration of the suspended inertial mass induces an electrical current that can be rectified and stored in a capacitor. For this three different mechanisms, namely, piezoelectric [5], electrostatic [120] and electromagnetic, stand as the feasible approaches.

The piezoelectric energy harvesting bases its operation principle on given materials that generate an electrical current when these are deformed [19]. This property has been leveraged by numerous researchers to implement energy harvesting for a wide variety of applications [10, 5, 32, 85]. Electrostatic energy harvesting consists of generating energy by moving the plates of a charged capacitor. When the plates are moved, the variations on the electrostatic force generates a voltage signal, which can be harvested [10, 120, 90]. Finally, electromagnetic energy harvesting is based on the Ampere law to generate electrical current by fluctuating the magnetic field around a coil [10].

2.2.3 Thermal Energy

Thermal energy can be also harvested through the action of thermoelectric generators, by leveraging the Seebeck effect [127]. This effect generates an electrical voltage that depends on the temperature difference at the junction of two dissimilar metals. In practice, this is generally implemented with a Peltier plate, where one side is connected to a heat source, whereas the remainder to a heat sink. However, the thermal to electrical energy conversion shows very poor efficiency, that is in the order of 5% [127]. Thermoelectric generators show an interesting approach to reuse the extra heat generated by human machinery, hence improving the energy efficiency of the system if considered as a whole [19].

2.2.4 Wireless RF Energy

Electromagnetic waves are widely employed as a method to broadcast and to propagate information. These are transmitted by base stations and aim at covering large geographical areas. Provided that the RF spectrum is a limited and scarce resource, frequency bands allocate a large amount of power, where sensors can harvest energy from.

To harvest the RF power, sensors integrate antennas. Antennas generate a voltage signal at the frequency of the received RF wave and its power is proportional to the power density of the RF wave. However, given that RF power can be neither stored nor used to supply the remaining sub-system units, the RF signal is down-converted by means of a rectifying stage [33] and, sometimes, a DC-DC converter to improve the conversion efficiency [56]. The design of antennas for

wireless RF energy harvesting does not pose additional challenges to those for signal reception. Alternatively, the concept of rectennas has also been well accepted in the research community [113]. These circuits refer to a combination of an antenna and rectifying, built for energy efficiency maximization.

The amount of harvestable power and size of the antennas depend in a great manner on the available RF power in the nearby spectrum. Accordingly, the size of an antenna is proportional to the wavelength of the RF wave, such that higher frequencies require smaller antennas and vice-versa. The received power, however, depends on the transmitter-receiver pair distance and frequency. The attenuation is proportional to the square of the distance and the frequency. It has been experimentally shown that it is possible to harvest up to 60 μW at a distance of 4.1 km in an urban environment [122].

Alternatively, wireless RF energy has also attracted the research community as a method to supply power on-demand on a wireless manner. This approach has given birth to wireless RF power transmission, which is discussed in Sec. 2.4

2.3 Energy Harvesting

In the recent years, several works ranging from the energy harvester circuit design to the network analysis has driven the research in the field of energy harvesting enabled WSN and IoT. Along these works, different type of energy sources have been characterized, energy scavengers, power electronics circuits and tools for low-power applications have been provided and a dense study on communications has been carried out [7, 84, 128, 133, 138].

These studies have remarkably shown the large degree of analytical complexity of energy harvesting systems. From a descriptive viewpoint, a generic system requires handling random processes at both input (harvested energy) and output (communications), while defining an energy state, also referred as residual energy, that varies in time in a non-predictable manner. Accordingly, energy modeling [102], optimal scheduling [7], dimensioning of the energy buffer [73] and design of the protocol stack have been some of the most active challenges that the research community has set to tackle.

Overall, energy harvesting conditions the design of the WSN at many different levels. This section overviews the design implications accross the different layers.

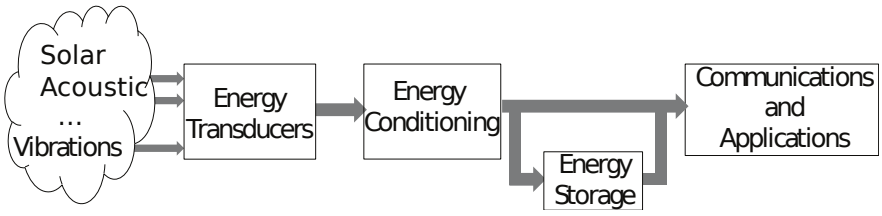

Figure 2.2: Depiction of the energy path.

2.3.1 Circuit Level

At the circuit level, the harvested energy is acquired through the action of the transducers. This is temporarily stored in an energy buffer. Finally, the energy is distributed to the different sub-system units to enable their normal operation. This flow is referred as the energy path and it is shown in Fig. 2.2.

An energy transducer is defined as a device which is capable of converting the energy of certain physical magnitude into electrical energy. i.e., the energy which is available in the close environment of the sensor is harvested through energy transducers and converted into electrical energy. In accordance with the energy sources, there also exist several types of energy transducers, depending on the nature of the energy source, such as MEMS and NEMS for vibrational and mechanical energy harvesting, which can be either resonant [116] or non-linear [52], antennas and rectennas for RF energy harvesting [51] or solar cells [65].

Energy transducers are very sensitive to size downscaling, since a modification in size or area of the transducer may affect critical parameters, such as oscillation frequency. As an example, in RF energy harvesting, the size of the rectenna is directly related to the targeted RF wavelength. i.e., the natural frequency for energy harvesting dramatically increases as the size downscaling in the rectenna is performed. In this context, nanotechnology-based novel transducers aim to provide similar properties of classical energy transducers at a much lower size. As an example, a graphene-based nano-antenna allows a reduction in size of two orders of magnitude (up to 100 times smaller), in comparison to metallic antennas, while still operating at the same frequency [69]. Accordingly, combining multiple energy harvesters to reduce the overall area, while meeting the user-defined requirements is set as a major research challenge that the community has set to tackle [22, 31]

The subsequent part of the energy path aims at conditioning the harvesting energy to the sensor requirements. As a result, the energy conditioning block provides the matching between the energy transducers to the sensor node [30, 8, 133]. As an example, in case of harvesting AC energy, this needs to be downconverted to DC current by means of a rectifying circuit [100].

By following the energy path, the harvested energy is required to be temporarily stored in an energy buffer, until this is used by the communication or processing unit of the sensor node. This block results of vital importance for the performance of the sensor node due to the fact that ambient energy sources provide not only low-power densities, but also they present a large sparsity and time-variant character [7].

The energy storage is usually composed of a battery or a supercapacitor [128]. Unfortunately, there is a huge compromise among both technologies. Particularly, batteries usually provide larger energy densities than capacitors. On the other hand, capacitors can handle faster energy fluctuations and have larger recharging cycles [132, 77, 112]. As a result, the strong compromise among technologies makes very challenging for the electronics designer to decide whether to use either one, another or both. Table 2.2 shows typical values for batteries.

Table 2.2: Comparison of battery technologies [132, 128]

Technology	Energy Density (MJ/kg)	Recharging cycles
Sealed Lead Acid	0.11-0.14	500-800
Ni-cadmium	0.14-0.22	1500
NiMH	0.11-0.29	1000
Li-ion	0.11-0.29	1200

2.3.2 Energy State Modeling

The existing state-of-the-art joint models, which are based on Markov queues, can be roughly classified into three types. In the first type the basic unit is the energy packet and -unlike classical communications queues- empty queues of energy packets entail an interruption of the normal operation of the sensor nodes. In such models the energy harvesters generate arrivals of energy packets that in turn, are stored in the energy buffer (representing a battery or a supercapacitor). The communication unit is modeled as a server which processes the energy

packets where the service time is associated to the generation of communications events[136, 70, 148]. The second type of models proposes the interconnection of two different Markov chains, namely a main queue for communications packets and a secondary queue for energy harvesting resources. Such type of models consider that a data packet can be effectively transmitted when it has been processed by the main queue and the queue of energy-packets is not empty [7, 102, 115]. And finally, the third type are based on state-dependent Markov chains where each state represents a combination of the amount of energy,data packets available in their respective buffers [88, 123].

Alternatively, existing joint models for solar energy harvesting account for daily temporal variations of the ambient energy. Due to the fact that solar energy provides a significantly larger amount of energy, and due to the fact that sensor nodes must store enough energy for several hours, these models are very source-specific, and therefore not general purpose [45, 73, 130, 83].

Overall, existing joint energy/information models suffer from a remarkable degree of complexity, at the same time extending them to account for multi-source energy harvesting systems is challenging since the energy harvesters are not considered as individual entities. Furthermore, they are not typically equivalent to classical communication models and as such, harder to solve. Developing a new type of model that it is simple, accurate and that naturally accounts for the multi-energy harvesting environment is set as a pending challenge.

2.3.3 Physical Layer Design

The physical layer is in charge of enabling a physical medium to transmit information. This layer aims at determining optimal power allocation and transmission policies to transmit in the best conditions [83, 7, 45, 58], as well as energy efficient modulations and transmission schemes to survive the large interferences of the transmitted power [96]. As one of the main research problems in this context we find the field of information theory. where, the channel capacity of energy harvesting enabled WSN and IoT have been extensely addressed [115, 104, 103, 134].

2.3.4 MAC Layer Design

It is widely accepted that communication in WSN requires more energy resources than computation. For this, reducing unwanted collisions and retransmissions of data packets becomes one of the challenges that the research community has mostly set to tackle. MAC protocols for energy harvesting WSN are thought as opposed to conventional energy-constrained MAC protocols. Provided that the energy state of the sensor is constantly changing, sensors aim at efficiently using the energy resources of the sensor, rather than employing energy-saving approaches [76, 61].

There exist a wide variety of MAC protocols designed for energy harvesting. These can be categorized in three main groups. First, polling-based protocols such as PP-MAC, EH-MAC and MTTP [76, 42]. Second, random access protocols, which, among others, considers ALOHA and CSMA-based protocols [61, 135]. Finally, scheduled protocols based on TDMA approaches [61, 135].

2.3.5 Energy Harvesting Wireless Sensor Networks

Energy harvesting changes the way in which networks are designed and considered. Non-energy harvesting powered IoT are constrained by the capacity of their batteries, such that nodes aim at optimizing the communication and network operation following an energy saving approach. On the contrary, energy harvesting defines energy as an unlimited resource, with scarce and non uniform availability, whereas the storage of energy is far limited. In this novel scenario, saving energy to extend the sensor lifetime is usually not the best approach, since it is likely to entirely fulfill the energy buffer. Accordingly, energy harvesting powered sensors need to follow energy efficient policies to maximize the use of the energy.

The study of WSN powered by energy harvesting starts from a simple transmitter-receiver pair [17]. From the networking viewpoint, studying the access of energy in large scales networks is posed as a major challenge. Among the different scenarios, mobile ad-hoc networks (MANETs) and cellular networks have attracted the interest of many research groups [59, 60].

2.4 Wireless RF Power Transmission

Wireless RF power transmission is emerging as a promising approach to enable battery-less wireless sensor networks (WSNs) [113, 144, 79, 145]. This technique aims to leverage RF energy harvesting [128, 141], which will allow controlled powering of nodes that may have insufficient residual energy in their batteries, or are unable to scavenge energy from the ambient environment (say, through solar, wind, vibration) at desired rates.

2.4.1 Circuit Design

The main circuits, which are required to implement an energy harvester for wireless RF power tranmission, are the antenna and a rectifying circuit, which converts the RF power into a DC current [138]. In case that both components are jointly integrated, this is referred as rectenna [51, 113]. However, employing separated circuits has been lately considered as an interesting approach to permit a dual operation of the considered antenna [82]. Hence acting for both communication and power transmission actions.

The non-linear behavior of semiconductor devices results in the dependency of the input impedance with the input power, such that the antenna and energy harvester impedances match only for a certain input power. The impedance matching makes two distinguished regions in any real implementation [33]: Increasing efficiency for low input powers and decreasing efficiency for high input powers. In region I, transmitting power in a time-varying manner leads to higher amounts of harvested energy [14]. On the contrary, in region II the power conversion efficiency at the high power range decreases with the input power [33], and a low peak-to-average received power ratio improves the efficiency of the energy harvester.

High-efficient energy harvesters integrate two separated and generic stages for energy optimization [56]. First, a rectifying circuit is employed that can convert with very high efficiency the harvested power. Then, a DC-DC boost converter operating in discontinuous conduction mode (DCM) is considered to transfer the accumulated energy in a temporal capacitor towards the energy storage unit (i.e., a super-capacitor or battery). The control unit handles the operation of this converter.

The aim of this dual-stage design is to optimize the transfer of energy by accurately matching the input impedance of the rectifying stage, which depends on its output load [100]. In particular, when connecting a rectifying stage for energy harvesting applications to an energy buffer, it shows a time-variable conversion efficiency, showing poor performance when the output capacitor voltage is either too low or too high [56]. For this, a small capacitor is connected to the output of the rectifier, which permits to rapidly skip the low-voltage operation regime (i.e., below a given voltage level). When its output voltage surpasses a given threshold the stored energy is high efficiently transferred to the output energy buffer through a DC-DC boost converter, leaving the voltage at the temporal capacitor at a low voltage (the duration time of this action is referred as *on-time*). As such, the voltage of the temporal capacitor approximates a saw-tooth waveform [34], and the output current of the energy harvester is in form of short time-scale spikes. Accordingly, the saw-tooth waveform period inversely depends on the input power.

2.4.2 Transmission of Energy

Given the relatively short charging range of one energy transmitter (ET), either mobile ETs or multiple ETs are required to cover large deployment areas [39, 40, 97] in WSN. The presence of multiple ETs reduces the average propagation distance to the energy harvesting sensors, and thus decreases the attenuation level of the energy waves and improve the RF power harvesting rates [55].

In multi-ET deployment scenarios, RF waves may interfere with each other when they are transmitted in the same medium. These interferences can be either constructive (i.e., the received power is larger than the average) or destructive (i.e., the received power is very low, or even zero) as shown in [97, 117], requiring ETs to implement energy multiplexing techniques for wireless RF power transimssion [144]. It can be observed that the constructive and destructive combination of RF waves generate very large peaks and drops of power in a non-controllable spatial-dependent manner.

Existing energy multiplexing approaches for wireless RF power transmission can be classified in two distinguishable groups. On the one hand, orthogonal methods can be utilized to mitigate interferences between transmissions of energy,

therefore providing separated access channels for each transmission of energy. In this group we find a large variety of multiple access methods that were proposed for communications and can be implemented for wireless RF power transmission as energy multiplexing methods, such as TDMA, FDMA, OFDMA [99], FHSS and DSSS [35]. This approach requires lightweight synchronization among ETs to guarantee non-interfering power transmissions [35]. Also, cooperative communication methods for many-to-single and many-to-many communication can also be considered [78]. On the other hand, distributed beamforming methods [94, 80] aim at constructively combining the RF waves at the recipient end to maximize the power transfer in a many (ETs)-to-many (sensors) configuration [144, 97, 80]. In this group, massive MIMO stands as the best alternative to optimize the power transfer. This was first showed in a two-user case [109] and later extended to a generic k-user [110]. However, this approach comes at the non-negligible cost of increasing hardware complexity by necessitating k antennas per ET, with k the number of deployed sensors, and requiring a node to ET communication link for channel state information reporting [110].

2.4.3 Energy and Communications

Using the RF spectrum for both energy and data transfer, however, may seriously affect network operations and performance, and require sophisticated hardware and devices that many systems cannot afford. For instance, transmitting energy and data on different frequencies [101] would require multiple or broadband access capabilities, since the frequency gap between energy and data communications cannot be very small [96]. Alternatively, when both energy and data share a single band, specialized MAC protocols are required [97]. In both cases, devices should feature two separate RF front-ends, for decoding the information and converting RF energy into DC [111]. Therefore, devising methods for energy provisioning without affecting data communications appears to be the challenge to tackle [48].

Simultaneous wireless information and power transfer (SWIPT) and full duplex energy harvesting have been presented in [82, 72]. These technologies aim to deliver information over a wireless medium during the simultaneous transmission of energy. However, SWIPT enables the transmission of data and energy from the same network device, thus enabling downlink communications, whereas

full-duplex energy harvesting aims at receiving energy as the device transmits it, thus targeting uplink communications. In these fields, significant work has been recently performed, which includes considering MIMO-based solutions [147] or simultaneous relay of energy and data [20]. In particular, a model for integrated data and energy transmission using SWIPT has been presented in [149].

Simultaneous transmission of energy and data is also provided by other technologies. For instance, RFID technologies inherently implement simultaneous transmission of energy and data, being based on backscatter communications [140]. In line with this approach, backscatter communications have recently been presented and experimentally demonstrated for wireless RF [84]. This approach leverages ambient RF waves produced by a third entity that are passively reflected from the transmitting to the receiving node. To reflect the RF wave and to modulate information, the impedance of the antenna is being constantly modified at the transmitter (i.e., short-circuiting and open circuiting the antenna to modify its reflection properties and to transmit logic '1's and '0's). Ambient backscatter enables ultra low power communications over an active transmission of energy. However, the transmitting node cannot allocate power as it reflects a portion of the power that it receives, whereas the allocated power in our approach is a design parameter. On the receiver side, no integrated data and energy receiver has been implemented, so the receiving sensor has to switch between activities, thus requiring synchronized MAC protocols to detect active data transmission.

Chapter 3

A general purpose Energy Model

3.1 Introduction

A major challenge in IoT is posed by the energy constraints of the nodes, where energy harvesting stands as a promising approach to perpetually re-charge the sensing and communicating devices yielding to self-powered IoT.

The available energy sources that a sensor can harvest can be originated from many natural sources and are present in many different forms. As an example, solar energy offers a slow pace time variation in cycles of 24 hours, with intense fadings in both temporal and spatial domains. Alternatively, the harvested energy from wireless RF sources, show a fast time-varying character with large dispersion. Overall, the harvested energy is then scavenged by a whole set of heterogeneous power processing techniques to maximize the conversion efficiency. Among other circuits, rectifiers and DC-DC converters show reasonably good power conversion performance. Finally, this is used to power a wide set of different applications.

As a result, the extremely large variation of approaches and alternatives to perpetually re-charge the IoT devices shows the need of general-purpose, energy-source-agnostic tools to model and characterize the ambient energy and the manner that sensors acquire and process it renders of major importance

This chapter presents the energy harvesting models, which are considered in the remainder of this work. First, the ambient energy is described. This is based in a separation of dynamics, being the slow dynamics a largely correlated in both time and space component which provides the average received power

at the node locations, whereas the fast dynamics stands for a dimension-less component which aims to capture the uncorrelated variations in both time and space. Then, the operation of the node and the flow of energy, referred as energy path is justified. This aims to provide a relation between the available energy at the close environment and the operations that the node can realize. Finally, a negative-energy queue model is provided to ease the modeling and simulation of energy harvesting enabled IoT devices. The negative-energy model aims at providing a one-to-one relation between the energy and the intensely devoted literature to classical communication queues.

3.2 Ambient Energy

The ambient energy can be harvested from a very large variety of physical phenomena. In particular, the most appealing energy sources for energy harvesting range from solar, thermal, mechanical, acoustic or RF. As it is shown in [128], the power that a sensor node can harvest depends upon many factors, such as nature of the source, power availability and dimensions of the energy harvester.

Among other physical phenomena, solar, human movement, vibrations or RF waves already present implementable transducers for sensors. In particular, the average power that it can be harvested from each energy source is in the order of 10 mW for solar, 1 mW for human movement, 10 μW for RF and 1 μW for vibrations [128]. However, the instantaneous power that it available at a given time and space is unpredictable.

In order to provide a model for the ambient energy, we require it to be as general as possible, we assume that the ambient energy, which is harvested, is spatio-temporal correlated and its value is given by what we define as the energy field. The energy field, $P_H(\mathbf{r}, t)$ in power units, is defined as a spatio-temporal function which provides the energy that would be harvested in case that a node is located at a certain location $\mathbf{r}$ at a time t.

To avoid an overhead in notation, in what follows, we will refer as $P_H(\mathbf{r}, t)$ the energy field, as $P_H(t)$ the power which is harvested from the energy field at the location of the sensor node under study and P_H as the average value of the energy field at the location of the sensor node.

Then, we assume that the energy field is given by the product of two separated

dynamics:

$$P_H(\mathbf{r},t) = P_S(\mathbf{r},t) \cdot p(\mathbf{r},t) \tag{3.1}$$

where $p(\mathbf{r},t)$ is a dimension-less, spatio-temporal-decorrelated random process, referred as the fast dynamics, and $P_S(\mathbf{r},t)$, in power units, stands for a random process with a slow variation in time as well as in space, here referred as the slow dynamics. The coexistence of these two dynamics is shown in Fig. 3.1.

The large temporal difference between both dynamics is such that it is accomplished that the average in time of P_H, can be separated by the product of both time-averages:

$$\langle P_H(\mathbf{r})\rangle = \langle P_S(\mathbf{r})p(\mathbf{r})\rangle = \langle P_S(\mathbf{r})\rangle \cdot \langle p(\mathbf{r})\rangle \tag{3.2}$$

where the $\langle\cdot\rangle$ operator stands for time average. Provided that the above equation holds, it is then obtained that we can approximate $P_H(\mathbf{r},t)$ at a time close to t_0 as:

$$P_H(\mathbf{r},t) \approx P_S(\mathbf{r},t_0)p(\mathbf{r},t) \tag{3.3}$$

for short time intervals, such that $P_S(\mathbf{r},t_0)$ can be considered constant within a node, while we can approximate P_H as:

$$P_H(\mathbf{r},t) \approx P_S(\mathbf{r},t) \tag{3.4}$$

for long time intervals. Therefore, depending on the length of the time interval, we can approximate the energy harvesting by just considering either the fast or the slow dynamics.

In addition, we define as e_H (and E_H its averaged value) the harvested energy over a fixed time T_H:

$$e_H = \int_{T_H} P_H(t)dt, \tag{3.5}$$

and alternatively, we define t_H (and thus, T_H its averaged value) as the time such that a given fixed amount of energy E_H has been harvested:

$$t_H \equiv \text{time s.t.} \int_{t_H} P_H(t)dt = E_H. \tag{3.6}$$

The spatio-temporal correlation of the slow dynamics is modeled with a cor-

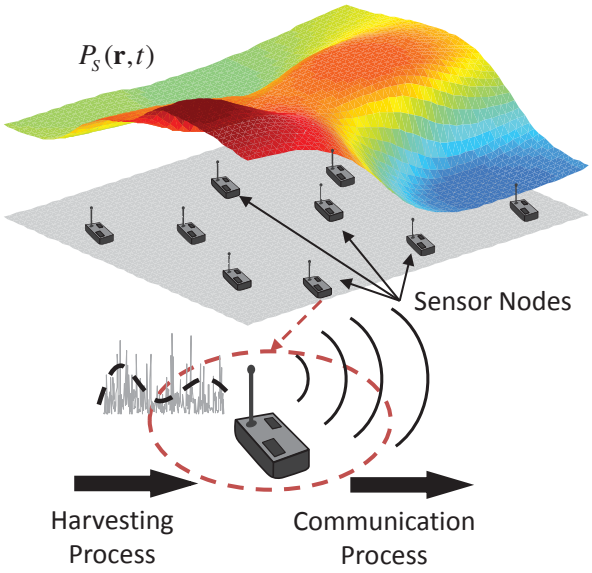

Figure 3.1: Separation of dynamics. The energy field is correlated in both time and space. The harvesting energy is bursty and random but it presents a smooth variation in temporal average.

relation coefficient. As a general definition, the correlation coefficient of the harvested power between the nodes i and j, located at $\mathbf{r_i}$ and $\mathbf{r_j}$ at times t_i and t_j respectively is given by:

$$\begin{aligned}&\rho_{ij}(\mathbf{r_i},\mathbf{r_j},t_i,t_j) = \\ &= \frac{E\left[(P_H(\mathbf{r_i},t_i) - \langle P_H(\mathbf{r_i})\rangle)(P_H(\mathbf{r_j},t_j) - \langle P_H(\mathbf{r_j})\rangle)\right]}{\sigma_H(\mathbf{r_i})\sigma_H(\mathbf{r_j})}\end{aligned} \tag{3.7}$$

where $\sigma_H(\mathbf{r_i})$ and $\sigma_H(\mathbf{r_j})$ refer to the standard deviation of the energy field at the locations of the nodes i and j.

Finally, we define the coherence time, t_c, as the minimum average time at which two points present no correlation between them. The concept of coherence time will result very helpful in the following sections in order to relate how fast the energy field varies in time and the impact that it has over the evaluated results.

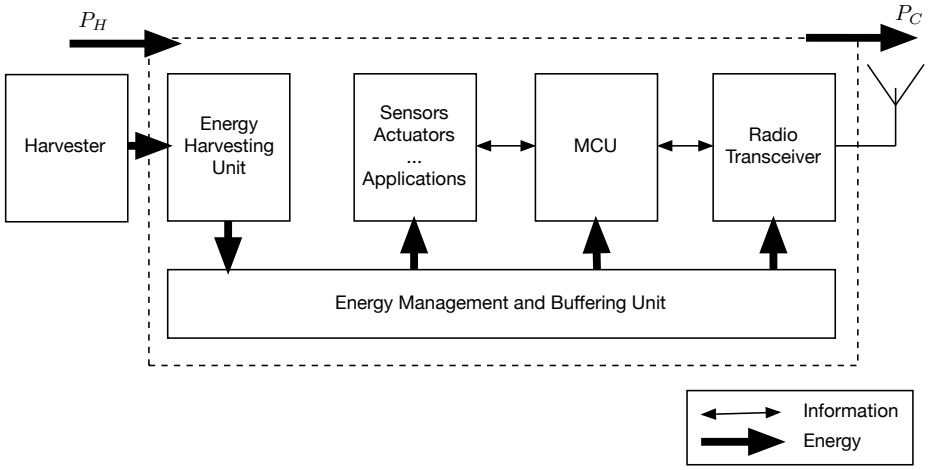

Figure 3.2: Considered system architecture of a node powered by energy harvesting. The harvesting power is denoted with P_H and the power which is efficiently converted into communications is shown as P_C

3.3 Sensor Node

In an energy-harvesting-enabled wireless sensor node, the energy which is used to enable the sensing, processing and communications is fully obtained from its close environment by means of ambient energy harvesters [128]. This energy would ideally present an ubiquitous and perpetual character, but it also generally has spatio-temporal-correlated properties [21]. Afterwards, this energy is conditioned in order to be stored in an energy buffer (e.g. a battery or a capacitor). Finally, this energy is used to power the sensing, processing and communications units [86]. This flow is here referred as the *energy path*.

The purpose of this section is two-fold. First, we aim to provide an overview of the sensor system architecture and to formarlly desribe the energy path. Second, we present the basic assumptions and relations among parts, as well as we define the dynamics-decoupled model for the ambient energy.

3.3.1 Sensor System Architecture

Environmental energy sources The energy found in the close environment of the sensor node can be presented in many different natures, such as thermal, solar, acoustic, RF and vibrations [128]. These energy sources ideally present an ubiquitous and perpetual character, as well as spatio-temporal-correlated prop-

erties among different nodes [21, 23]. However, their properties show a variation in time and frequency for a given node, because they also present a pulse-based, burst-mode, time-domain behavior.

Energy transducers The energy from the environment is scavenged through energy transducers. There exist several types of energy transducers, depending on the nature of the energy source, such as MEMS and NEMS for vibrational and mechanical energy harvesting, which can be either resonant [93] or non-linear [52], antennas and rectennas for RF energy harvesting [51] or solar cells [49].

Energy conditioning The subsequent part of the energy path requires the energy to meet a set of requirements, such as a regulated voltage. The energy conditioning block provides the matching between the energy transducers to the sensor node [133]. In this work, an adaptive front-end in the energy conditioning block is proposed to improve the overall efficiency in the energy path.

Energy storage Given the low-power density of the environmental energy sources, and their burst mode nature, there is the need of temporal energy storage [21, 23], so that the sensor node can access to the energy when the application requires more energy, despite severe time asynchronicity between time-dependent energy access and energy consumption. The energy storage unit is usually composed of either batteries, capacitors or supercapacitors.

Communications and applications The harvested energy is finally used to carry out the communication among nodes or perform a certain task, such as sensing, processing, or interacting with the environment [4].

3.3.2 The Energy Path

To model the access of energy in the node, we propose the use of the energy path function. This is a function which relates the average energy which is required to transmit a information packet to the actual energy which must be harvested from the environment. In other words, this function represents the power conversion efficiency along the energy path of an energy harvesting enabled sensor node. In

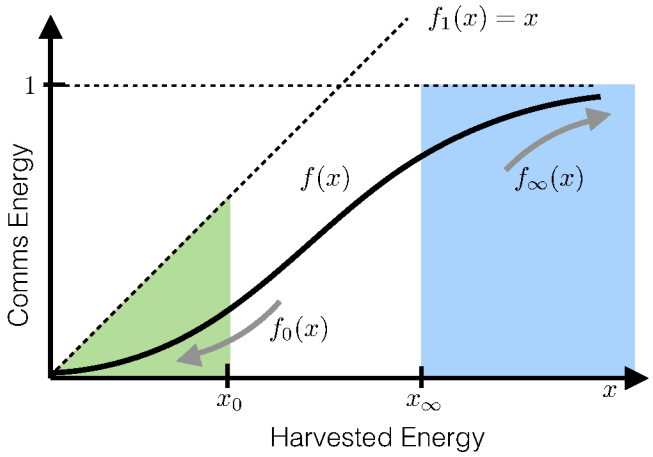

Figure 3.3: A generic energy path function, its theoretical bounds and the asymptotic approximations. In the green region, the EPF approximates an over-dimensioned sensor, with $f(x) \approx f_0(x)$. In the blue region, the EPF approximates a miniaturized sensor, with $f(x) \approx f_\infty(x)$.

this section, we will provide a general mathematical description, as well as its general implications.

We define the energy path function, as

$$\frac{E_C}{C_B} = f\left(\frac{E_H}{C_B}\right), \tag{3.8}$$

where E_C is the energy requirement of the communications unit, C_B stands for the energy buffer capacity and E_H refers to the harvested energy from the environment. As it is defined, the f function relates input-to-output energy normalized by the energy buffer capacity and it is then defined as dimensionless. As it follows, we define x as the fraction $x = E_H/C_B$ and we refer it as normalized harvested energy. We observe that the f function has the following properties:

- $f(x) \geq 0$. Provided that the energy is defined as a non-negative magnitude, the energy path function is also non-negative.

- $f(x) \leq x$. Provided that energy harvesting is the only source of energy, the acquired energy in this unit is always greater or equal than the energy that is required from the communications unit. The equality in this condition refers to the ideal case, such that the node converts the ambient energy and

uses it with 100% efficiency.

- $f(x) < 1$, i.e., the energy which is used for communications cannot exceed the capacity of the energy buffer. Intuitively, if during the transmission of two information packets the energy harvester receives more energy than the capacity of this, the excess of energy is lost.

- The efficiency of the energy path can be defined as $\eta(x) = h(x)/x$. We observe that the efficiency decays as $1/x$ for x sufficiently large.

Fig. 3.3 shows an example of the energy path function. As it is shown, the f function is bound by $f_1(x) = x$. It is also depicted the asymptotic behavior of this function. We define as f_0 as the f when it approaches $x \to 0$ (denoted with the interval $x \in (0, x_0)$), that is, the energy buffer is very big compared to the required energy to communicate, whereas we define as f_∞ when it approaches $x \to \infty$ (denoted with the interval $x > x_\infty$), that is, the energy buffer capacity is similar to the size of a communication data packet. These two particular cases are described in detail as follows:

A Miniaturized Sensor We refer as miniaturized sensor to a device with very limited energy buffering capabilities. Regardless of the available power that these sensors can harvest, the energy buffer is able to only store a very small portion of the energy. If the sensor does not use the energy immediately after it is harvested to communicate, it stops buffering extra harvested energy. Notice that the miniaturized sensor refers to the particular case $E_H \gg C_B$. According to the definition of such system, we can model $f(x) \approx f_\infty(x)$ as a function which, regardless of the input energy, it provides a constant output energy $f_\infty(x) = k$, with $k = E_C/C_B$. Therefore, the energy harvesting efficiency of a miniaturized sensor is given by:

$$\eta_\infty(x) = \frac{f_\infty(x)}{x} = \frac{k}{x}, \tag{3.9}$$

.

An Overdimensioned Sensor An over-dimensioned sensor refers to a device that, even though it operates in a low-end network (low data rates and low power requirements), it has been designed to operate at higher power and

information rates. These devices are generally bigger in terms of area, capabilities and also power losses than optimized devices. As such, the energy buffer is over-dimensioned and, thus, the energy of a single data packet renders negligible compared to the capacity of the energy buffer, i.e., $E_C \ll C_B$. An over-dimensioned sensor refers to a sensor such that its energy path function approximates $f(x) \approx f_0(x)$, and its efficiency depends on the harvested energy. Experimental results in micro-scale energy harvesters show that energy harvesters operating at lower rates than designed show an efficiency which is power-dependent on the input power [100]. Without loss of generality, we therefore consider:

$$\eta_0(x) = \frac{f_0(x)}{x} = \beta x^{\gamma}, \tag{3.10}$$

where β and $\gamma > 0$ are technology-dependent values which are left as parameters.

3.3.3 A Model for the Energy Path

In this section, we propose a Markov chain model to characterize the energy path function of a sensor node powered by energy harvesting. To do this, we first establish the primary assumptions, and then we evaluate the equations to show the energy path function of in the context of RF energy harvesting.

Overview

By following the energy path, the harvested energy is temporarily stored in an energy buffer, until this is used by the communication unit of the sensor node. This energy buffer of maximum capacity C_B, in energy units, (e.g. a battery or a supercapacitor) is used in order to absorb the time-varying random variations of both the energy harvesting and communication processes. We define the energy state, $s(t)$, as the energy which is stored at a time t in the energy buffer. This is a random process, which, in turn, is a function of the energy harvesting and the communication processes. This is given by:

$$\begin{gathered} \frac{\partial}{\partial t} s(t) = P_H(t) - P_C(t) \\ \text{Subject to: } 0 \leq s(t) \leq C_B \ \ \forall t \end{gathered} \tag{3.11}$$

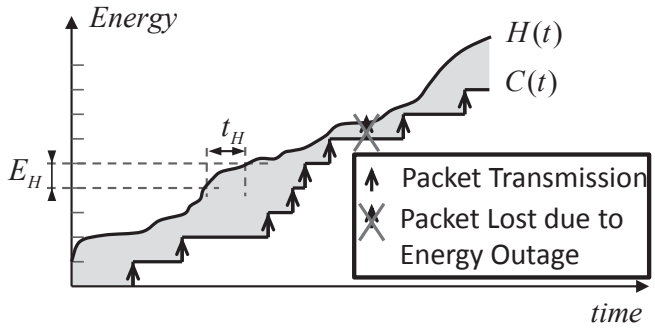

Figure 3.4: Depiction of the three elements which interact n the energy path/ The harvested energy, the energy stored in the energy buffer and the energy used for communications.

where $P_H(t)$ is the energy which is harvested by the sensor node and $P_C(t)$ stands for the power which is requested by the communications unit.

For a better understanding of the three elements which interact in the energy path, they are shown in Fig. 3.4. $H(t)$ refers to the aggregation of the energy which is harvested starting from the time $t = 0$ plus the initial stored energy. $C(t)$ stands for the aggregated energy which has been used for communications. In addition, the energy which is stored in the energy buffer, $s(t)$, is represented as the shaded area between the curves $H(t)$ and $C(t)$. Finally, we have also represented the data transmission requests as arrows.

The communication process in a WSN is characterized by the transmission of short data packets. A data packet has an associated energy, e_C, which is required in order to guarantee that the transmitted data can be recovered at the receiver node. This energy, e_C, is a function of the link capacity, link distance and transceiver constraints, and it is provided by the Shannon's link capacity.

Characterization of the Energy State

The energy state is a key parameter in the design and evaluation of any scheme of the protocol stack, ranging from the PHY layer to the application. In this work, we aim to characterize the energy state and to estimate the probability of each state.

The packetized patterns of the communications unit enables the discretization of (3.11). Such discretization has been performed in previous works [115, 45]

by providing a Markov chain and defining a virtual energy harvesting packet which arrives every certain time. However, given the unpredictable patterns of the energy harvesting process, the assumption of a markovian energy harvesting packet might not hold as a general case.

Therefore, we discretize in time the energy state equation. It is done at the time, t^k, produced by the communication event k. Thus, the energy state at the communication event $k+1$, s^{k+1}, is given by:

$$\begin{gathered} s^{k+1} = e_H^k - e_R^k + s^k \\ \text{Subject to: } 0 \leq s^{k+1} \leq C_B \ \ \forall t \end{gathered} \tag{3.12}$$

where s^k refers to the energy state after the k-th communication event, e_H^k is the harvested energy during the times t^{k+1} and t^k. Finally, the term e_R^k stands for the requested energy to transmit the data packet k.

The harvested energy during communications events needs to be modeled since this time usually randomly varies. As such, we find that the harvested energy during time events, e_H, is actually the result of the integration of random processes, P_H during a random time. As such, we proceed to characterize e_H by means of the law of total probability, which states the cumulative distribution function (cdf) of e_H, here referred as F_{E_H}, is given by:

$$F_{E_H} = \mathbf{E}[F_{E_H^{t_C}} | T_C] \tag{3.13}$$

which can be rewritten as:

$$F_{E_H} = \int_0^\infty F_{E_H^{T_C}}(t_C) f_{T_C}(t_C) dt_C \tag{3.14}$$

where $F_{E_H^{t_C}}(t_C)$ is the cdf of the harvested energy during a fixed time t_C and $f_{T_C}(t_C)$ stands for the probability density function (pdf) of the time between communications events, t_C.

The energy which is actually used to transmit the data packet, the communication energy e_C^k, equals to the requested energy, as long as there is enough stored energy:

$$e_C^k = \begin{cases} e_R^k & \text{if } s^k > e_R^k \\ 0 & \text{otherwise.} \end{cases} \tag{3.15}$$

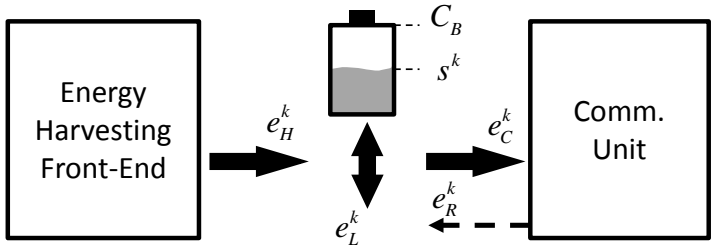

Figure 3.5: Energy balance at the sensor node, where e_H^k is the harvested energy, s^k stands for the energy state of the energy buffer, C_B stands for the maximum capacity of the energy buffer, e_L^k refers to the energy which is lost due to battery fulfillment, e_R^k is the requested energy, e_C^k stands for the communication energy,

In addition, we denote as e_L^k the energy which is lost when the node is not able to store the energy due to energy buffer fulfillment. This is given by:

$$\begin{gathered} e_L^k = e_H^k - (C_B + s^k) \\ \text{Subject to: } e_L > 0. \end{gathered} \tag{3.16}$$

The relation among energies is referred as the energy balance. This is shown in Fig. 3.5. Finally, we have that, in average, the input energy must equal to the output energy. Therefore:

$$E_H = E_C + E_L \tag{3.17}$$

where E_H, E_C and E_L refer to the average value of the harvested, communications and lost energies. As it follows, we will refer as e_H, e_C, e_R, s, e_L and t_C the discrete random processes of energy and time, such that a given random process x accomplishes that $x^k = x(t_k)$. The random processes e_R and t_C are communications-related, which both are provided by the application.

By having defined a time-discretized energy state equation, (3.12), and by having modeled the cdf of the ambient harvesting energy which arrives at each discrete time, (3.14), the energy state probability can be mathematically obtained through a Markov model.

Markov Modeling of the Energy State

In order to model the sensor node through a Markov chain, the energy state is discretized into N_B states. In addition to this, we have assumed Poisson arrivals

only produced by the communications unit. After an event arrival, the transition probability is estimated by means of the difference between the harvested energy, with cdf defined by F_{E_H} (3.14), and the statistics of e_R, which are provided by the application.

Then, we define the transition matrix, $\mathbf{P}$ as the N_B-by-N_B matrix, where each element of the matrix, p_{ij}, refers to the transition probability from the state i to the state j. This probability is given by:

$$p_{ij} = \begin{cases} p_1(i,j) & \text{if } j \leq i \\ p_1(i,j) + p_2(i,j) & \text{otherwise} \end{cases} \tag{3.18}$$

where the first term, $p_1(i,j)$, is common for both cases and refers to the probability that $e_R - e_H = (i-j)C_B/N_B$, i.e., the probability that the difference between e_R and e_H equals to the distance between both states. In addition, the second therm, $p_2(i,j)$, refers to the probability that $e_H + iC_B/N_B < e_R$, i.e., the sensor node does not have enough energy to communicate, and also that $e_H = (j-i)C_B/N_B$, i.e., e_H coincides with the distance between both states.

Therefore, we define $\boldsymbol{\pi}$ as a horizontal vector of N_B elements, which contains the state probabilities. In order to be the $\boldsymbol{\pi}$ vector the probability vector in steady state, it must be accomplished that *i)* $\boldsymbol{\pi} = \boldsymbol{\pi}\mathbf{P}$, i.e., $\boldsymbol{\pi}$ is left-eigenvector of $\mathbf{P}$, with eigenvalue $\lambda_\pi = 1$, and that *ii)* $\sum_{N_B} \pi_i = 1$, i.e., the sum of every element of the vector is equal to one.

Derivation of the Energy Path Function

In order to obtain the average function, we first estimate the f function for a fixed C_B and average E_H. By considering the markovian model, we have x as the normalized harvesting energy, y_R as the normalized requested energy to transmit the data packet, y_C as the normalized communications energy. We define z_S as the energy which is not lost, i.e. $z_S = x - z_L$. The energy z_S is highly dependent on the current energy state. Indeed, in large energy states, the chances that the energy buffer is over-flooded, thus causing a loss of the harvested energy is larger than in low energy states. As a result, the average $Z_{S,i}$ at the state i of the

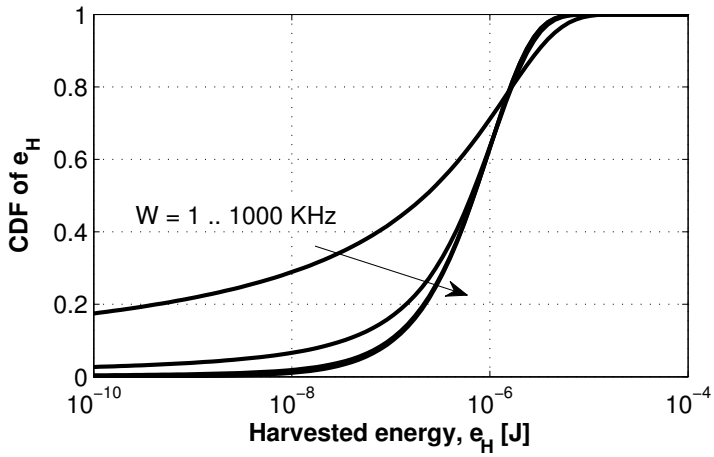

Figure 3.6: Cumulative distribution function of the harvested energy for different values of the bandwidth in RF energy harvesting ($W \in \{1, 10, 100, 1000\}$ kHz).

Markov chain is given by:

$$Z_{S,i} = E[z_{S,i}] = \int_0^{N_B - i} x f_X(x) dx + \int_{N_B - i}^{\infty} (N_B - i) f_X(u) dx \tag{3.19}$$

where f_X refers to the pdf of the energy normalized harvesting process. This is obtained through (3.14), by computing its derivative. Then, the average harvested energy which is stored in the i-th state can be obtained by:

$$Z_S = E[Z_{S,i}] = \sum_{i=0}^{N_B} E[Z_{S,i}] \pi_i \tag{3.20}$$

where π_i stands for the i-th state probability in the Markov chain.

As a last step, by assuming that the energy which is stored will be eventually used to communicate, we obtain that in average $Y_C = Z_S$.

3.3.4 A Case Example

As a case example, we evaluate the energy path function in case of RF energy harvesting. Firstly, we assume that the RF energy source is generated by an AWGN noise-like power source with bandwidth W and two-sided spectral density $P_H/2W$, such that the resulting received power at the sensor node is P_H.

It is well known that the energy, E_H, which is harvested from an AWGN-like power source over a fixed time T can be modeled as a chi-square distribution with $\nu = 2TW$ degrees of freedom random variable. This probability density function is expressed in terms of the normalized random variable $Y = 2E_H W/P_H$, and is given by:

$$f_Y(y) = \frac{1}{2^{\nu/2}\Gamma\left(\frac{\nu}{2}\right)} y^{(\nu-2)/2} e^{-y/2}. \tag{3.21}$$

However, the integration time is given by the communication block, which is modeled as an exponential random variable. Therefore, by the law of total probability, which is given by (3.13) and (3.14), the cumulative distribution function (cdf) of the chi-squared distributed harvested energy, e_H over an exponentially distributed time t is given by:

$$F_{E_H}(e_H) = \int_0^\infty \frac{\gamma\left(tW, \frac{e_H W}{P_H}\right)}{\Gamma(TW)} \lambda_t e^{-\lambda_t t} dt \tag{3.22}$$

where γ stands for the lower incomplete gamma function. This integration does not have a close-form expression, thus it must be numerically solved. Afterwards, the estimation of the cdf is used in order to compute the transition matrix $\mathbf{P}$ from the Markov model and the energy state probabilities are found. Finally, the state probabilities of the energy state are used in order to compute the h function.

In order to evaluate these results we have assumed the following configuration: $P_H = 1$ mW, $\lambda_t = 1000$ packets/second, $W \in \{1, 10, 100, 1000\}$ kHz and $e_C = 1$ μJ. In Fig. 3.6 we evaluate the CDF of the harvested energy, F_{E_H}, from (3.22). As it is shown, the bandwidth of the energy harvester has a strong effect on the statistics of the harvested energy. Afterwards, we show in Fig. 3.7 the cdf of the energy state, when considering RF harvesting energy. In order to characterize the energy state, a total capacity of the energy buffer has been chosen as 1 mJ. It is observed that larger bandwidths provide a more uniform distribution of the energy state at the sensor node. Finally, we evaluate the energy path function in Fig. 3.8. The energy path function is shown for different values of bandwidth. Consistently with the energy state distribution, larger values of bandwidth uniformly distribute the energy state, thus reducing the probabilities of not having enough energy to transmit.

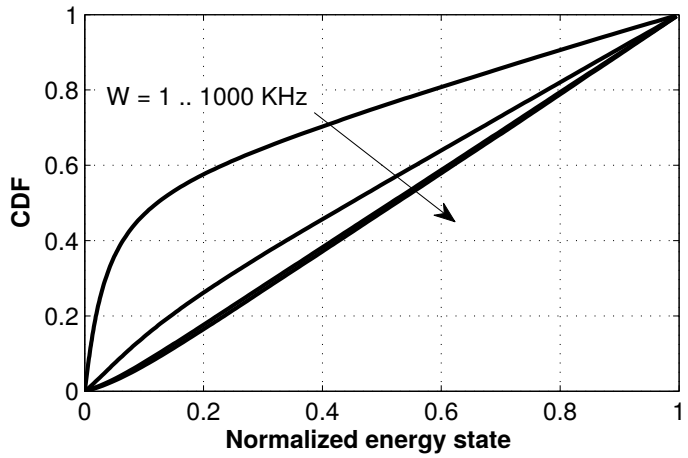

Figure 3.7: Cumulative distribution function of the energy state, using an energy buffer of 1 mJ, for different values of the bandwidth in RF energy harvesting ($W \in \{1, 10, 100, 1000\}$ kHz).

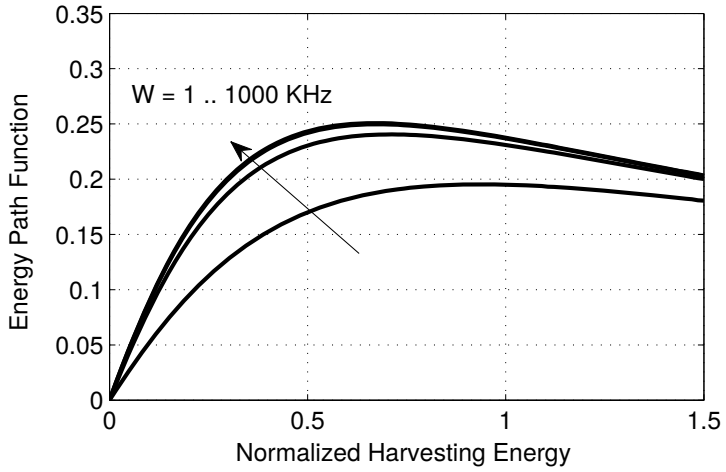

Figure 3.8: Evaluation of the energy path function for different values of bandwidth ($W \in \{1, 10, 100, 1000\}$ kHz).

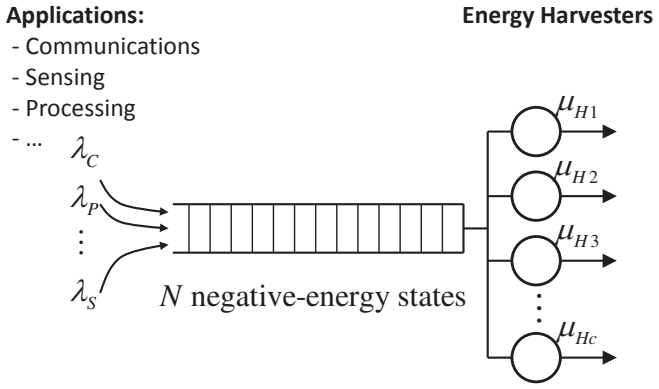

Figure 3.9: The negative-energy queue model. The arrivals of negative-energy packets are produced by the applications of the sensor node. The negative-energy packets are processed by the energy harvesters.

3.4 The Negative-Energy Queue Model

Given the large amount of literature devoted to queue theory for communication models, we consider that a queue model for EHE-WSN nodes should have the same properties than a communication queue. That is, we pursue an energy model such that:

- The stability condition must be $\rho < 1$.
- The idle state must be defined as the state of having an empty queue.
- The loss of communication must be assigned to a full queue.

Thanks to such queue model, we would be capable of using the well known results and closed-form expressions for communications, and to translate them into energy harvesting requirements.

Therefore, we define the negative-energy queue model for EHE-WSN as in Fig. 3.9. As it is shown, the arrivals of this queue are generated by the set of applications of the sensor node. i.e., every time an application spends one unit of energy, it generates an arrival of negative-energy. Each type of application has an associated generation rate (e.g. λ_C for communications, λ_P for processing and λ_S for sensing). On the other hand, the service time, $T_H = 1/\mu_H$, is the time that an energy harvesting unit needs to process one negative-energy packet. In other words, T_H is the time that it takes for the energy harvesting unit to harvest

the required amount of energy that has been consumed by a certain application (3.6).

In order to account for power losses [86] in our negative-energy queue model we assume them as constant. This assumption is valid for a wide set of values of the energy buffer state while does not apply for very low or very high energy buffer states [29]. Below a certain threshold of stored energy the sensor node stops its operation, this is taken into account by our model as a full negative-energy queue. Similarly, the energy harvested by sensor nodes with very high energy stored is lost because of the leakage, this represents the maximum achievable capacity of the energy buffer. We consider this case in our model as an empty negative-energy queue.

In addition to this, recent trends in sensor node design is pointing to multi-source energy harvesting [8, 108, 141]. Multi-source energy harvesters can be considered in this queue model by connecting them in parallel, such as multiple servers in a communication queue (e.g. M/M/c/N and M/G/c/N).

Finally, the queue of negative-energy packets refers to the energy buffer but observed upside down. A queue which is empty of negative-energy packets refers to a fulfilled energy buffer, while a fulfilled queue stands for an empty energy buffer. Thus, the number N of negative-energy states is related to the energy buffer capacity as:

$$N = \frac{C_B}{E_H} \tag{3.23}$$

where C_B is the energy buffer capacity and E_H refers to the energy which is harvested over a time T_H. Additionally, if at a certain time t_k the queue has L^k negative-energy packets, then the energy state s^k at the energy buffer is given by:

$$s^k = C_B - L^k E_H. \tag{3.24}$$

It is observed that when the queue does not have any negative energy packet, the energy harvester unit can remain in idle state, alike communications queues.

For further evaluation along this work, we have considered communications processes, with Poisson arrivals, as the generator of negative-energy packets and a single energy harvester. Therefore, as it follows, we can use the literature of M/G/c/N queues, so that we can evaluate the system for any arbitrarily chosen statistic distribution for the energy harvesting source.

The Energy-Erlang

By having provided the negative-energy queue model for EHE-WSN, we can now define the energy utilization as:

$$\rho_E = \frac{\sum_i \lambda_i}{\mu_H} = \frac{\sum_i P_i}{P_H} \tag{3.25}$$

in Energy-Erlang [E2] units. As it can be observed, the energy utilization of the negative-energy queue model, unlike the utilization which was defined in typical queue models for EHE-WSN, is now stable for $\rho_E < c$, where c stands for the number of energy harvesters.

In general terms, the Energy-Erlang is a dimension-less unit which is proposed here as a statistical unit of energy harvesting resources.

As an example, let us assume that an energy harvester is able to harvest $P_H = 10$ μW. If, in order to communicate, it requires $P_C = 25$ μW, then the required energy harvesting resources result in $\rho_E = 2.5$ Energy-Erlangs, which means that at least 3 energy harvesters are required in order to enable a correct operation of the sensor node ($\rho_E < c$).

Due to the fact that the Energy-Erlang is a ratio between the available and the required energy resources, it provides significant advantages in the design and dimensioning of sensors. In particular, this can be used to dimension energy harvesters, since we can relate the required harvesting power to meet certain user-defined requirements by $P_H = P_C/\rho_e$. In addition to this, it is also possible to dimension energy buffers for fixed available energy and requirements, through the evaluation of the negative-energy queue model. This is provided in the following sections through the evaluation of the energy outage probability.

The Energy Outage

As a metric for evaluation of the energy model to provide guidelines in dimensioning of energy buffer, we define the energy outage. The energy outage is defined as the time interval during which the sensor node does not have enough stored energy, and thus its operation is temporarily interrupted. This situation can be observed in Fig. 3.4. The probability that this occurs equals to the probability that the queue of negative-energy is full, and so, it equals to the expression for

blocking probability of a queue model for communications [89]. Therefore, by means of queue theory on M/G/1/N, we can obtain that the outage probability, p_{out} is given by:

$$p_{out} = P_N = 1 - \frac{1}{\pi_0 + \rho_E} \tag{3.26}$$

where π_0 refers to the probability that there are 0 negative-energy packets left within the queue right after the last negative-energy packet was processed by the energy harvester. π_0 is found as a solution for:

$$\begin{gathered} \pi_n = \sum_{n=0}^{N-1} \pi_j p_{jn}, \quad 0 \leq n \leq N-1 \\ \text{and} \quad \sum_{n=0}^{N-1} \pi_n = 1 \end{gathered} \tag{3.27}$$

where, equivalent to π_0, π_n refers to the probability that there are n negative-energy packets left and p_{jn} stands for the state transition probability of remaining negative-energy packets from the state j to the state n, considering each state right after a negative-energy packet has been processed by the energy harvester.

3.4.1 Model Evaluation

Time-domain Simulation Set-up

In order to validate the negative-energy queue model, we have first performed a time-domain simulation which implements a one-to-one transmission of RF energy in a multi-path environment. The energy transmitter (ET) generates an RF wave, which is propagated through a multi-path Rayleigh channel with coherence time $t_c = 0.5$ s [117], the average power at the receiving node is set to 10 μW, which is reasonable as reported in [100]. A block diagram of the simulation set-up is shown in Fig. 3.10. At the receiving node, a rectenna is used to harvest the energy of the RF wave [51]. The power which is harvested is power processed and stored in a continuous manner in an energy buffer of variable capacity. The communications unit transmits data packets with a variable Poisson distributed inter-arrival rate.

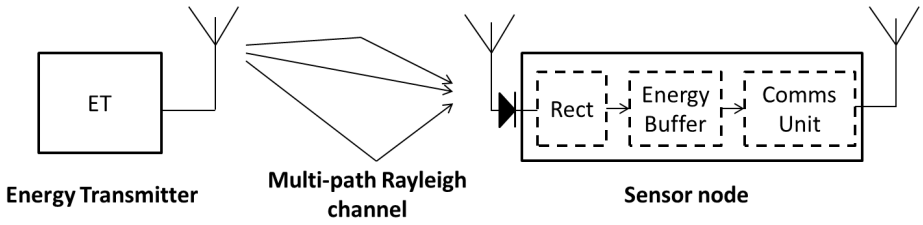

Figure 3.10: Considered set-up in the time-domain simulation.

Negative-energy Model Simulation Set-Up

We assume that the energy harvester processes these negative-energy packets at a rate of $\mu_H = 1$ negative-energy packets per second, following both Poisson and chi-squared statistics. Then, the communications unit generates Poisson arrivals of negative-energy packets at a rate of $\lambda_C = \rho_e/\mu_H$.

A Poisson distribution might not hold as a general case, however it studied due to two main reasons. Firstly, the energy outage probability has a closed-form expression, which is given by:

$$p_{out} = \frac{1-\rho_E}{1-\rho_E^{N+1}}\rho_E^N. \tag{3.28}$$

And, secondly, a Poisson process has very large entropy [143], thus becoming the energy outage probability of a M/M/1/N as an upper bound in the energy outage probability in many environments.

Alternatively, a chi-squared distribution is of special interest in the context of energy harvesting, since this distribution is given as a result of harvesting energy from a Gaussian noise-like energy source [92]. In particular, the energy which is harvested during a time T from a Gaussian noise-like source of bandwidth W is modeled as chi-squared distribution with $k = 2TW$ degrees of freedom. In this simulation, we have chosen $k = 4$, since it is the result of approximating the time-domain simulation parameters with a time $T = 1/\mu_H$ and $W = 1/t_c$.

Performance Evaluation and Comparison

In Fig. 3.11 we compare, in terms of the energy outage probability, the time-domain simulation results to the negative-energy queue model results assuming *i)* a Poisson distribution for the energy harvesting process (black continuous lines)

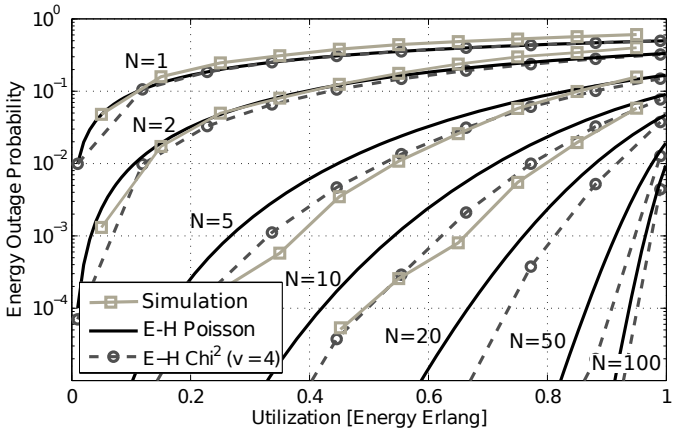

Figure 3.11: Comparison between the energy outage probability obtained by assuming both a Poisson process and a chi-square distributed process for the energy harvesting. It is shown as a function of the energy utilization for different values of the normalized energy buffer capacity.

and *ii)* a chi-squared distribution for the energy harvesting process. The energy outage is evaluated as a function of the energy utilization for different values of the normalized energy buffer.

As the results show, the negative-energy model well predicts the behavior of time-domain simulation, although significantly reducing the computational cost. In addition, we observe that the energy outage probability is upper bounded by the results from the M/M/1/N queue and it tends to $p_{out} = 1/(N+1)$ when the energy utilization tends to one. As an example, if considering that the sensor node has the following requirements: $E_C = 10$ μJ, $\lambda_C = 0.9$ packet/s, and the node is able to harvest $P_H = 10$ μW from an environmental source, then we find that the energy utilization equals to $\rho_E = 0.9$ E2. By considering a target of $p_{out} = 10^{-2}$ in the energy outage probability, it is obtained that we would require a normalized energy buffer capacity of $N = 20$. Finally, if we express the energy buffer capacity in terms of energy, we would require an energy buffer capacity of $C_B = 200$ μJ.

3.5 Summary and Conclusion

The large amount of sources of available ambient energy has yield to application-specific models. This chapter has introduced a general-purpose energy-source-agnostic definition of the ambient energy by defining the energy field, and has provided an implementation-independent system model, through the energy path function. This has enabled a generic framework to model arbitrary sources of energy and to characterize the access that sensors do with it. In the following chapters, we will employ the presented definitions to address the research challenges that appear during the network planning and sensor design.

Chapter 4

Scalability of Network Capacity in WSN Powered by Energy Harvesting

4.1 Introduction

A critical parameter in the design and evaluation of Wireless Sensor Networks (WSN) is the throughput capacity. In bandwidth-limited conditions, this was bounded by Gupta and Kumar [50] showing that when n identical nodes, each capable of transmitting W bits per second, the uniform throughput per node decreases with n as $\Theta\left(\frac{W}{\sqrt{n \log n}}\right)$ where Θ refers to the asymptotic bound and n is the number of nodes. In addition, in [98] it has been shown that in cases where the system is constrained by power, the uniform throughput capacity per node increases as $\tilde{\Theta}(n^{(\alpha-1)/2})$ where α is the path loss exponent and $\tilde{\Theta}$ stands for soft order (i.e., the same as Θ bound with the powers of $\log n$ neglected). More recently, the throughput capacity has been largely studied, finely modeled and evaluated for several network topologies, physical layers, mobility and energy constraints [47, 126, 71, 119].

In this chapter, we bound for the per node throughput capacity as a function of the number n of nodes in energy harvesting powered wireless sensor networks. This bound sets an important guideline for feasibility and deployability during the design process of a network powered by energy harvesting. Among others, the

scalability of such networks will decide whether these kind of networks support large deployments of sensors of whether these will require additional infrastructure to properly operate.

As a result, we find that the per node uniform throughput of a network powered by energy harvesting is upper bounded by the power constrained bound [98]. That is, the operation of an energy harvesting enabled powered WSN operates as a power constrained network if the energy conversion is perfectly performed. However, we show that affordable hardware brings several non-idealities of the sensors, such as a limited size of the energy buffer or a standby leakage current, which alter this bound showing that: the former causes worse resilience to node failure than power constrained wireless networks (i.e., the throughput rapidly decays as the number of nodes decrease), while the latter makes the network to become non-scalable. For this, it is observed that different strategies have to be followed to come across these restrictive bounds. In particular, it is required to increase the number of deployed nodes improve the scalability of low resilient to node failure networks, while appropriate network protocol design is required to improve non-scalable networks.

The rest of this chapter is organized as follows. In Sec. 4.2, we present the main assumptions of this work at the different design levels. Sections 4.3 and 4.4 provide an upper and a lower bound for the throughput capacity. In Sec. 4.5 we discuss the bounds in throughput capacity and consider a non-ideal operation. Sec. VI presents a model to derive the energy path function. Finally, in Sec. 4.6 we conclude our work.

4.2 Energy, Hardware and Network Architecture

This section overviews the hardware and network architectures which are considered in this work.

4.2.1 Sensor Node Considerations

Sensors integrate the sub-system units which are described in Chapter 3. In summary, the considered sub-system units are:

- **Harvester:** This unit interacts with the environment to transform the ambient energy into electric current.

- **Energy Harvesting Unit:** This unit aims to optimize the AC to DC power conversion.

- **Energy Management and Buffering Unit:** This unit is in charge of distributing the harvested energy to the remaining units of the node.

- **Sensors, actuators and applications:** Nodes are intended to monitor their close environment and to occassionally interact with it.

- **MCU:** The microcontroler unit (MCU) is the central unit of the node.

- **Radio Transceiver:** This unit actually establishes the communication among nodes.

In order to achieve an energy neutral operation (i.e., a node can uninterruptedly operate for an unlimited time) the harvested power must be greater or equal than the power demands in temporal average [73]. In addition to this condition, the capacity of the energy buffer plays a key role during this operation. Given that the energy buffer separates the time-varying dynamics of both the energy harvesting and energy demands, the capacity of the energy buffer must be sufficiently large to supply the remaining units when the energy source is temporarily unavailable.

To capture the interaction between the access and demand of energy we employ the concept of energy path function, derived in Chapter 3. Accordingly, this translates the average energy which is required to transmit an information packet to the actual energy which must be harvested from the close environment.

4.2.2 Network Considerations

We describe next the network considerations, including network topology and physical, MAC and routing layers

Network Topology

This work assumes a wireless Ad-Hoc network topology of n nodes, which is deployed over a spherical surface of unitary area. The deployed nodes are assumed to be equal in energy harvesting, processing and communication capabilities, as well as in traffic generation. It is assumed that each node generates information, which is intended to be delivered to a single, yet different, node located in a random destination of the network, such that for a sufficiently large n, we can assume that each node receives and generates the same amount of information.

Physical Layer

The expected data-rate of the nodes is expectedly lower than the allocated bandwidth [128]. In real context applications, it has been shown that nodes powered by energy harvesting techniques are able to generate just a few bits per second, while the communication channel allocates a few tens of kbps. This fact conveys to establishing the infinite bandwidth approximation as a starting hypothesis, and to be a reasonable approximation.

We assume a flat channel, which is a function of the distance. This is given by:

$$g_{ij} = g_0 d^{-\alpha}, \tag{4.1}$$

where g_0 refers to the attenuation at a distance of 1 m, d is the distance between the transmitting node i and destination node j and α stands for the path-loss exponent. Usually ranging from 1.9 to 6 in real context applications [117]. Finally, we assume that sensors have full channel state information (CSI) and perform perfect power allocation. That is, given a communications link, these achieve the required data-rate with the minimum power.

Medium Access Control Protocol

MAC protocols are required to synchronize nodes and to coordinate data packet transmissions. Substantial work has been published in this matter to achieve near-optimal solutions.

In this work, we assume an optimal MAC layer, which ensures perfect coordination among nodes and avoid destructive interference among data packets

(i.e., each packet which is transmitted is perfectly decoded at the receiver end). Ideal MAC layer can be demonstrated for infinite bandwidth approximation. In particular, as it is shown in [98], CDMA is demonstrated as an optimal multiple access method, with a bandwidth scaling of $\Theta(n(n^2 \log n)^{\alpha/2})$.

Routing Protocol

The routing layer is a key aspect in the throughput capacity of a network and it requires further optimization. Routing protocols for these types of networks show that factors, such as the stored energy at the nodes and the available energy, modulate the cost functions during the design of optimal routes.

Notice that in accordance to the network topology description (i.e., there are no edge effects, each node has the same capabilities, is both source and destination of the same amount of information and each sensor generates information towards a single random destination node), every node in the network is expected to have, in average, the same residual energy. As such, optimal routing in this scheme must be based on the least-energy path.

We observe that the shortest-path accomplishes this condition. Intuitively, given that sensors have the same capabilities and requirements, there is no reason to justify any traffic diversion towards any specific area of the network. In other words, the least-energy consumption route matches the route with less relaying nodes.

We define the route R_i as the route that is generated to propagate the generated data packet from the i-th node towards its destination. Then, we refer as the throughput produced by a route, $r(R_i)$ as both the generated and the relayed traffic required to propagate the data packet along the route R_i

In case of considering the effect of a non-constant energy field, traffic routes should be obtained by means of a convex optimization problem. This problem is similar to the optimal routing for wired networks [12]. Additionally, optimal routing for massively deployed wireless sensor networks has been addressed in [18]. However, notice that the spatial dependence of the energy field does not have an impact upon the per node throughput scalability, since, the energy field can be both upper and lower bounded by a constant value.

4.3 An Upper Bound in Throughput Capacity

In this section we provide an upper bound on the throughput capacity for networks powered by energy harvesting as a function of the number of nodes. In order to obtain this upper bound, the f function is used to relate the requirements in the communication unit to the available environmental energy.

4.3.1 Relating Link Capacity to the Ambient Energy

First, we have that the link's Shannon capacity between a generic pair of nodes i and j, assuming the infinite bandwidth approximation, is given by:

$$r_{ij} = \frac{P_{ij} g_{ij}}{N_0} \log_2 e \tag{4.2}$$

where P_{ij} is the output power, g_{ij} refers to the channel attenuation from (4.1) which is a function of the distance between nodes and N_0 stands for the noise level.

Provided that nodes communicate employing data packets and the link capacity can be rewritten in terms of the energy needed to transmit a single packet, E_C, during the communication process as:

$$r_{ij} = c_0 \frac{E_C}{N_0} \frac{d^{-\alpha}}{T} \tag{4.3}$$

where c_0 is a certain constant, which does not depend on the link distance, and T refers to the time between communication events.

Then, by fixing a target energy per packet, E_{C0}, at the receiving node such that the receiver requirements are accomplished, it is then obtained that the energy of the packet at the transmitter, E_C, is given by $E_C = E_{C0}/g_{ij}$. Given that the node relies on the available energy stored at the energy buffer, the time between communication packets equals to the time that it takes for the energy harvester to acquire an exact amount of E_C. As such, the product $E_C T$ is constant and equal to the output power P_{ij}. Therefore, the time between communication events also depends on the distance between nodes and can be rewritten as:

$$T = \frac{P_{ij}}{E_C} = T_0 d^{\alpha}, \tag{4.4}$$

where T_0 refers to a given constant in time units.

Thus, knowing from Sec. 4.2.1 that E_C is related to E_H by means of the f function, as shown in (3.8) and in Fig. 3.3, and that E_H is the average available harvested energy, which equals to the power P_H harvested during $T = T_0 d^\alpha$, the link capacity can be rewritten in terms of the available harvesting power as:

$$r_{ij} = c_1 \frac{f(P_H T_0 d^\alpha / C_B)}{T_0 d^{2\alpha}}, \tag{4.5}$$

which actually predicts the shape of the information capacity of energy harvesting nodes as a function of the harvested energy, reported in the existing literature [115]. Then, we simplify the equation by only considering the dependency of the link capacity with the distance between nodes:

$$r_{ij}(d) = c_2 f(c_3 d^\alpha) d^{-2\alpha}. \tag{4.6}$$

4.3.2 Relating Link Capacity to the Overall Throughput

Once the ambient energy is related to the link capacity, we need to relate this to the overall traffic of the entire network. This overall traffic considers both the generated and relayed traffic of the nodes and it can calculated as:

$$\sum_i r(i) = \sum_i r(R_i), \tag{4.7}$$

where $r(i)$ is the traffic of the i-th node, defined as the addition of the generated traffic and the relayed information from neighboring nodes, and $r(R_i)$ refers to the throughput generated by the route R_i.

Intuitively, we find that the link capacity of the i-th node must be grater than its traffic, $r_i \geq r(i)$. Otherwise, the node is not capable of supporting the communication and its operation remains interrupted. By combining this principle with (4.7), we find that the link capacity of all nodes relates to the overall traffic of the network as:

$$\sum_i r_i \geq \sum_i r(R_i). \tag{4.8}$$

We find that there appears a significant symmetry in the network topology

and routing layers. In particular, (i) there exist n routes in the network (i.e., one per transmitting node). (ii) These routes are handled by the n sensors using a shortest-path routing. (iii) Each node is considered identical in terms of capabilities and requirements. For this reason, we find that, the summation of both sides can be simplified. In other words, in order for the network to operate, the throughput generated to forward the information from a source-destination pair along its route, must be able to be entirely handled by the source node. Thus, we have that:

$$r_i \geq r(R_i). \tag{4.9}$$

The overall throughput of the route R_i, $r(R_i)$, which considers both the generated and relayed data, can be calculated as the number of hops, N, times the throughput capacity of the source node, $r(n)$. Thus we have:

$$r_i \geq r(R_i) = Nr(n). \tag{4.10}$$

To derive the per node throughput capacity as a function of the number of nodes, we need to relate the average distance between nodes, d, and the number of hops, N, to the overall number of nodes, n. First, defining the source-destination distance as D_i, it is found in [50, 98] that the number hops, N, required to forward the packet along D_i can be lower bounded by:

$$N \leq c_1 \log n + c_2 L_i \sqrt{n \log n} \tag{4.11}$$

where L_i is the addition of the distance between hops. We find that this distance can be lower bounded by D_i, according to the triangle inequality:

$$L_i \equiv \sum_{k=1}^{N} \left| X_i^k - X_i^{k-1} \right| \geq \left| X_i^N - X_i^0 \right| \equiv D_i, \tag{4.12}$$

where the term X_i^k refer to the position of the k-th node of the route R_i. The relation of these distances is depicted in Fig. 4.1 As such, neglecting the term which depends on $\log n$ as it vanishes in from of the second term in the number of hops, and bounding L_i by D_i, we find that the number of hops, N, is upper bounded by:

$$N \leq c_2 D_i \sqrt{n \log n}. \tag{4.13}$$

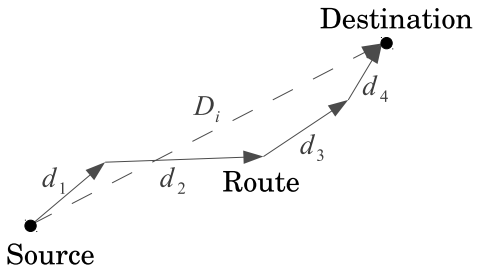

Figure 4.1: Relation between distances between hops d_j, end-to-end distance D_i. According to the triangle inequality, the addition of the distance between hops is greater or equal than the end-to-end distance, $L_i = \sum_j d_j \geq D_i$.

Then, the average distance, d, between hops can be calculated as:

$$d = \frac{L_i}{N} \geq \frac{L_i}{c_1 \log n + c_2 L_i \sqrt{n \log n}}, \tag{4.14}$$

where, again, bounding L_i by D_i and neglecting the term which depends on $\log n$ as it vanishes in from of the second term in the number of hops, we find that the average distance between hops is given by:

$$d \geq \frac{1}{c_2 \sqrt{n \log n}}. \tag{4.15}$$

4.3.3 Obtaining the Upper Bound

As a last step in the upper bound derivation, we must substitute d and N with the actual dependence with the number of nodes n. Recall that the term D_i is set as a design parameter, and thus it does not depend on the number of nodes it is found that the upper bound scales as:

$$c_6 h (c_5 \sqrt{n \log n}^{-\alpha}) \sqrt{n \log n}^{2\alpha - 1}. \tag{4.16}$$

4.4 A Lower Bound in Throughput Capacity

In this section we provide a lower bound on the throughput capacity to tie the gap between the upper bound and the actual throughput capacity of an energy

harvesting powered network. For this, we assume a sub-optimal communication protocol stack such that: *(i)* nodes do not know the exact location of the neighboring nodes, thus these must allocate more power to reach further distances. *(ii)* The network is divided into small cells such that the shortest-path route is calculated at the cell level. In this routing layer, a random node located in the next cell is chosen as the next hop in the route.

4.4.1 Network Topology

Similar to the upper bound, we assume that the nodes are deployed over a spherical surface of unitary area. Then, we first subdivide the networking area into smaller cells. These cells are determined by a Voronoi Tessellation which accomplishes the following conditions:

- Every Voronoi cell contains a disk of area $100 \log n/n$. Thus we define $\rho(n)$ as the radius of a disk of area $100 \log n/n$. The radius ρ in the sphere is given by:
$$4\rho \leq \sqrt{\frac{3200 \log n}{\pi n}} \tag{4.17}$$
- In addition, every Voronoi cell is contained in a disk of radius $2\rho(n)$.
- There is at least one sensor node at each Voronoi cell, with high probability (probability approaching 1 as n tends to ∞).

We refer the reader to [50, 98] for additional details on the network planning.

4.4.2 Routing Protocol

The considered routing protocol is defined as follows. First, a straight line between source and destination sensors is traced. This line crosses a given number of cells. Then, the traffic is relayed from one cell to the following cell through a randomly chosen node located at each cell until it reaches the destination. Notice that this routing scheme is a implements shortest-path sat the cell level. However, given that the intermediate relaying nodes are randomly determined at each cell, this node may not be the optimum relaying node in terms of energy requirements. We show in Fig. 4.2 an example of the routing scheme considered and we compared to the shortest path.

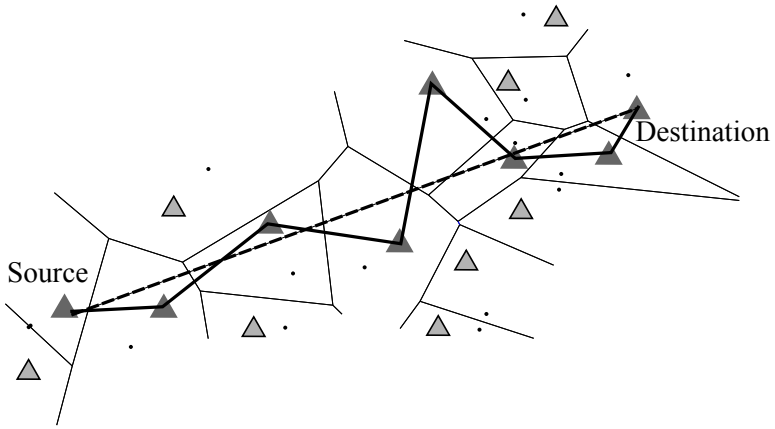

Figure 4.2: Routing scheme considered in the calculation of the lower bound. A straight line between source and destination is traced. A relaying node is selected at each crossing cell.

Under these assumptions, it is then found that the amount of routes that intersect a certain Voronoi cell, V, is bounded by [50]:

$$\mathbf{E}\left[\text{Routes intersecting } V\ \right] \leq k_4\sqrt{n\log n} \tag{4.18}$$

Then, being $r(n)$ the traffic of a single route, the traffic that is carried in a cell is bounded by:

$$\mathbf{E}\left[\text{Traffic carried by } V\ \right] \leq k_4 r(n)\sqrt{n\log n} \tag{4.19}$$

4.4.3 Obtaining the Lower Bound

According to the definition of the Voronoi cell, there is at least one node per cell. As such, we find that the most restrictive case in terms of the throughput of a cell refers to the situation where the traffic carried in the cell is supported by just a single node. Then, we can relate the link capacity of the single node to the traffic that this must carry:

$$k_4 r(n)\sqrt{n\log n} \leq c_2 f(c_3 d)d^{-2\alpha}, \tag{4.20}$$

where d is the distance between nodes.

Provided that the nodes do not have CSI, nodes must allocate sufficient power

to reach the following node. As such, nodes need to choose a range for the transmission sufficient to guarantee that the node is always able to forward the information to any adjacent cell. We select a transmission range of two times the maximum diameter of a cell, i.e., the transmission range is set to 8ρ. Thus, (4.20) remains:

$$k_4 r(n)\sqrt{n\log n} = c_2 f(c_3(8\rho)^{\alpha})(8\rho)^{-2\alpha} \tag{4.21}$$

As a last step, we substitute ρ by (4.17) and we isolate the generated traffic, $r(n)$. By doing so, we find that the lower bound in the per node throughput capacity scales as:

$$c_9 f\left(c_8\sqrt{\frac{\log n}{n}}^{\alpha}\right)\frac{\sqrt{n}^{2\alpha-1}}{\sqrt{\log n}^{2\alpha+1}}. \tag{4.22}$$

4.5 Discussion

In this section we first derive an expression for the soft-order bound in the throughput capacity and evaluate it. Then we discuss the main implications of this bound and discuss system design rules to improve the performance of energy-harvesting-enabled WSN.

4.5.1 The Soft-order Bound in Throughput Capacity

A soft-order bound $\tilde{\Theta}(g(n))$ is defined as the regular bound of $\Theta(g(n)\log^k g(n))$ for some k. Essentially, this bound neglects logarithmic factors because it assumes that it is more important predicting large trends with the input parameters than fine-grained details.

We find that by neglecting the logarithmic powers, the throughput capacity in an energy-harvesting-enabled network is both upper and lower soft-bounded by the same expression. Therefore, we can say that the throughput capacity is soft-bounded by:

$$\tilde{\Theta}\left(f\left(n^{-\alpha/2}\right)n^{(\alpha-1/2)}\right). \tag{4.23}$$

Finally, we use the definition of energy efficiency from Sec. 4.2.1 with (4.23) to relate the bound in throughput capacity to the energy efficiency of the node.

Table 4.1: Evaluation of the soft-order bound in our considered case scenarios.

Case	Bound
Ideal (power constrained [98])	$\tilde{\Theta}\left(n^{(\alpha-1)/2}\right)$
Miniaturized sensor ($\eta(x) = k/x$)	$\tilde{\Theta}\left(n^{(2\alpha-1)/2}\right)$
Overdimensioned sensor ($\eta(x) = kx^{\gamma}$)	$\tilde{\Theta}\left(n^{(\alpha-\alpha\gamma-1)/2}\right)$

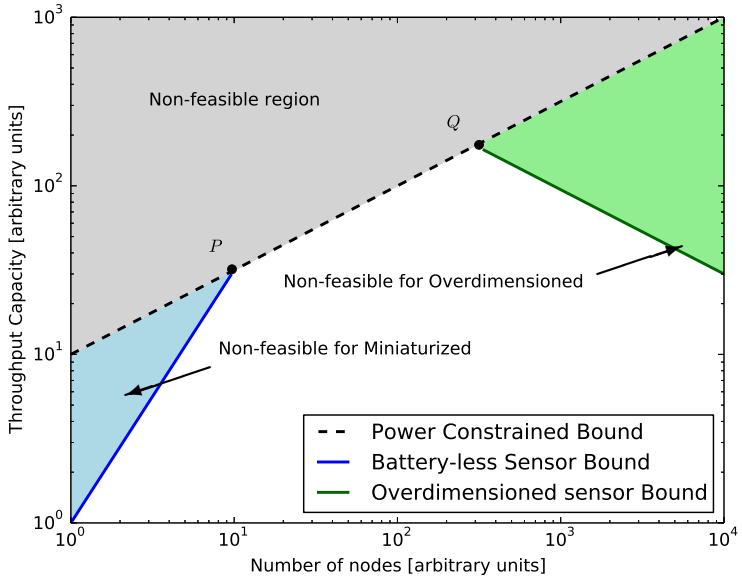

Figure 4.3: Throughput capacity bounds of energy harvesting powered networks. Comparison among the ideal, the miniaturized and the over-dimensioned sensor particular cases.

We find that the throughput capacity scales as:

$$\tilde{\Theta}\left(\eta\left(\sqrt{n}^{-\alpha}\right)\sqrt{n}^{\alpha-1}\right). \tag{4.24}$$

4.5.2 Evaluation of the Throughput Capacity

We particularize the efficiency of the energy path in the considered case examples from Sec. 2. That is, we consider the ideal case $\eta = 1$, the miniaturized sensor with efficiency $\eta(x) = k/x$ and the over-dimensioned sensor with efficiency $\eta(x) = kx^{\gamma}$ with $\gamma < 0$. These bounds are shown in Table 4.1. We observe that a miniaturized sensor device scales *faster* than the ideal case, whereas an over-dimensioned sensor scales *slower* or, even it does not scale for $\gamma > 2 - 1/\alpha$. To better show these

bounds, we observe in Fig. 4.3 the bounds in throughput capacity assuming a path-loss exponent $\alpha = 2$ and a $\gamma = 1$. We observe the following:

Throughput Capacity of Ideal Sensors

Energy harvesting powered networks which implement ideal energy harvesters and management units show the same bounds than power constrained wireless networks. Clearly, if a sensor can efficiently convert the environmental energy and unlimitedly store it until required, the random character of both the communications and harvesting processes become independent to each other. As a result, the sensor will operate as a power constrained sensor, where its output power equals to the average harvested power.

In addition, we observe that any sensor which is able to operate in a region such that the energy efficiency is approximately constant as a function of the energy demands and generation, i.e., $\eta(x) \approx \eta_0$, with $\eta_0 \in (0, 1)$ will have a reduced throughput capacity in comparison to the ideal case, but it will show the same scalability trend. As a general case, this is the desired operation region

Throughput Capacity of Miniaturized Sensors

Miniaturized sensors show similar performance than ideal energy harvesting sensors for a large number of deployed sensors. However, we observe that the throughput capacity rapidly drops if the number of sensors falls below a given value (the intersection between curves is denoted with the point P in Fig. 4.3). Intuitively, as the number of sensors decreases, the distance between neighbors grows. Then, miniaturized sensors are unable to reach the next hop as it cannot allocate enough power in the data transmission. As a result, the communication is interrupted and the throughput capacity drops. The location of the intersection point P is related to the energy path function. In particular, it is related to the point, x_∞ such that the f function can be approximated by $f_\infty(x)$ (see Fig. 3.8).

In order to improve the throughput capacity, as well as its scalability, EHE-WSNs show an interesting trade-off in terms of sensor affordability and number of devices, such that a large number of devices relax the sensor requirements and vice-versa. On the one hand, high-end sensors equipped with large energy storage

units and high energy efficient transceivers can sustain the normal operation of the network, since these store larger amounts of energy and to reach further distances by transmitting signals with more instantaneous power. As a result, deploying high-end sensors would shift the intersection point P between bounds towards low values of number of nodes. On the other hand, deploying a very large number of inexpensive devices can sustain the normal operation of the network. In this case, nodes are located closer to each other, thus requiring a significantly lower amount of energy to enable communication among them, which can be stored in a smaller energy buffer.

Throughput Capacity of Over-dimensioned Sensors

Over-dimensioned sensors show similar performance than ideal energy harvesting sensors for small number of deployed sensors. However, we observe that the throughput capacity stops being scalable when the number of sensors is greater than a given point (denoted as Q in the figure). The intersection point Q depends, among many other factors, on the power losses which become non-negligible. Intuitively, when the number of sensors increase, the distance between neighbors is reduced. Then, the required power to reach the next hop becomes very small and the power losses associated to a data transmission (e.g., turning ON and OFF the transmitter) become noticeable.

In order to improve the throughput capacity and its scalability, EHE-WSNs show an interesting trade-off in terms of circuit design and protocol complexity. On the one hand, designing high-efficiency circuits and reducing leakage and standby power losses make their associated power losses to become noticeable for reduced required power. This shifts the intersection point Q between bounds towards larger number of nodes. On the other hand, the throughput scalability can be improved through avdanced protocol design: first, optimized MAC scheduling may reduce standby power losses by implementing accurate duty-cycled transmissions [97] or by implementing wake-up radio protocols [63]; second, we find that optimal routing differs from shortest path in over-dimensioned sensors. That is, we find that the optimal number of hops cannot arbitrarily grow with the number of deployed nodes. Instead, this becomes a fixed value, which is independent to the number of deployed nodes. In this context, optimal routing design, imposes that each hop skips an optimal amount of intermediate relaying nodes making

the distance between relaying hops to be independent of the distance between nodes, and thus the overall number of nodes. By finding the optimal distance between relaying nodes constant throughput scaling (i.e., $O(1)$) can be achieved (see Sec. 5.C). That is, a wireless network powered by energy harvesting can undefinitely scale with the number of nodes, without showing any improvement in the overall throughput.

4.5.3 Upper Bound in Throughput Capacity for an Over-dimensioned Node

In this section, we aim to provide a bound in throughput capacity for over-dimensioned nodes. To do this, we find that the constraints imposed by these devices alter the number of relaying nodes between a source-destination pair. As such, the distance between hops and traffic carried by a sensor must be recalculated.

Let us consider that a node s_S intends to transmit a data packet to the destination s_D located at a distance D_i. Then, let us assume that the amount of deployed nodes between the s_S and s_D pair of nodes is massively large [18] and equals to N_R. We find that the optimal number of hops N_O is fixed and independent to the overall number of intermediate nodes.

Provided that the optimal route must guarantee the least energy consumption, we find that finding the number of hops becomes a linear optimization problem that can be formulated as:

$$N_O = \arg\min_{N_h} \sum_{i=1}^{N_h} E_R(D_i/N_h) \tag{4.25}$$

where N_h refers to number of hops, E_R is the required energy to forward a data packet, which depends on the distance between hops, $d = D_i/N_H$.

In order to illustrate this equation, let us particularize this equation for the following link budget model:

$$E_R(d) = E_0 + E_C(d) = E_0 + E_{C0} g_0 d^{\alpha}, \tag{4.26}$$

where E_0 refers to the standby losses for transmitting a data packet, E_{C0} refers to

the required energy to be received at the receiver end, g_0 stands for the channel attenuation at a distance of 1 m, d is the distance between nodes and α stands for the path-loss exponent.

We find that the optimal number of hops, N_O can be easily obtained by differentiating (4.25) and equalizing to zero. This shows that the optimum number of hops does not depend on the overall number of nodes. Particularly, the optimal number of hops is determined to:

$$N_O = D_i \sqrt[\alpha]{\frac{E_{C0} g_0}{E_0}(\alpha - 1)}. \tag{4.27}$$

Then, substituting the distance between hops, $d = D_i/N_O$ in the link capacity of the nodes and the number of hops, N, by N_O from (4.10), we have:

$$r_{ij}(D_i/N_O) \leq r(n)N_O. \tag{4.28}$$

which does not depend on the number of deployed nodes. As such, we find that the per throughput capacity of over-dimensioned senors is upper bound by

$$O(1). \tag{4.29}$$

4.5.4 Discussion

In this section we have addressed three particular case examples, namely an ideal, a miniaturized and an over-dimensioned operation. We find that these three cases cover a great part of possible non-idealities of the sensor nodes, and show interesting trade-offs in terms of hardware affordability, number of deployed nodes and protocol complexity.

Actual nodes powered by energy harvesting techniques will show an energy path function which depend on many factors. As a result, the eventual characterization of a given set of nodes will combine the addressed case examples. This will show a throughput scalability which will depend upon the number of deployed nodes.

We find that the throughput capacity and its scalability can be improved by means of deploying nodes with improved hardware design. However, redesigning these system components is often rendered unfeasible, as it increases the monetary

costs of the network planning, it is time consuming and it may require replacing all the deployed nodes. Instead, this work shows that small-size, inexpensive nodes can be deployed over a networking area and achieve similar performance than expensive nodes by simply deploying additional nodes in the network and designing optimal approaches at the routing layer.

4.6 Summary and Conclusion

In this chapter, the bounds for throughput capacity of energy-harvesting-enabled wireless sensor networks have been studied. These bounds set an important guideline for feasibility and deployability during the design process of a network powered by energy harvesting. It has been shown that for such networks these bounds coincide with the bounds in power constrained networks when the energy conversion is ideal. However, non-ideal factors during the energy acquisition and buffering can alter the scalability of such networks, making them less resilient to node failure or even non-scalable. This chapter has overviewed the main factors which affect the proper scalability of these networks and motivates a joint network deployment and sensor co-design in order to guarantee a successful operation of energy harvesting powered wireless sensor networks.

Chapter 5

Design Space Exploration of Multi-Source Energy Harvesting

5.1 Introduction

In the previous chapter, a thorough analysis on the scalability of the network has been provided. For this, a homogeneous energy field with no slow-temporal evolution has need to be been considered. However, as provided in Chapter 2, the available energy at the close environment of the sensor shows a temporal correlation, causing the energy state at the sensor to be time-varying.

Accordingly, the energy buffer (e.g. a supercapacitor or a battery) is constantly charging and discharging in a random manner [23]. For this reason, one of the main challenges in the design of such devices lies in the dimensioning of both the energy harvesting and energy buffer units [23]. Considering both subsystem units to be sufficiently large solves undesired interruptions during the normal operation of the sensor and, accordingly, on the wireless network. However this comes at the cost of precluding desirable miniaturization of the sensors, caused by the relatively small power densities of existing ambient energy sources and low energy density of energy buffers [128, 112]. As an example, in order to harvest 0.2 mW vibrational energy and to store 1 J of energy, an energy harvester of approximated 1 cm^2 and an energy buffer of approximated 2 cm^3 would be required.

Recently, multi-source energy harvesters are gaining interest as a robust alter-

native to power wireless sensors [8]. To implement multi-source energy harvesters, there appear two feasible approaches. On the one hand, these can be implemented through platforms which combine a few number of energy harvesters, each devoted to each source of energy [8, 108, 141]. On the other hand, self-tunable approaches permit tuning their oscillating frequency, therefore enabling multi-band capabilities to harvest energy from multiple energy sources [38, 67].

These platforms are more robust than the single-source ones. Indeed, if a certain energy source renders unavailable for a certain time period, due to the time asynchronicity among energy sources the sensor node can still maintain its normal operation. An additional, but less explored, advantage of heterogeneous multiple-source energy harvesters, which aids the miniaturization of the sensor nodes, is that when the ambient energy presents large temporal variations (i.e., the harvested power randomly varies over a wide range during time) the combination of multiple statistically independent energy sources lowers the sparsity of the overall energy which is harvested. This causes that devices, which are powered by multi-source energy harvesters show lower outage probabilities in contrast to single-source configurations. Equivalently, the requirements in terms of energy buffer capacity can be relaxed while maintaining the same performance. As an example, Fig. 5.1 shows three wireless motes that implement one, two or four energy harvesters which occupy the same overall area, in a chip-like planar implementation.

In this chapter, we first analyze the need of proper battery dimensioning and its impact over the energy outage probability. Then, we motivate the use of multi-source energy harvesters and derive and derive a model to characterize the overall occupied area by both the energy harvesting and the energy buffer units. On top of these results, we explore the capabilities of self-tunable energy harvesters as a feasible alternative to multi-source platforms [38]. In this context, we evaluate their performance in terms of harvested power and compare it to the performance of multi-source energy harvesting platforms. Finally, we address the spatial correlation between nodes, by characterizing the expected energy state.

This framework shows that harvesting energy from multiple sources by using either multi-source platforms or self-tunable energy harvesters provides significant improvements in energetically sparse scenarios. These improvements, jointly considered with an optimal dimensioning of the energy buffer will pave the way to

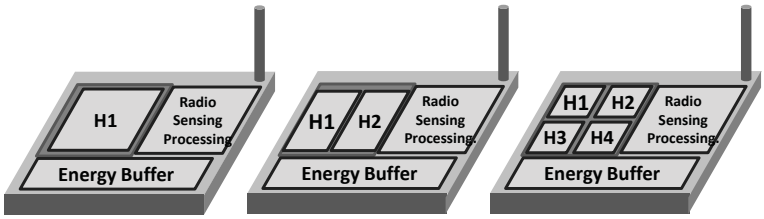

Figure 5.1: Architecture of a multi-source energy harvesting sensor. Increasing the number of sources reduces the efficient area for harvesting but maximizes the probability of finding an active energy source.

smaller energy management units and, therefore, actual miniaturization of eventual networking devices.

5.2 Sparse Energy Sources

Ambient energy is generally generated by the aggregation of an extensive number of physical entities which simultaneously radiate power [128]. Then, the random contribution of each entity, in both magnitude and time duration, entails a time-varying character in the aggregated power.

Accordingly, we refer to any physical phenomena which produces an aggregated power in a sparse, time-varying manner, such that this power cannot be known or estimated and the magnitude of the instantaneous power falls within a wide range, as a sparse energy source. In fact, sparse energy sources are present in a wide variety of physical phenomena. Among others, acoustic energy, mechanical, vibrational or RF energy [143, 141, 52] are considered representative examples of such sources, when considering a large time scale.

In this work, we propose the peak power to average power ratio as a metric to enable the comparison of performance of ambient energy sources. This metric is given by:

$$C = \frac{P_{peak}}{P_H}, \tag{5.1}$$

where P_{peak} is the average peak power and P_H refers to the average harvested power. Fig. 5.2 shows examples of two random energy sources with different peak power to average power ratio ($C = 8$ and $C = 3$). As it is shown, energy sources with large peak power to average power ratios are characterized by short

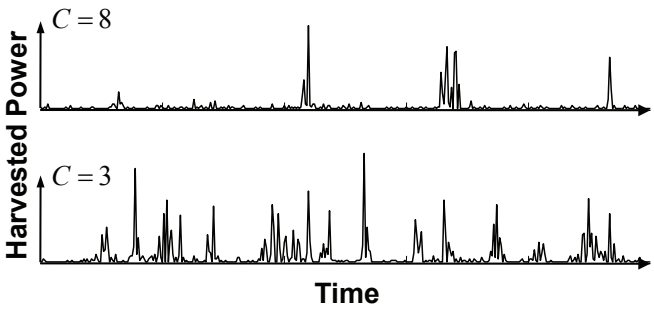

Figure 5.2: Harvested power from a sparse ambient source of peak power to average power ratio of (upper) $C = 8$ and (lower) $C = 3$.

but powerful bursts of energy, while leaving large inter-burst times where the available energy is far below the average value. On the contrary, energy sources with low values of this metric are characterized by being more constant and predictable.

5.3 Evaluation of the Energy Outage

In this section we evaluate the energy outage probability in terms of the utilization in Energy-Erlangs and the normalized energy buffer capacity.

In a real environment, the ambient energy is time-varying. This is, the actual harvesting rate slowly evolves with time in an unpredictable manner, within a wide range of orders of magnitude. As a result, the power which is being harvested at the node location is affected by deep fadings.

Given the large variety of ambient energy sources, in this section we focus on RF energy harvesting affected by multi-path propagation. It is well known that multipath propagation is a very common effect during the reception of RF power within an urban area. The multipath is defined as the propagation of an RF signal through two or more paths, giving as a result constructive or destructive interference and phase shifting. When the number of interferences is large and it is very environment-dependent, the received power is affected by the Rayleigh fading [117]. In general terms, this model is mainly characterized by a certain coherence time, t_c, or, equivalently, with the doppler frequency.

In Fig. 5.3 we show an example of the harvested power, $P_H(t)$ over time when assuming that the harvesting source is affected by the Rayleigh channel.

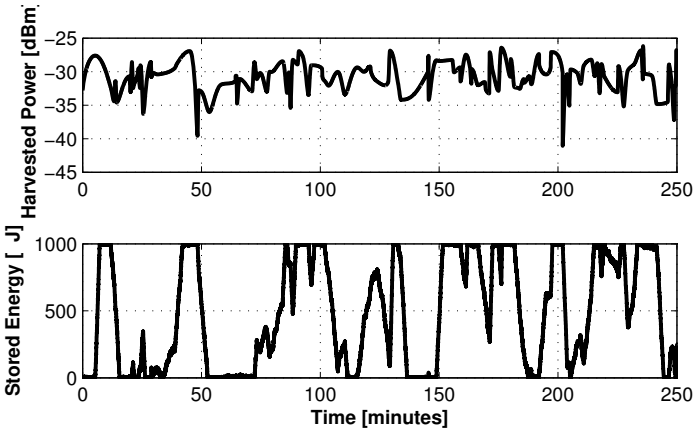

Figure 5.3: Model of the Rayleigh channel and evolution of the energy state at the sensor node.

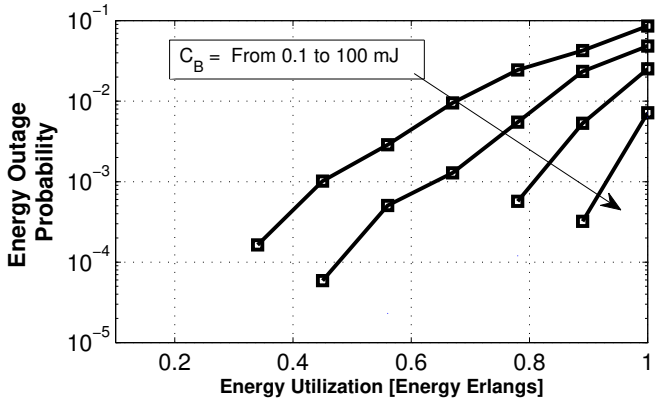

Figure 5.4: Energy outage probability assuming Rayleigh fading with coherence time $t_c = 10$ s as the slow dynamics in the energy harvesting power source. An average $P_H = 10$ μW and $E_C = 10$ μJ has been considered.

In addition, it is also shown a depiction of the energy state at the energy buffer of the sensor node. As it is shown, given the variation of the harvested power, the energy state is unable to reach a steady-state. On the contrary, deep fadings tend to completely deplete the energy buffer. Alternatively, when the multipath propagation provides constructive interference, the sensor node is able to store large amounts of energy.

Thus, in consideration of the multipath propagation, it is observed that the energy buffer does not only have to store enough energy to handle the random patterns of both communication and energy harvesting processes, but it also does have to be able to store large enough amounts of energy to overcome deep fadings in the harvested energy.

5.3.1 Energy Outage Probability

The lack of a steady state leads to evaluate the energy outage probability throughout event-based simulation of the negative-energy queue. In order to do so, we have assumed that the average energy harvesting rate, μ_H, evolves in time by following a Rayleigh distribution. The temporal evolution of μ_H is related to the coherence time, t_c. In Fig. 5.4 and Fig. 5.5, we show the results of the energy outage probability as a function of the energy utilization in Energy-Erlangs, for different values of the energy buffer capacity. In order to obtain these results, the average ambient power has been set to $P_H = 10$ μW and the energy per packet has been set to $E_C = 10$ μJ. As it is shown, the effect of the slow dynamics is clear. While in Fig. 5.5, an energy buffer of 200 μJ was enough to guarantee a $p_{out} < 10^{-2}$ for $\rho_E = 0.9$ E2, in this case, by assuming slow dynamics, we would now require an energy buffer of 5 mJ or 50 mJ to meet the same requirements for $t_c = 10$ s and $t_c = 100$ s respectively.

As we would expect, the most critical situation refers to an energy utilization of $\rho_E = 1$ E2. That is, the communications unit requires the whole amount of energy which is harvested. As it is shown in the previous figures for both dynamics, this case has for any energy buffer capacity the worst energy outage probability. In Fig. 5.6, we show the energy outage probability of the sensor node in terms of the energy buffer capacity. As it can be observed, by increasing the size of the buffer, the node is able to temporarily store more energy to satisfy the

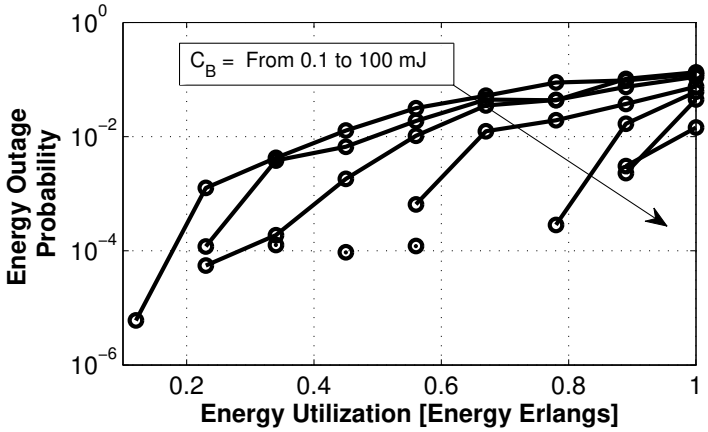

Figure 5.5: Energy outage probability assuming Rayleigh fading with coherence time $t_c = 100$ s as the slow dynamics in the energy harvesting power source. An average $P_H = 10$ μW and $E_C = 10$ μJ has been considered.

energy requirements for larger fadings. It is found that the relation between the buffer size and the energy outage probability follows an exponential relationship.

5.3.2 Average Time to Energy Outage

Another relevant parameter which is set as a metric for design and dimensioning of energy buffers is the average time to energy outage. This metric evaluates the average time it takes for the node to fail in the communication due to energy outage. This time has large implications in the network protocol designs, such as routing. As an example, when a node is temporarily disconnected from the network, any existing route which would go through this node must be reassigned to neighboring nodes. Then, a larger average time to the energy outage represents a reduction in the network reconfiguration, and thus it represents a reduction in communication, control and energy overhead. In fact, a similar concept in battery-powered WSNs is defined. The network lifetime in a WSN is defined as the time it takes for any node to deplete its battery, thus causing an alteration in the network topology.

In figures 5.7 and 5.8 we show the average time to energy outage as a function of the energy utilization in Energy-Erlangs, for different values of the energy buffer capacity, considering a coherence time of $t_c = 10$ s in Fig 5.7 and a coherence

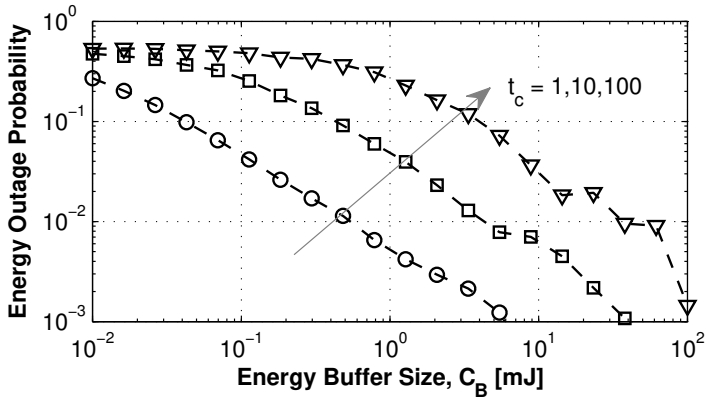

Figure 5.6: Dependency of the energy outage probability in terms of the energy buffer size. It is represented for three different coherence times of the energy source: 1, 10 and 100 seconds.

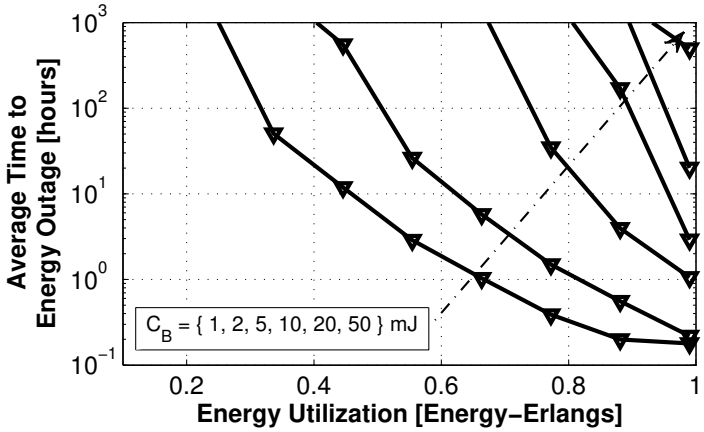

Figure 5.7: Average time to energy outage assuming Rayleigh fading with coherence time $t_c = 10$ s.

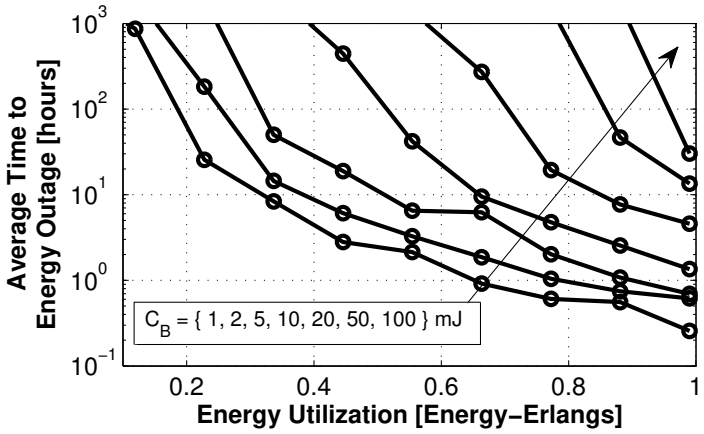

Figure 5.8: Average time to energy outage assuming Rayleigh fading with coherence time $t_c = 100$ s.

time of $t_c = 100$ s in Fig 5.8. In order to obtain these results, we have set the same parameters as in the evaluation of the probability of energy outage. As it is shown, the average time to energy outage rapidly decreases as the energy utilization tends to one. On the contrary, this time increases rapidly for larger energy buffer capacity, thereby establishing a relevant design guideline.

In addition to this, for a better understanding on the dependence of the energy buffer capacity on the average time to energy outage, we show in Fig. 5.9 this average time as a function of the energy buffer for a coherence time of $t_c = \{10, 100, 1000\}$ s. As it is shown, channels with large temporal correlation need larger energy buffers in order to overcome long deep fadings. Interestingly, it is observed that for small sizes of the energy buffer, the average time to energy outage tends to the coherence time. However, as the energy buffer capacity is increased, the average time increases faster for those environments with smaller t_c.

5.4 Multiple Source Energy Harvesters

Multi-source energy harvesters are able to combine the energy from multiple energy sources. This reduces the chances that the sensing system is in a deep energy fading, where it is not able to harvest energy for a significant amount of time, since whenever an energy source is faded, any other energy source can

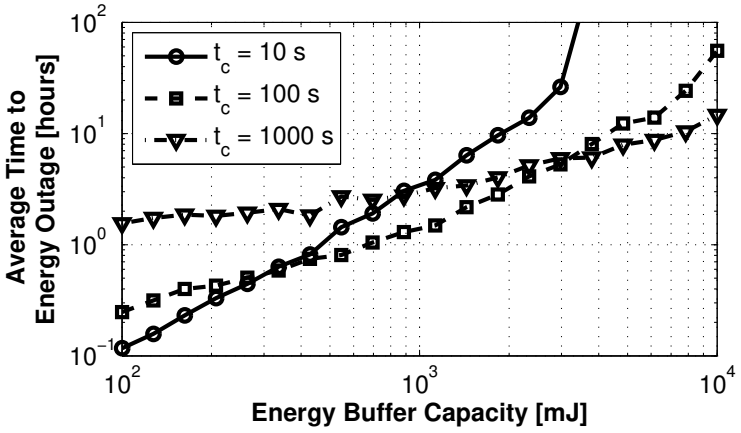

Figure 5.9: Average time to energy outage assuming Rayleigh fading with coherence as a function of the energy buffer capacity.

be supplying energy. In other words, combining independent energy sources, the sparsity of the overall process is reduced and thus the energy fadings are potentially reduced, as well. In this section we provide a model for multi-source energy harvester platforms and we evaluate the improvement on performance that using multiple energy harvesting platforms has when contrasted to single harvester platforms.

5.4.1 Performance of a Multiple Source Energy Harvester

We have considered an average communications rate of $\lambda_c = P_C = 100$ μW. Then, we have considered each negative energy packet to be of 10 μJ. Finally, we have set the overall harvesting rate $N\mu_H = P_H = P_C/\rho$, where ρ_e has been set as an evaluation parameter. Therefore, each harvester harvests an average power of $P_C/\rho_e N$. These energy harvesting rates can be achieved by means of vibrational harvesters [128].

In order to generate the sparse energy sources, we have approximated the ambient energy by a random process generated by exponentially distributed energy bursts of power $P_H C/N$, with an inter-burst time of $0.1/C$ seconds. An exponentially distributed random process has been chosen as it presents the largest entropy, thus estimating the worst case [143].

Fig. 5.10 and Fig. 5.11 compare the improvement over p_{out} that using multiple harvesters has as a function of the energy buffer capacity, C_B, for a peak power

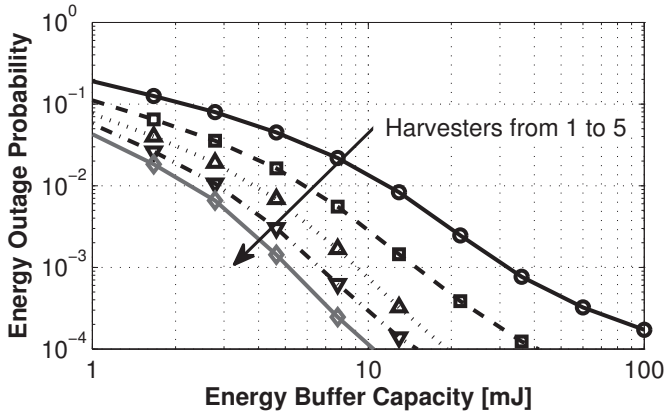

Figure 5.10: Energy outage probability as a function of the energy buffer capacity. $\rho_E = 0.9$ E2 and $C = 10$.

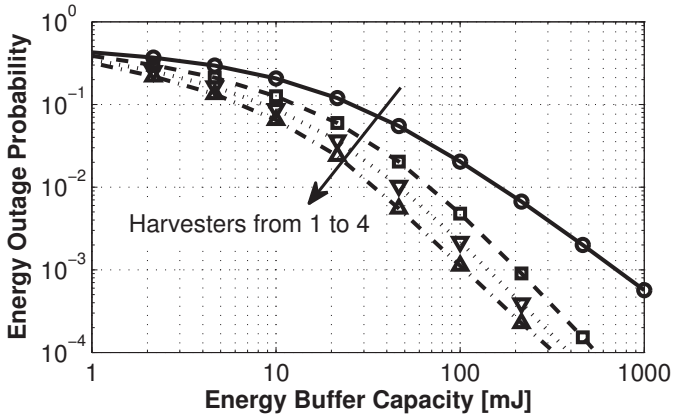

Figure 5.11: Energy outage probability as a function of the energy buffer capacity. $\rho_E = 0.9$ E2 and $C = 100$.

to average power ratio of $C = 10$ and $C = 100$ respectively. These results have been obtained by assuming in the negative energy queue model $\rho_e = 0.9$. As it is shown, there is a clear improvement, since varying from one to five harvesters, the energy buffer capacity can be reduced from 30 mJ to just 5 mJ and from 600 mJ to just 100 mJ, while still maintaining $p_{out} < 10^{-3}$.

In addition to this, Fig. 5.12 and Fig. 5.13 compare this improvement as a function of the ρ_e for peak power to average power ratios of $C = 10$ and $C = 100$ respectively. In order to obtain these results, the energy buffer capacity has been set to $C_B = 10$ mJ in Fig. 5.12 and to $C_B = 100$ mJ in Fig. 5.13. As it is shown, multi-source energy harvesters are able to provide similar performance, but at

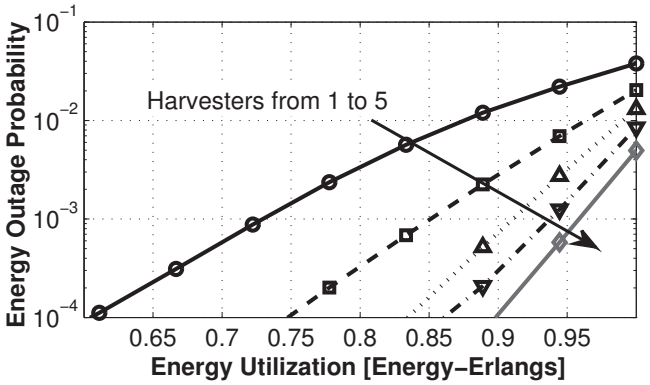

Figure 5.12: Energy outage probability as a function of the energy utilization. $C_B = 10$ mJ and $C = 10$.

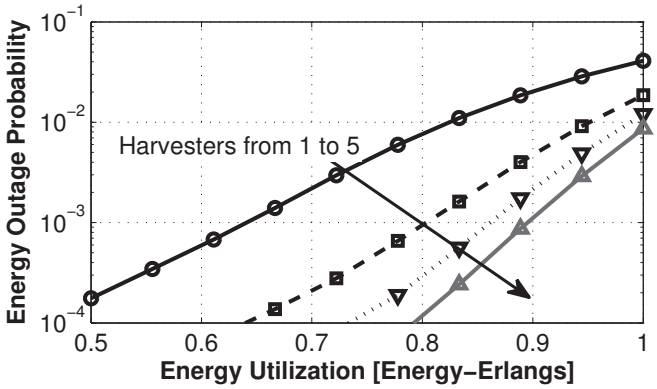

Figure 5.13: Energy outage probability as a function of the energy utilization. $C_B = 100$ mJ and $C = 100$.

larger ρ_e values and, therefore, requiring smaller energy harvesting area.

As a result, we observe that multi-source energy harvesters can help reducing both the energy buffer capacity, as well as the energy harvesting requirements, while still providing the required performance.

5.4.2 Circuit Area Model

As seen in the previous section, additional energy harvesters have a positive impact upon the performance. Nonetheless, this technique produces a non-negligible area overhead, since each energy harvester requires some additional circuitry and separation space.

An additional compromise is that low values of ρ_e help reducing the energy

buffering capacity at the cost of proportionally increasing the energy harvesting requirements.

These compromises motivate a framework for circuit area optimization which considers the user-defined requirements, the area overhead of multiple harvesters and the energy buffer capacity. In order to do so, we first relate the required power, harvesting power, number of harvesters and energy buffer capacity which are able to achieve the required performance in energy outage probability, through the energy model presented in Sec. 5.4. Afterwards, this is translated into circuit area by means of the following model.

We then define the overall area of the system as:

$$A_{TOTAL} = A_H + A_B + A_A, \tag{5.2}$$

where A_H refers to the area of the harvesting unit, A_B stands for the area of the energy buffer unit and A_A is the area of the applications units (i.e., processing, sensing and communications unit). In particular, since A_A is fixed and provided by a certain application, A_A is not considered in the following circuit area optimization.

Area of the Energy Harvesting Unit

The area of the harvesting unit depends on mainly two factors, the number of energy harvesters and the power that these aim to harvest. As shown in [128], the ambient power is generally characterized by a given power density. As such, the overall area is expectedly proportional to the desired power to be harvested. Alternatively, integrating more than one energy harvester requires additional circuitry, which increases the eventual size of the unit. In this work, we linearly approximate the area of the energy harvesting unit in terms of the number of energy harvesters and desired power rate:

$$A_H = A_{H0} + A_{HN} N_H + A_{HP} P_R / \rho_e, \tag{5.3}$$

where A_{H0} refers to a constant area, A_{HN} to the partial contribution of A_H with respect to the number, N_H, of energy harvesters and A_{HP} to the partial contribution of A_H with respect to the required power P_H.

Table 5.1: Values used in the Optimization Framework

Parameter	Value	units
A_{H0}	0.01	cm^2
A_{NH}	.01	cm^2
A_{NP}	6.66	$\text{cm}^2\ \text{mW}^{-1}$

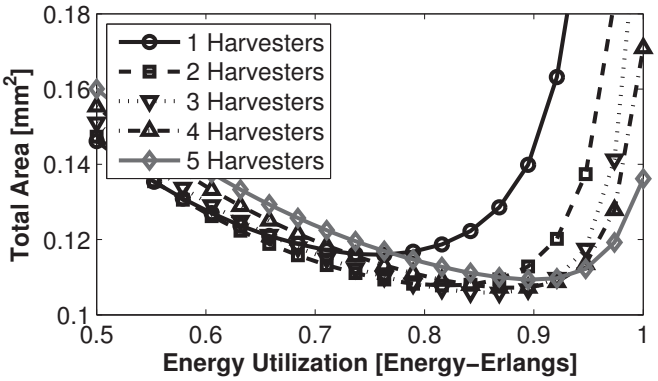

Figure 5.14: Overall area in terms of the Energy Utilization. $C = 10$.

The considered values in this works are shown in Table 5.1. These correspond to reasonable values that have previously been reported [128].

Area of the Energy Buffer

In line with recent advancements in energy buffering [112], each technology presents an associated energy density. In this context, we have considered consistent values for this density of $D_B = 2\ \text{J/cm}^3$ and a fixed height of 1 cm. Similar to A_H, we may linearly approximate the overall area of the energy buffer as:

$$A_B = A_{B0} + C_B D_B, \tag{5.4}$$

where A_{B0} is a fixed area overhead and C_B is the required capacity of the energy buffer in mJ units.

5.4.3 Evaluation of the Area Model

In order to optimize the area, we have simulated the wireless sensing system through the same energy model as described in the previous sections. Then, we

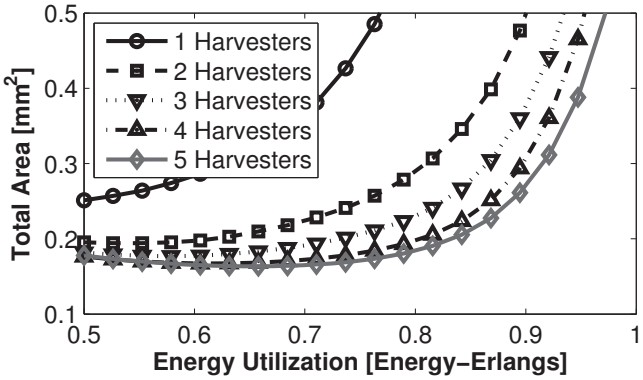

Figure 5.15: Overall area in terms of the Energy Utilization. $C = 100$.

have assumed a tolerable performance of a wireless device, when its energy outage probability is below $p_{out} = 10^{-4}$.

We show in Fig. 5.14 the overall occupied area for the joint energy harvesting and energy buffer unit, such that the user defined requirements in terms of output power and energy outage probability are met. This area corresponds assuming that the environmental energy is characterized by a peak power to average power ratio of $C = 10$. As it is shown, the overall area is shows an optimal minimum for $\rho_e = 0.87$ E2. This is due to the fact that for fixed values of power requirements, a large energy utilization ratio reduce the amount of harvested energy, therefore reducing the size of the energy harvester. However, this reduction of the energy harvester comes at the price of increasing the size of the energy buffer.

Similarly, Fig. 5.15 shows the results of the circuit area optimization when considering the same system requirements, but assuming a peak power to average power of $C = 100$. As it is shown, an increase in this ratio enlarges the size of the overall area, regardless of the number of energy harvesters and their operation point. This increase is caused by the fact that the sensing system runs on the stored energy for a longer time. In this case, it is found that increasing the number of energy harvesters shows a significant benefit, since the sparsity of the energy is reduced. In particular, the minimum area is found at a $\rho_E = 0.66$ E2, considering five energy harvesters. The outcomes of this design, which are required for the energy harvesting unit and an energy buffer to minimize the area can be found in Table. 5.2 for both cases.

Table 5.2: Component requirements

C	**Parameter**	**Value**	**Units**
10	Harvesters	4	—
	Area Harvester (total)	7.7	mm^2
	P_H (each)	27.7	μW
	Area Energy Buffer	3	mm^2
	Capacity Energy Buffer	15	mJ
100	Harvesters	5	—
	Area Harvester (total)	8.3	mm^2
	P_H (each)	40	μW
	Area Energy Buffer	5	mm^2
	Capacity Energy Buffer	25	mJ

5.5 Self-tunable Multi-band Energy Harvesters

In case that the considered energy sources are of the same type and the differences among them is that each is produced at a different frequency band, self-tunable energy harvesters emerge as an encouraging alternative to multi-source platforms. These devices have the property of tuning their oscillating frequency over a wide range to adapt it to the frequency band of the harvestable energy [38].

This technology aims to provide a much higher performance compared to independent multi-source platforms in cases where the ambient energy is very sparse and the frequency bands are uncorrelated to each other. In this case, a single energy harvester can generate more power than small energy harvesters. However, this improvement compared to multi-source platforms is not always achieved because of two main reasons. On the one hand, when the different bands generate power simultaneously, self-tunable energy harvesters can only tune a one of the frequencies, thus disregarding the other bands. On the other hand, a similar concept to cognitive-radio communications [16], these devices must implement spectrum sensing techniques to detect which frequency band generates a larger amount of power, therefore requiring power to generate power.

To exemplify this, consider the time diagram shown in Fig. 5.16. In the figure, two IoNT platforms (one equipped with a multi-source platform, and one equipped with a self-tunable harvester) harvest power from bands #1 and #2. We consider that both platforms integrate an energy harvester of the same overall occupied area. Therefore, the self-tunable energy harvester integrates a

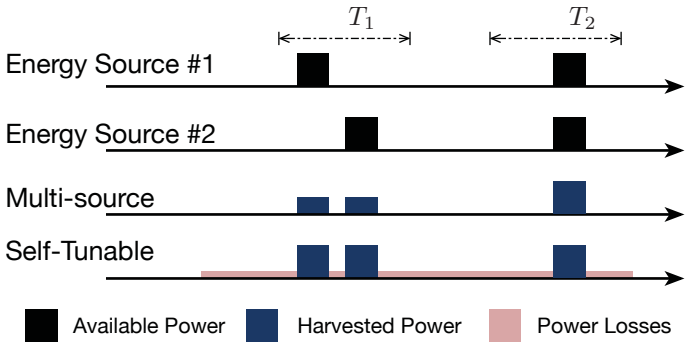

Figure 5.16: Comparison between multi-source and self-tunable platforms.

single energy harvester which can select the operating frequency band, whereas the multi-source energy harvester is divided by two energy harvesters, one for each frequency band. Then, we observe that during the time T_1 both energy sources generate power at different times, whereas during T_2 the energy sources simultaneously generate power. As a result, the self-tunable energy harvester shows potential improvement during T_1 since it can harvest twice power, whereas the multi-source platform scavenges more energy during T_2 since both harvest the same amount of power while this does not requires to spend power in sensing the environment.

In this section we provide a generic model for a self-tunable energy harvester and provide compare their performance to multi-source approaches as a function of critical factors which affect their performance.

5.5.1 A Self-tunable Energy Harvester

We show a generic model block diagram of a self-tunable energy harvester in Fig. 5.17. This is composed of four sub-units, namely the broadband sensor, harvester, energy harvesting front-end and tuning circuit. As the figure shows, the harvester is the only sub-unit which generates power, whereas the remaining units require power to realize their operation. We define the net harvested power as the net contribution of power generated by the harvester, broadband sensor and tuning circuit:

$$P_H = \eta P_{EH}(t, B) - P_B - P_T \tag{5.5}$$

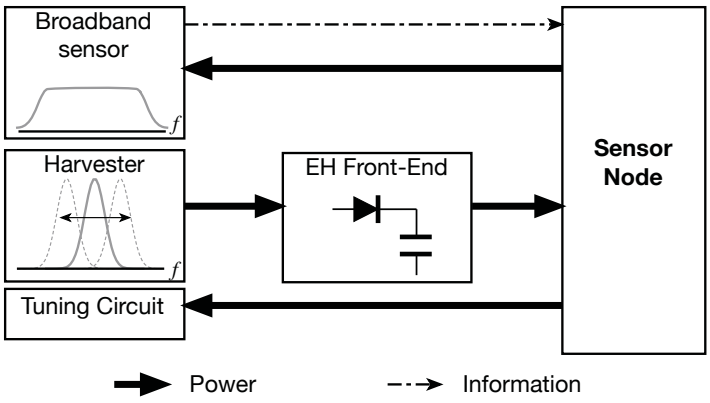

Figure 5.17: Generic block diagram of an energy harvesting powered device that employs a self-tunable energy harvester.

where η stands for the efficiency of the EH front-end , P_{EH} is the power generated in the harvester sub-unit, which is tuned at the band B, P_B refers to the required power from the broadband sensor to operate, P_T stands for the power which is consumed in the tuning circuit. As it follows we briefly describe the operation of each unit.

Harvester

The tunable energy harvester stems as the key element in the energy harvesting unit. This is the only component which generates energy by converting environmental energy into electric current. This component has tunable properties, i.e., its oscillating frequency can be modified by adjusting its electrical parameters. Provided that this component generates energy, there is a direct relation between its occupied area and the power that it is able to harvest. As such, it is desired that this component occupies the largest area allocated for the energy harvesting unit. The harvested power is given by:

$$P_{EH}(t, B) = (S(t) * h(t, B))\, A_{eff}, \tag{5.6}$$

where S is the spectral power density of the available energy source, in power/area units, $h(t, B)$ stands for the transfer function of the harvester, which is tuned to the band B, and A_{eff} refers to the effective area of the harvester.

Broadband Sensor

In order to choose the optimal oscillating frequency of the energy harvester, a broadband sensor is integrated to detect most powerful band.These devices show remarkable properties to detect oscillations at a significantly wide frequency range. Unfortunately, they cannot be used as energy harvesters. As it is shown in Fig. 5.17, this unit requires a supply power to operate and to reports the sensed information. The sensing system must integrate spectrum sensing tools to process this information to decide whether to re-tune the harvester. The power consumed by this unit, P_B is assumed constant during the normal operation of the device.

Tuning Circuit

This circuit accommodates the natural frequency of the energy harvesting depending on the processed results retrieved by the sensed data of the broadband sensor. The basic element of this circuit is a capacitor. By selecting a capacitor voltage, V_C, the natural frequency of the energy harvester is tuned to a different frequency. Recent studies show approximately linear dependency between the frequency and this voltage [38]. As such, the tuned band B is selected according to:

$$B = kf_0V_C, \tag{5.7}$$

where k is a given constant, f_0 is the center frequency of the harvester and V_C refers to the capacitor voltage Provided that the number of bands depends on the capacitor voltage, switching to additional bands requires additional voltage levels. Unfortunately, charging a capacitor to a higher voltage has an associated quadratic loss of energy. Accordingly, the energy required to switch from one band to another is given by:

$$E_{sw} = \frac{1}{2}C(\Delta V_C)^2 \tag{5.8}$$

where ΔV_C refers to the difference between voltage levels.

Energy Harvesting Front-End

This unit is in charge of adapting the power which is generated by the energy harvester to generate a DC current which is delivered to the energy buffer and the remaining sub-system units of a wireless sensing system. As a result of this power processing operation, the actual power which is delivered to the device is always lower than the produced by the energy harvester [23]. This is generally referred as the efficiency of the energy harvester.

5.5.2 Performance Evaluation

We evaluate the performance of a self-tunable energy harvester in terms of the average power which is able to generate. For this, we consider the energy balance at the energy harvester by calculating the generated power and the power losses derived from sensing the spectrum and retuning the harvester.

To derive the generated power, we have assumed that a self-tunable energy harvester occupies the same area as the optimized case in multi-source energy harvesting platforms and is able to generate the same power. Alternatively, we have assumed that the power that the energy harvester consumes to sense the spectrum, to process this information and to tune the oscillating frequency of the energy harvester, referred as P_{loss}, quadratically depends on the voltage range applied, V_C, to an equivalent capacity of $C_{eq} = 1$ μF, which is a reasonable value as reported in [38]. The voltage applied at the capacitor linearly depends to the number of frequency bands, as shown in (5.7).

We show in Fig. 5.18 the harvested power as a function of the peak power to average power ratio, C, for different number of available bands. In addition, we compare the results to the multi-source energy platform which has been optimized in the previous section for $C = 10$ with 4 energy harvesters. In order to calculate these results, we have considered that the voltage difference to tune between consecutive bands is 0.5 V. As the figure shows, when the peak power to average power ratio increases, the power of the energy sources is more compacted in time. Then, the likelihood that two energy sources are generating power at the same time is reduced. This permits the energy harvester to maximize the harvestable energy, thereby showing a better performance than multi-source energy harvesters. However, as this factor becomes large, the energy devoted to perform

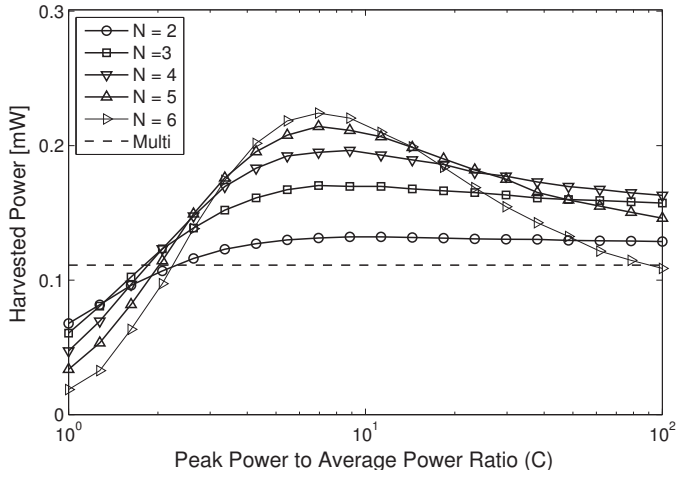

Figure 5.18: Harvested power as a function of the peak power to average power ratio in self-tunable energy harvesters.

spectrum sensing and tuning the oscillating frequency gains significance, thus negatively impacting upon the performance of the energy harvester. In addition, it is observed that the number of frequency bands plays an important role in the performance of the energy harvester. In fact, considering more energy bands improve the likelihood of a given band being active, but significantly increases the power losses.

We then show in Fig. 5.19 the harvested power as a function of the applied voltage at the equivalent capacitor. In addition, we compare the results to the multi-source energy platform which has been optimized in the previous section for $C = 10$ with 4 energy harvesters. To calculate these values, a peak power to average power ratio of $C = 10$ has been assumed. As it is shown, the applied voltage has a very strong impact upon the performance of the energy harvester. In fact, as this voltage approaches zero, increasing the number of bands can provide a very large improvement compare to multi-source energy harvesting platforms. As an example, using a self-tunable energy harvester to harvest from 4 bands generates almost 3 times the energy that an optimized multi-source energy harvester with the same number of bands. However, as the required capacitor voltage increases, the performance of the energy harvester is being affected, therefore showing equal performance at a capacitor voltage of approximately $V_C = 0.65$ V. This shows the need of sophisticated sensing schemes to minimize the power consumption.

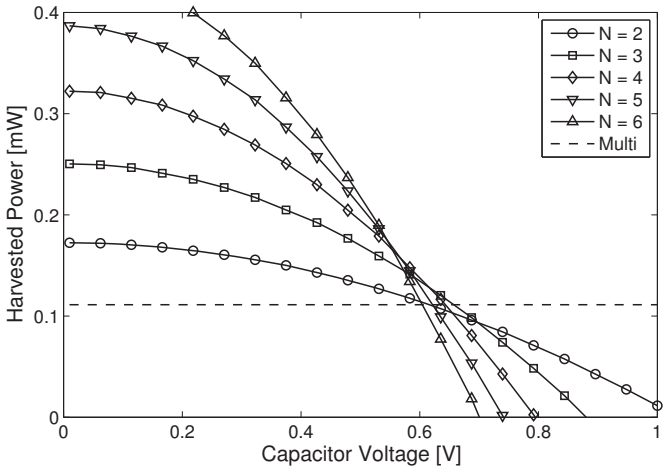

Figure 5.19: Harvested power as a function of the capacitor voltage in self-tunable energy harvesters.

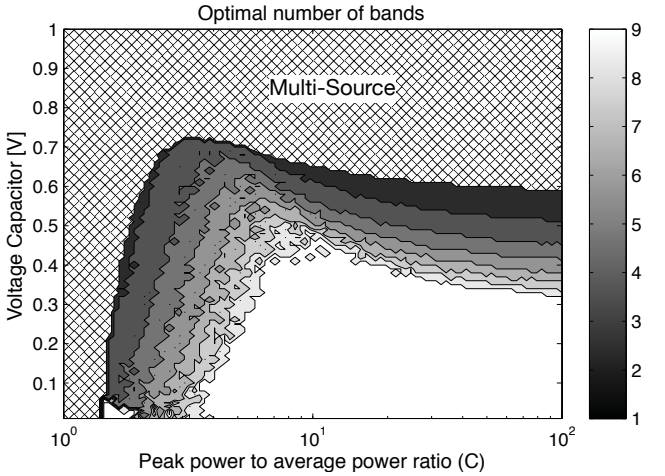

Figure 5.20: Design space of self-tunable energy harvesters. Optimal number of bands as a function of the capacitor voltage and peak power to average power ratio.

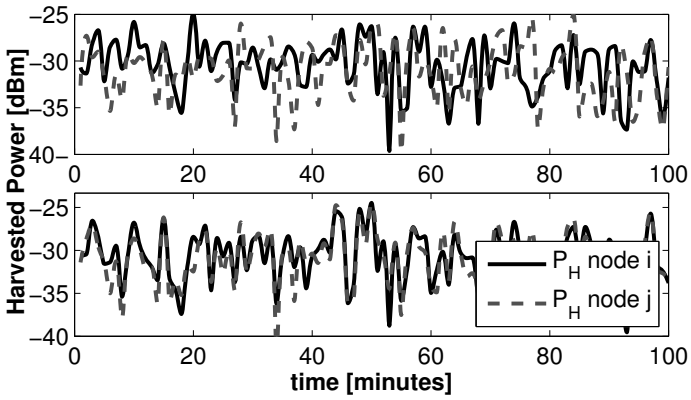

Figure 5.21: Correlation of the ambient energy: comparison of the harvested power in two neighboring nodes with spatial correlation $\rho_d = 0.155$ (top) and $\rho_d = 0.844$ (bottom).

Finally, we optimize the number of bands of a self-tunable energy harvester as a function of the peak power to average power ratio and capacitor voltage in Fig. 5.20. In addition, this performance is compared to the performance of multi-source energy harvesting platforms. As the figure shows, regardless of the associated power losses of the energy harvesting unit, multi-source energy harvesting platforms outperforms self-tunable harvesters, in terms of outage probabilities, for moderately low values of C. Then, as this parameter increases, the effect of the capacitor voltage becomes significant. In particular, it is observed that low number of bands show more robust performance in terms of both studied parameters, whereas considering a large number of bands require low capacitor voltages and large peak power to average power ratios.

5.6 Spatial Correlation of the Energy State

In previous sections, the energy outage has been addressed for just a single sensor node. It has been assumed that the sensor node can transmit any time it has enough energy to transmit. Intuitively, in order to successfully deliver a data packet from the node i to the node j, not only the transmitter node must be energetically charged, but also the receiver must be active.

In this section, we evaluate the correlation of the energy outage probability of neighboring nodes. In order to do so, this work accounts for the spatial correlation

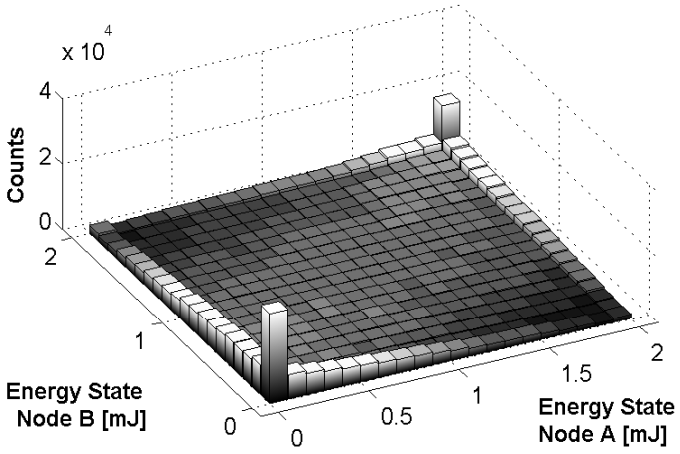

Figure 5.22: Energy state correlation between two nodes, for a correlation factor of $\rho_d = 0.4$.

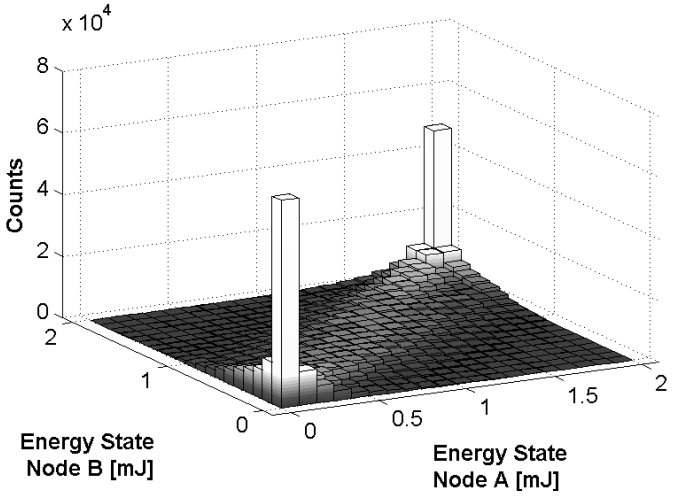

Figure 5.23: Energy state correlation between two nodes, for a correlation factor of $\rho_d = 0.9$.

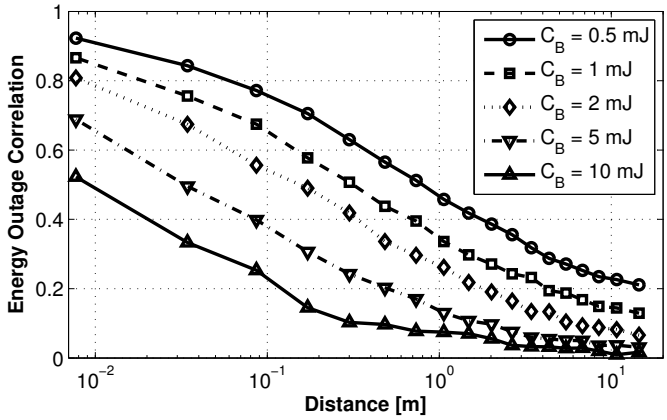

Figure 5.24: Correlation of the energy outage probability in terms of the correlation among sensor nodes.

of the energy field. The spatial correlation, ρ_d, defined as a function of the distance between nodes can be simplified from (3.7), if considering only spatial variations by:

$$\rho_d(d) = \frac{E\left[P_H(\mathbf{r_i})P_H(\mathbf{r_j})\right] - \mu_H^2}{\sigma_H^2} \tag{5.9}$$

where $d = \|r_i - r_j\|$ refers to the distance between nodes i and j, and μ_H refers to the average power of the ambient energy source. The spatial correlation as a function of the distance is assumed to decrease monotonically with the distance and bounded to 1 when $d = 0$ and 0 when $d \to \infty$. This spatial correlation depends upon the physical phenomena, which can be generally classified into several groups [68, 11], e.g., spherical, power exponential, rational quadratic or *matérn*. As an example of physical phenomena, electromagnetic waves present a power exponential correlation function, with $\theta_2 = 1$ [139]. The exponential correlation function is given by:

$$\rho_d(d) = e^{(-d/\theta_1)^{\theta_2}}; \quad \theta_1 > 0, \theta_2 \in (0, 2] \tag{5.10}$$

In order to evaluate the correlation of the energy outage among neighboring nodes,we focus on a RF energy harvesting environment, where the correlation of the slow-dynamics of the harvesting energy between two locations is given by (5.10). Then, we use a Rayleigh channel model from Sec. IV. To evaluate this correlation, we proceed to simultaneously perform a time-varying simulation

of two neighboring nodes which harvest correlated RF power. Fig. 5.21 shows an example of the harvested power from two neighboring nodes when there is a spatial correlation of $\rho_d = 0.15$ (top) and $\rho_d = 0.85$ (bottom).

In Fig. 5.22 and Fig. 5.23, we show the bivariate histogram of the energy state of two energy harvesting enabled sensor nodes which present a correlation in their harvesting rates of $\rho_d = 0.4$ and $\rho_d = 0.9$. In order to obtain these results, an energy buffer capacity of $C_B = 2$ mJ has been chosen. As shown, the relatively small capacity of the energy buffer, leads to a noticeably large probability of energy outage. As it is also observed, as the correlation of the energy source decreases, the bivariate histogram the energy states spreads, thus becoming challenging to estimate the energy state of neighboring sensors.

In addition to this, Fig. 5.24 shows the probability that a certain node j is in energy outage, when it is known that the node i is already in energy outage. This probability is shown as a function of the distance, when considering the values of $\Theta_1 = 5$ and $\Theta_2 = 1$ in the correlation model shown in (5.10). As the figure shows, at short distances, if a node is in energy outage, neighboring nodes of this sensor node will probably be in energy outage as well. Alternatively, as the distance among nodes increases, this probability tends to the energy outage probability. Alike temporal variations of the slow dynamics, the energy buffer has a significant effect in counteracting the impact of the spatial distribution of the energy.

5.6.1 Applications of the Spatial Correlation

The correlation of the environmental energy and the energy state of the sensor nodes is of special interest for network designers. As an example, in the MAC-layer, sensors can increase the success rates in packet delivery in a point-to-point communication, since they can estimate whether the destination node has sufficient energy to receive the packet.

However, we expect that the majority of the benefits of this model will lay on the routing layer. State-of-the-art routing protocolss for energy harvesting include the energy state in their cost function [97, 53, 41]. With this, the network tries to avoid nodes which have significantly less remaining energy and, therefore extending the network operation. When considering spatially distributed energy

fields, routes bend to energetic networking areas [53]. This aims to balance the overall energy availability to the energy requirements.

Unfortunately, in order to optimize the routes in these environments, the network must take decisions upon the up-to-date energy state and energy availability of the sensors. As a result, this information must be constantly exchanged among nodes -or, even, reported to the base station (BS)- to generate the optimal solutions.

In this context, having knowledge of the spatial distribution of the ambient energy and the correlation among energy states can improve the network operation: on the one hand, sensor nodes can potentially take decisions on behalf of their neighboring nodes, thus suppressing the local exchange of overhead information. On the other hand, in case of reporting the energy state to a BS, the reporting overhead can be also reduced, since fewer nodes are required to report updated information.

5.7 Summary and Conclusion

Multi-source energy harvesting is gaining popularity as an alternative to power wireless sensor networks. The benefits that this alternative provides when the ambient energy is largely time-variant is two-fold: on the one hand, it provides robustness to the sensors, while on the other hand, the sparsity of the overall contribution is reduced, and thus its operation lifetime is improved. In this context, circuit area optimization which considers both energy harvester and energy buffer and takes advantage of the improvement in performance of multiple-source energy harvesters has been addressed. As it has been shown, this joint effort can help reducing the overall area, thus enabling circuit area optimization to pursue a future miniaturization of the communicating devices. In addition, the performance of self-tunable energy harvesters has been compared to an optimized multi-source energy harvester. Self-tunable harvesters have shown better performance especially when the presented environmental energy is very sparse. However, the operation of these devices require sensing and computing tasks to actively select the optimal energy band.

Chapter 6

Scalability of power of Multi-ET Wireless RF Power Transmission

6.1 Introduction

Wireless RF power transfer has transitioned from proof-of-concept deployments to commercial products over the recent years [113], indicating its feasibility in powering unattended Internet of Things (IoT). This approach consists of harvesting the RF radiation from controllable energy transmitters (ETs) to supply the power demands of the networked nodes [144]. Thus, this technology can impact the growing market for wearables, intra-vehicle charging, industrial safety sensors, among others.

The high path-loss of the RF signal in free-space constrains the range of the transmission of energy to relatively short distances (i.e., up to a few tens of meters) [138]. Hence, considerable efforts have been undertaken for extending the power transfer range to cover a large area of deployed nodes, within the limitations of the regulatory bodies (e.g., FCC) imposed maximum threshold on the transmitted power, ET hardware installation costs, and the specific capabilities of the transceiver system of the ETs [144]. One such viable direction involves using antenna arrays and directional antennas that allow harvesting energy from 60 μW of incident power, with the receiver placed a considerable distance away from the energy source (i.e., 4.1 km). However, this setup increases the dimensions of the antenna to a few tens of centimeters, since it requires a typical broadband

UHF TV antenna [122]. MIMO-based approaches, on the other hand, permit on-demand energy beam-forming, thereby reducing the energy spread [146]. However, despite these methods, multiple ETs may be needed to cover the entire area of interest leading to concerns of scalability [144].

This chapter aims at presenting wireless RF power transmission from multiple ETs as a feasible approach, by answering the following fundamental question: *In order to guarantee sufficient power at the deployed nodes, is it better to increase the number of ETs, to increase their transmitted power or to increase their system complexity?* For this, a scalability analysis of the cumulative power that ETs need inject into the network to guarantee the sensor nodes operation is provided for three different multiple access methods for multi-ET transmissions, namely cellular-based planning, orthogonal multiple access methods and distributed beamforming. To analyze the former, a closed-form expression of the minimum cumulative injected power is derived. Then, this is numerically evaluated to analyze and compare the three proposed methods. The presented analysis is agnostic of any underlying physical layer capability.

It is found that this power metric is bounded, in its worst case, by $O(s^{1-\alpha/2})$, where α refers to the propagation path-loss exponent. That is, the injected power is independent of the number of deployed ETs in free-space conditions, whereas it is decreasing in typical indoors propagation environments ($\alpha > 2$). By implementing optimal power transmission schemes, this bound scales up to approximately s times faster in ideal transmission channels, whereas this improvement becomes less noticeable at higher values of the path-loss exponent.

In summary, this chapter shows that increasing the number of deployed ETs is scalable in terms of aggregated transmitted power and that the propagation channel conditions the way in which multiple ETs should coordinate to mitigate mutual interferences and generate maximum constructive signal addition at the energy-receiving sensors. We show that for the correct operation of such networks it is necessary to research and develop sophisticated interference-aware schemes for near-ideal channel conditions, and also demonstrate that simple approaches can provide similar performance when the channel degrades.

The rest of this chapter is organized as follows. In Sec. 6.2, we briefly overview the fundamentals of wireless RF power transfer. In Sec. 6.3, discusses the design of multipe access for wireless RF power transfer. Sec. 6.4 derives a theoretical

bound for the scalability of power. Sec. 6.5 numerically evaluates this work. In Sec. 6.6 we discuss the obtained results and conclude this chapter in Sec. 6.6.

6.2 A Channel Model for Power Transfer

In this section we revise the fundamentals of wireless RF power transfer and the channel model considerations.

6.2.1 Point-to-point Power Transfer

We consider the following path-loss model, which is described by the transmitted power, P_T, the path loss at 1 meter distance, L_0, the transmission distance, R and the path-loss exponent, α [143]. L_0 also accounts for additional multiplicative constants that play a role in the wireless medium and do not depend on the distance, such as the antenna gain or directivity. The power which is received at the antenna is given by:

$$P_H = P_T L_0 R^{-\alpha}. \tag{6.1}$$

As a general case, α is generally comprised between 2 (free space) and 6 within urban areas (both outdoors and indoors) [2].

6.2.2 Multiple Power Transfers

When multiple ETs are required to cover a large networking area, the wirelessly propagated RF waves may constructively or destructively combine. We find that the received power at the harvesting antenna, when it harvests from a number s of ETs is given by [110]:

$$P_R = \sum_{i=1}^{s} P_{Hi} + \sum_{\substack{i,l=1 \\ i \neq l}}^{s} \rho_{il} \sqrt{P_{Hi} P_{Hl}} \tag{6.2}$$

where P_{Hi} refers to the received power from the i-th ET and ρ_{il} stands for the correlation between the i and l transmissions, in case of random signals, or orthogonality factor in case of deterministic signals. This value is bound in such that $-1 \leq \rho_{il} \leq 1$.

In order to exemplify this factor, let us consider two deterministic RF sine waves that arrive at a receiver node with same power $P = P_1 = P_2$, frequencies f_1 and f_2 and phases ϕ_1 and ϕ_2. If $f_1 \neq f_2$, we have that $\rho = 0$, then the received power equals $2P$. If $f_1 = f_2$ and $\phi_1 = \phi_2$, the RF waves constructively combine and the received power equals $4P$. Finally, if $f_1 = f_2$ and $\phi_1 = \phi_2 + \pi$, the RF waves destructively combine and the received power is zero.

6.3 Multiple Access for Multi-ET Transmissions

In this section, we revise the design space in multiple access for multi-ET transmissions. Multiple access methods to handle interference in wireless RF power transfer can be classified as follows:

6.3.1 Cellular-based planning

Each ET has an associated region in the space, where this is in charge of transferring the energy. To avoid neighboring interferences, each ET has an associated transmission slot (either in frequency or in time). After a certain distance, cells could re-use slots [117]. The received power from a given node is simplified to:

$$P_R = P_{H\,\max}, \tag{6.3}$$

where $P_{H\,\max}$ refers to the most energetic reception from the set of ETs. Given that ETs do not cooperate to maximize the power tranfer, this approach stands as the worst case.

6.3.2 Orthogonal Methods

Classical orthogonal approaches appear as a second approach to mitigate the signal destruction due to interferences. In this group, simple schemes such as FDMA, TDMA or advanced modulations, such as CDMA, FHMA or OFDMA can be implemented at the ETs [35, 27, 28]. This approach aims at vanishing the correlation factors between RF waves ($\rho_{il} = 0\ \forall i, l$) hence, reducing the received

power equation to:

$$P_R = \sum_{i=1}^{s} P_{Hi}. \tag{6.4}$$

These methods have been employed to implement off-the-shelf ETs and potentially offer better performance than Cellular-based planning. Pseudo-random codes for CDMA and FHMA, as in [35] permit an unattended operation and deployment of the ETs.

6.3.3 Distributed beam-forming Methods

This last approach aims at leveraging the constructive combination of RF waves, hence optimizing parameters, such as the transmission phase at each ET to either maximize the received power at all locations or to guarantee a minimum delivered power. In this direction, energy-on-demand (EoD) MAC protocols have been proposed to maximize the constructive combination of RF waves [97]. Recent works in massive MIMO for energy transmission has shown that ETs can constructively combine at all sensor node locations if each ET has at least k separated antennas, being k the number of users or deployed nodes in the network [110]. Due to the large number of required antennas per ET and the excessive node to ET channel state information (CSI) communication feedback, this approach may render unpractical. Accordingly, it sets the upper bound in performance of transmission of energy and, then, the lower bound in minimum cumulative injected power.

Analytically, this approach aims at providing the best correlation factors, hence being upper bound (i.e., $\rho_{il} = 1$) by:

$$P_R = \sum_{i=1}^{s} P_{Hi} + \sum_{\substack{i,l=1 \\ i \neq l}}^{s} \sqrt{P_{Hi} P_{Hl}} \tag{6.5}$$

As reported in [94], the received power considering this approach shows a gain of s, with s being the number of considered ETs, compared to orthogonal methods.

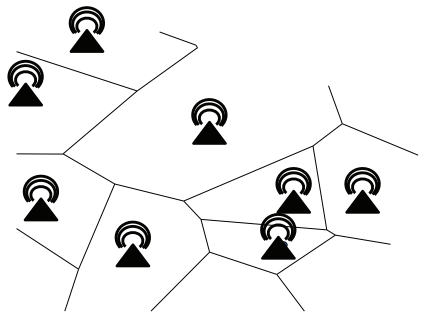

Figure 6.1: Voronoi tesselation generated by the energy transmitters.

6.4 A Theoretical Bound for Cellular Planning

In this section, we bound the minimum cumulative injected power per unit area as a function of the number of ETs in a cellular-based planning set-up. In this context, nodes are able to harvest power only from their nearest ET and disregard the received power from any other ET.

Let us define a Voronoi Tessellation where the set of s ETs spatially distributed, following a Poisson Point Process, along the area $\mathcal{A}$ are used as center of each cell. Then, we find that a given node k located at an arbitrary location harvests power from the i-th ET if the node is contained in the cell V_i. In this study, each deployed ET injects the same amount of power into the network. To exemplify this, we show in Fig. 6.1 an example of an ET deployment and their associated cells, based on closer distance.

Then, we bound the distance between the ET i and the node in its cell that is located at the furthest distance from the ET. This distance is bound by one of the vertices of the Voronoi cell, which, in turn, for arbitrarily large number of ES, s, and any integer $j > 0$, we can bound it by defining a disk of diameter R_j [37], which is given by:

$$R_j = 4 \cdot 3^{-1/4} \sqrt{\frac{j}{s-1}} \tag{6.6}$$

with probability $\geq 1 - 6e^{1-j}$. In other words, the maximum possible distance between the ET i and the furthest node that can be deployed within the ET cell V_i is bounded by:

$$d_{max,i} < \frac{R_j}{2} < c_1 s^{-1/2} \tag{6.7}$$

with probability tending to one when $s \to \infty$, being c_1 a multiplicative term

which does not have dependence on s.

Let us, then, define the minimum cumulative power density $\mathcal{P}$, defined as the sum of the transmitted power of every ET deployed in the networking area $\mathcal{A}$. The minimum cumulative power density refers to the total power per unit area which is transmitted by the ETs to guarantee the power requirements at the sensor node locations. In this sense, requiring a single ET transmitting 4 W of power or four ETs transmitting 1 W of power each to cover a 10x10 m area, yield to the same minimum cumulative power density of 0.04 Wm^{-2}.

We then set the transmitted power at each ET to be such that the node located at the furthest distance from the ET is able to receive the minimum required power P_0 set IoT communication layer. Therefore, the minimum cumulative power density can be calculated as:

$$\mathcal{P} = \frac{\sum_{i=1}^{s} P_0 L_0^{-1} d_{max,i}^{\alpha}}{\mathcal{A}} \tag{6.8}$$

where P_0 refers to the requirements of power at the node location, L_0 stands for the path loss at the distance of 1 m, $d_{max,i}$ stands for the distance between the ET s_i and the furthest node located within its Voronoi cell V_i and α stands for the path-loss exponent.

Provided that the maximum distance from the center of a Voronoi cell to any point within its cell is bounded by $d_{max,i} < c_1 s^{-1/2}$, we can now obtain that the transmitted power density can be upper bounded by:

$$\mathcal{P} < \sum_{i \in \mathcal{S}} P_0 L_0 (c_1 s^{-1/2})^{\alpha} < c_2 s^{1-\alpha/2}, \tag{6.9}$$

which is a function of the number of ETs. Finally, we can say that the minimum cumulative power density is upper bounded by:

$$O\left(s^{1-\alpha/2}\right). \tag{6.10}$$

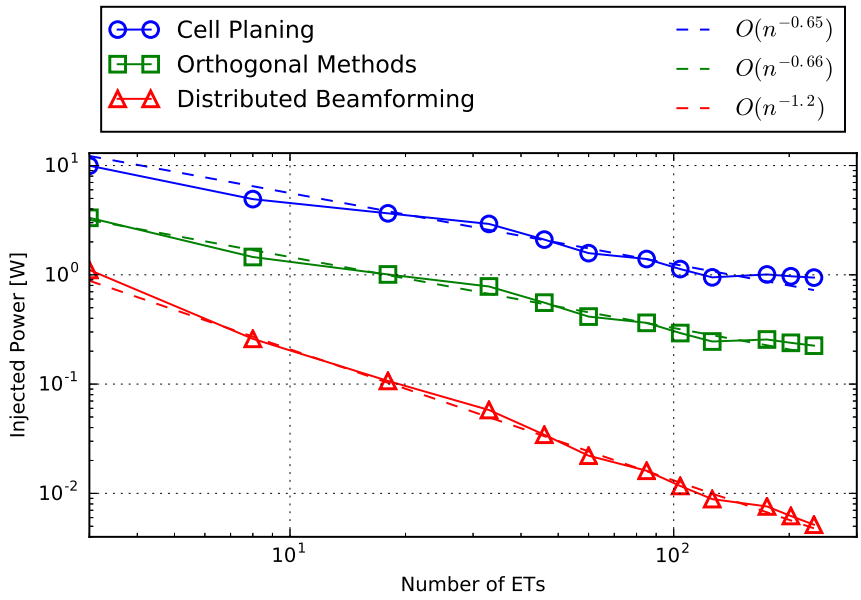

Figure 6.2: Minimum cumulative power injected by the ETs to guarantee sufficient harvested power at any location, considering a regular hexagon deployment grid.

6.5 Numerical Results

We numerically evaluate the scalability of the three considered approaches. For this, we assume the ideal operation of the multiple access methods. We calculate the required power that it needs to be allocated at each ET, such that a sensor node placed at any point in the networking area can harvest a minimum power of $P_0 = 10$ μW. The minimum cumulative power is then calculated by summing the allocated power at every ET. The network is placed over a 20x20 m^2 squared area. The deployed ETs are deployed over the networking area following two different topologies, namely regular hexagons and random positioning.

We first show in Fig. 6.2 the minimum cumulative injected power as a function of the number of deployed ETs. This numerical evaluation considers the office environment channel model provided in [2], which provides an $\alpha = 3.3$. In the figure, we compare the different multiple access methods. In addition, we also show the scalability trend that each curve offers. As it is observed, cellular planing offers the worst performance, requiring larger amounts of injected power. Nonetheless, we observe that it scales as predicted. Orthogonal methods, show

very similar scalability as cellular planing, whereas offering an approximately three-fold performance improvement in terms of the injected power. Finally, we find that distributed beam-forming offers a substantial improvement with respect to the other approaches, in terms of injected power and its scalability. Particularly, this scales as $O(s^{-1.2})$, instead of the theoretically obtained $O(s^{-0.65})$.

Then, we show in Fig. 6.3 the design space for multiple access methods for Multi-ETs. In the figure we show the *scalability exponent* as a function of the path-loss exponent. The scalabilty exponent refers to the obtained exponent of s in the scalabiltiy trend (i.e., $1-\alpha/2$ for cellular planing). We first see that the numerically evaluated cellular planing matches the theoretical bound derived in the previous section. Then, we find that distributed beam-forming achieves the best performance, as predicted in Sec. 6.3 These two bounds define the design space of multiple access methods for wireless RF power transfer.

6.6 Discussion

In this section, we assess the question asked in Sec. I: *In order to guarantee sufficient power at the deployed nodes, is it better to increase the number of ETs, to increase their transmitted power or to increase their system complexity?* To provide an answer, we consider the following two use-cases:

The case $\alpha = 2$ refers to free-space or ideal propagation. In this scenario, the injected power scales as $O(1)$ in cellular-based planning. That is, the injected power is independent of the number of deployed ETs. As such, there is no preference between increasing the allocated power or increasing the number of deployed ETs, without taking into account practical constraints in the maximum power per ET. In these conditions, it is observed that implementing sophisticated interference-aware schemes extends this bound to $O(s^{-1.1})$, which responds to the theoretical s gain of distributed beam-forming over orthogonal methods predicted in [94].

The cases where $\alpha > 2$ generally apply to indoors and/or urban environments. In such cases, larger densities of ET reduce the cumulative injected power. That is, larger path-losses constrain the power transfer to very few meters distance from the ETs, and this power very rapidly decays with the separation distance. For a fixed deployment, increasing the number of ETs reduces the transmitted power,

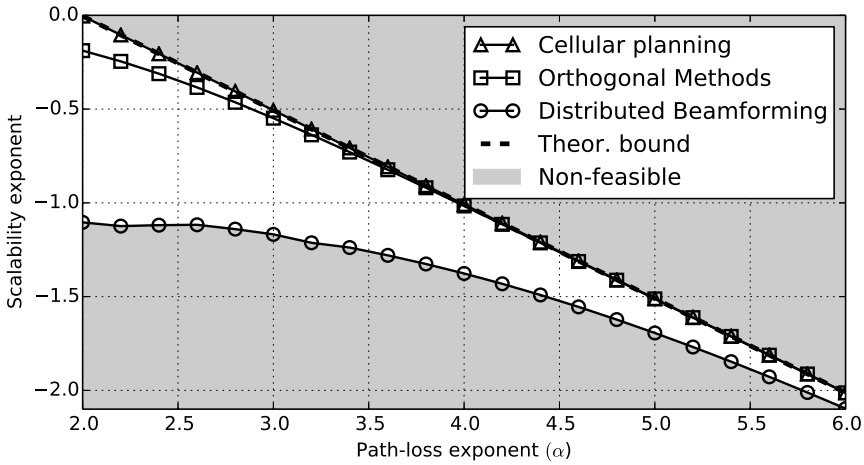

Figure 6.3: Design space of multiple access methods for Multi-ETs.

Table 6.1: Summary of the results and proposed recommendation

Channel	**Scalability**	**Recommendation**
Free-space	$O(s^{-1.1})$	Multiple ETs, sophisticated methods
Indoors	$O(s^{1-\alpha/2})$	Multiple ETs, simple cellular approach

therefore yielding towards more sustainable environments. It is noteworthy that as α increases, the large dispersion of the medium causes that the transmitted RF waves do not propagate over long distances and cannot combine among them. Hence, the derived bounds for optimal multi-ET transmissions approach the theoretical bound.

The provided use-cases provide strong design guidelines in the deployment of ETs. It is first shown that large deployments of low-power ETs help reducing the overall transmitted power. Then, it is shown that the path-loss exponent conditions the multiple access for multi-ET design. We advocate for sophisticated methods in near-ideal or line-of-sight environments, whereas simple multiple access methods for inter-ET interference mitigation can offer similar power saving in highly- dispersive channels. Table 6.1 summarizes the achievable scalability of the minimum cumulative injected power and the recommended design guidelines, depending on the type of considered channel.

6.7 Summary and Conclusion

In this paper, the bounds for the cumulative power that energy transmitters (ETs) need to inject to supply a wireless RF powered Internet of Things have been addressed. These bounds compare the performance of different multiple access methods for multi-ET transmission, and define the design space for ET deployment. It has been shown that the required injected power decreases with the number of deployed ETs, hence motivating the deployment of a supporting network of ETs. It has been shown that near-ideal channel conditions can leverage sophisticated interference-aware schemes to further reduce the required injected power, whereas dispersive simple approaches can provide similar performance when the channel degrades.

Chapter 7

Energy Multiplexing for Multi-ET Wireless RF Power Transmission

7.1 Introduction

In the previous chapter, a thorough analysis on the scalabilty of the cumulative injected power as a function of the number of ETs has been provided. As the results show, this metric decreases when the number of ETs grows, hence motivating the deployment of multiple ETs to cover large networking areas. This potential benefit has been already experimentally validated [39, 40, 97], showing that the presence of multiple ETs reduces the average propagation distance to the energy harvesting sensors, and thus decreases the attenuation level of the energy waves and improve the RF power harvesting rates [55].

When deploying multiple ETs over a an area, the propagated RF waves spatially overlap. Fig. 7.1 shows a many-to-many power transmission in a WSN, where more than one ET delivers power to multiple sensors. In this network RF waves may interfere with each other when they are transmitted in the same medium. These interferences can be either constructive (i.e., the received power is larger than the average) or destructive (i.e., the received power is very low, or even zero) as shown in [97, 117], requiring ETs to implement energy multiplexing techniques for wireless RF power transimssion [144]. It can be observed that the

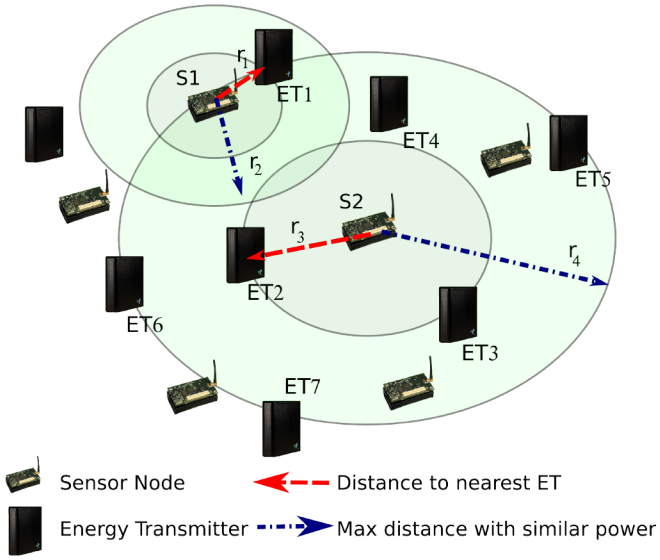

Figure 7.1: Example of a WSN powered by wireless RF energy transfer. The number of coinciding RF waves generated by ETs with similar magnitude depends on the distance from the sensor to the closest ET. Larger distances imply more coinciding sources.

constructive and destructive combination of RF waves generate very large peaks and drops of power in a non-controllable spatial-dependent manner.

In this chapter, we lay the foundations of a Duty-Cycled Random-Phase (DCRP) energy multiplexing method for wireless RF power transmission. DCRP relies on the fundamental assumption that efficiency is maximized when the input power varies in time as much as possible, since the energy harvesters operate with increasing efficiency as a function of the input power [106, 33, 13, 14]. This approach not only is able to handle the interferences of multiple ETs but it also benefits from them to broaden the input power range of existing energy harvesters at the sensor nodes. The key idea here is to leverage time-synchronized transmission of bursts at a single frequency (i.e., every ET transmits the power burst at the same time), where each of these bursts is transmitted with a random phase. The combination of these bursts with random phases approximate a temporal sequence of bursts with random amplitude. We evaluate the performance of DCRP through both simulation and experimental test-beds. The results show that DCRP, which requires a similar system complexity than orthogonal methods, is able to broaden the input power range of the energy harvesters by 5 dB, hence

approaching distributed beamforming performance in our considered scenario.

The main contributions of this chapter are as follows:

- We analytically describe a new duty-cycled RF transmission and modulation approach for energy multiplexing wireless RF power transmission sensor networks.
- We perform an experimental study to validate the key working principles of the approach. This study involves a scaled evaluation of DCRP on a testbed composed of USRP radios with RF amplifiers as ETs and energy harvesting sensors.
- We show the performance of DCRP for large-scale sensor deployments using network level simulation. This simulation studies the statistical power distribution in space and demonstrates the charging action of many ETs to many sensors.

The rest of the chapter is organized as follows. In Sec. 7.2, we overview the hardware and network considerations. In Sec. 7.3, we present and analyze our DCRP approach. In Sec. 7.4, we experimentally evaluate the performance of DCRP in a many-to-one environment using both analysis and experiments. In Sec. 7.5, we simulate the performance of the experimentally validated model for many-to-many transmissions. Finally, we conclude our work in Sec. 7.6.

7.2 Overview

This section overviews the hardware and network architectures which are considered in this work.

7.2.1 Network Model

We consider a network composed of multiple ETs which permanently transfer energy through RF waves to power a wireless sensor network, as shown in Fig. 7.1. Each node is equipped with an energy harvesting circuit, which converts RF energy into DC current. The received power at a sensor node located in an arbitrary location of the network is the result of the combination of the RF

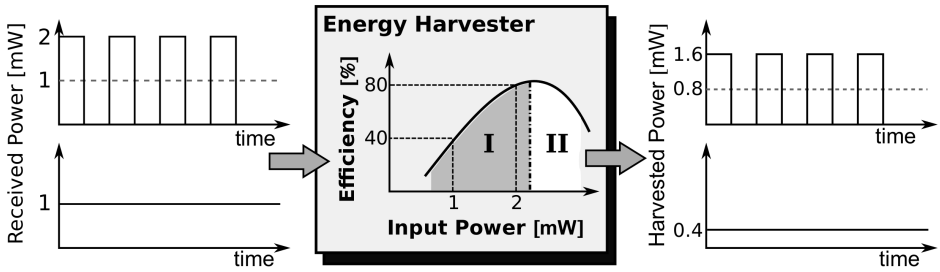

Figure 7.2: Low and high power regions of operation of an energy harvester (denoted as I and II) and benefits of transmitting power with large peak-to-average power ratios in region I. A duty-cycled transmission of energy is compared to a constant transmission.

waves that are transmitted from multiple ETs. Due to the propagation path-loss, sensors will receive a large amount of power from their closest ETs, whereas the nodes located far from any ET will receive significantly less power that is generated by the small contributions of many ETs. We show an example of a network in Fig. 7.1. In the figure we observe that the sensors S1 and S2 are located at a distance r_1 and r_3 from their closest ETs, respectively. Then, we show the distances r_2 and r_4 which represent the maximum distance where an ET could generate an RF, such that it can interefere. We see that due to the short distance r_1 between S1 and ET1, S1 only receives power from a single ET. Alternatively, provided that S2 is located at a further distance from any ET, S2 receives a lower input power, which is the sum of power from ETs with indices ranging from 1 to 7.

7.2.2 Hardware Considerations

The non-linear behavior of semiconductor devices results in the dependency of the input impedance with the input power, such that the antenna and energy harvester impedances match only for a certain input power. The impedance matching makes two distinguished regions in any real implementation [33], as shown in Fig. 7.2: Increasing efficiency for low input powers (denoted as region I) and decreasing efficiency for high input powers (denoted as region II). In region I, transmitting power in a time-varying manner leads to higher amounts of harvested energy [14]. On the contrary, in region II the power conversion efficiency at the high power range decreases with the input power [33], and a low peak-to-average

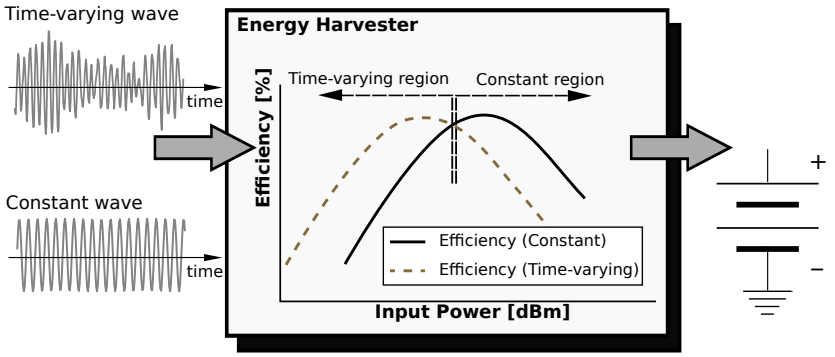

Figure 7.3: Time-varying input power improves the efficiency at the low input powers, whereas it shows lower efficiency at the high input power region.

received power ratio improves the efficiency of the energy harvester.

As an example, Fig. 7.2 also compares two power transmission schemes, namely continuous and duty-cycled (with a peak-to-average power ratio of 2) with equal average received power of 1 mW. Without loss of generality, we assume a 40% efficiency for 1 mW input power and a 80% efficiency for 2 mW input power. Accordingly, in the case of continuous power transmission, a constant power of 0.4 mW would be harvested, while in the case of duty-cycled power transmission the harvester provides a duty cycled instantaneous power of 0 mW for an input power of 0 mW and 1.6 mW for an input power of 2 mW. Overall, this results in 0.8 mW average harvested power. In contrast to this example, if the efficiency curve decreases with the input power, receiving a constant power provides a larger efficiency.

7.3 Duty-cycled Random-phase Energy Multiplexing

Our proposed Duty-Cycled Random Phase (DCRP) energy multiplexing for wireless RF power transmission exploits the two energy regions in order to maximize the efficiency of the energy harvester at each node. In particular, it generates time-varying power at the input of the the sensors which receive low power levels and to generate constant input power at the sensors which receive high power levels. As it is shown in Fig. 7.3, this action optimizes the operation of the energy harvesters in both low and high power regions. For this, our scheme leverages

multiple transmissions at the sensors which receive low power levels (i.e., sensors located at further distances from any ET receive low power and this power is generated by the combination of multiple ETs) and single transmission at the sensors which receive high power levels (i.e., sensors located nearby an ET receive high power from their nearest ET, thus neglecting the combination from further ETs). To generate time-varying input power, ETs transmit time-synchronized bursts of power in a duty-cycled manner (each *on* duration is here referred as a *burst*). Each burst is a single frequency, continuous sine wave RF transmission, generated with a randomly selected phase $\phi_{jk} \in (0, 2\pi]$. At the start of every *on* time, the ETs select a random, different phase. Fig. 7.4 shows a time-diagram of the DCRP scheme, where S1 and S2 are nodes in Fig. 7.1, whereas No RP stands for a generic energy multiplexing for wireless RF power transmission method which ensures perfect channel orthogonality, such as FDMA or DSSS.

By employing this scheme we modulate the peak-to-average power ratio in two stages: First, the duty cycled transmission increases the peak-to-average power ratio of all input powers. Unfortunately, the maximum peak power that can be transmitted is constrained by regulatory organizations, hence the duty cycle cannot be arbitrarily reduced to create large peaks of power. Second, the combination of multiple RF waves with random phases deliberately generates both destructive and constructive interferences. These interferences modulate the overall received power at the sensor locations, thus increasing the peak-to-average power ratio. Given that the time-varying power is generated by intentionally interfering the RF waves from the ETs, only sensors which receive power as the combination of multiple ETs receive a time-varying power. Accordingly, it is shown in Fig. 7.4 that S1 receives power only from one source (ET1), thus harvesting from a low peak-to-average power ratio signal. Alternatively, S2 receives power from many ETs (ET1 to ET7), thus harvesting from a very large peak-to-average power ratio signal. We also show the case of a generic orthogonal method, such as FDMA or DSSS, referred in the figure as No RP (no random-phase). As the figure shows, the received power at each burst is constant in time, since these methods avoid both constructive and destructive interferences.

The period T in DCRP depends on the design and circuital properties of the energy harvesting, as well as it depends the average input power at the sensors. These parameters must be experimentally adjusted for any given technol-

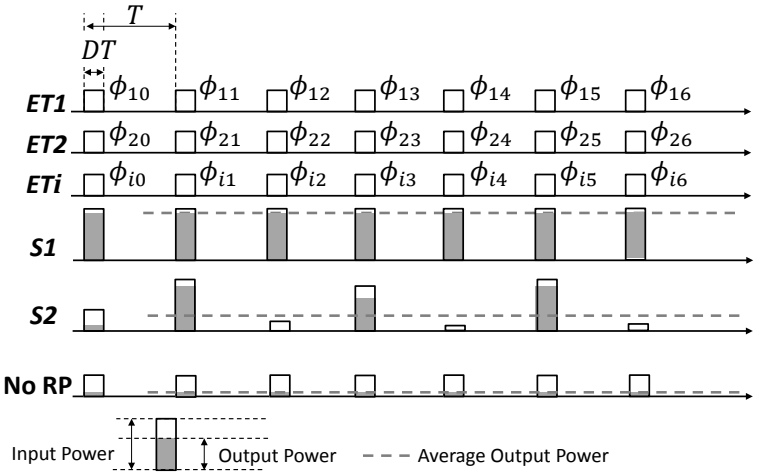

Figure 7.4: DCRP scheme. Each ET propagates RF waves with random phases ϕ_{ik} in a duty-cycled manner with period T and duty cycle D.

ogy. In particular, we have experimentally found that for a P1100 Powercast harvester [33], values of T in the order of 10 ms to 100 ms provide a good performance. This selected time range is important as the burst must be significantly larger than the synchronization time, and the transient time of the energy harvesters at the receiving node. Note that synchronization errors between ETs can be kept several orders of magnitude below the time-scale of DCRP. In particular, a precision of a few tens of microseconds can be achieved using inexpensive off-the-shelf software over wireless [129, 54]. This precision can be improved to 200 ns if ETs integrate typical GPS receivers [87].

The selection of the duty cycle is constrained due to regulatory organizations. As a general case, the allocated peak power will be assigned by considering the maximum permitted transmitted power, either by regulation (e.g., 4 W according to the FCC [1]). Thereafter, the duty cycle will be assigned, such that it is possible to meet the power requirements of the deployed sensors with the least amount of power.

7.3.1 Analytical Model of DCRP Performance

Combined Input Power

We first model the input power at the sensor node destination. We denote m as the number of ETs and n as the number of sensors which are deployed over the networking area. Without loss of generality, we locate the sensor node under study at the center location of the Cartesian plane. Then, we denote P_T as the average power that is transmitted from an ET (P_{Ti} if particularized by the i-th ET).

We utilize the concept of signal $s(t)$ as the squared-root of the instantaneous input power, $p(t) = |s(t)|^2$, in $\mathrm{W}^{1/2}$ units. Notice that the concept of signal does not directly correspond to voltage, since the signal is $s(t) = \sqrt{v(t)i(t)}$, where $v(t)$ is the voltage drop across the terminals, and $i(t)$ is the current flowing through them. According to operational method of the DCRP scheme, *the power is transmitted in bursts of energy and each ET transmits at the same time with same frequency and with random phase*, the duty cycled signal which is generated at a given ET can be described as the addition of independent bursts of RF signal delayed in time:

$$s(t) = \sum_{k=0}^{\infty} \sqrt{\frac{P_T g(r)}{D}} \cos\left(2\pi f_0 t + \phi_k\right) \Pi\left(\frac{t - kT}{DT}\right), \tag{7.1}$$

where k refers to the burst, P_T is the average transmitted power, $g(r)$ stands for the path loss, which is a function of the distance r, D is the duty cycle, f_0 stands for the carrier frequency, $\phi_k \in (0, 2\pi]$ refers to the phase shift of the k-th burst, $\Pi(x)$ is the rectangular function (defined as $\Pi = 1$ if $0 \leq x \leq 1$ and $\Pi = 0$ otherwise), finally, T refers to the time period of the duty cycle. Moreover, the signal parameters D, f_0 and T are fixed for all the ETs, such that each ET concurrently transmits in-time and in-frequency. On the contrary, the sequence of phase shifts, ϕ_k, is random in-time and different ETs have different sequences.

Notice that pure squared signals cannot be effectively modulated, since this would require infinite bandwidth capabilities. However, given that the timescale of DCRP is in the order of 100 ms and above, approximating the rise and fall time of the transmitted bursts by pure squared signals in (7.1) is a reasonable approximation.

To reduce further notation, we denote the received power from a given ET as $P_i = P_{Ti}g(r)$. Also, we focus on a specific burst time and use phasor notation, such that the signal that a sensor receives from a the i-th ET is simplified to:

$$s = \sqrt{P_i/D}e^{j\phi_i}. \tag{7.2}$$

The received signal, composed as the combination of concurrent m ETs at a given burst time, is a sine signal of same carrier frequency, amplitude $\sqrt{p_R}$ and phase θ, which is given by:

$$s_R = \sum_{i=1}^{m} \sqrt{P_i/D}e^{j\phi_i} = \sqrt{p_R}e^{j\theta}, \tag{7.3}$$

where p_R is the instantaneous received power and can be easily obtained as:

$$p_R = D^{-1}\sum_{i=1}^{m} P_i + D^{-1} \sum_{\substack{1\leq i,j\leq m \\ i\neq j}} \sqrt{P_i P_j}cos(\phi_i - \phi_j). \tag{7.4}$$

As observed, the received signal amplitude and instantaneous power depend on the phases among RF waves. Since these phases are kept constant during the transmission of each burst, but randomly changed at each one, the received signal amplitude and its instantaneous power at each burst define decorrelated random processes.

Given that the input power is a random process, we statistically analyze its properties. First, we observe that the expected value of the received power at the sensor node location during the duration of a burst of energy equals to the sum of the contributions ($\mathbb{E}[p_R] = \sum_i P_i/D$), since

$$\mathbb{E}\left[\cos\left(\phi_i - \phi_j\right)\right] = 0, \ \forall i \neq j. \tag{7.5}$$

The expected value refers to the received power that a sensor node receives on average, if the phases are randomly chosen. In DCRP, since the phase shifts are randomly varied in time, the temporal average tends to the expected value multiplied by the duty cycle as a consequence of the weak law of large numbers. Then, the input power in temporal average, P_R, equals to the sum of the received

power from each ET:

$$P_R = D^{-1} \sum_{i=1}^{m} P_i. \tag{7.6}$$

We find that this guarantees that DCRP operates as an energy multiplexing method for wireless RF power transmission , as it does not suffer from interferences in temporal average, as the time tends to infinity. Also, we observe that the use of duty cycled bursts generates large instantaneous power for the same averaged power.

The variance of the received power, σ_R, is given by:

$$\sigma_R^2 = \mathbb{E}[p_R^2] - \mathbb{E}[p_R]^2 = D^{-2} \sum_{\substack{1 \leq i,j \leq m \\ i \neq j}} \mathbb{E}\left[P_i P_j\right]. \tag{7.7}$$

In order to exemplify this result, if we assume that the received power from each ET is equal, i.e., $P = P_1 = P_2 = \cdots = P_m$, we obtain that the relation between the standard deviation and the average value is given by:

$$\frac{\sigma_R}{P_R} = \sqrt{\frac{m-1}{m}}. \tag{7.8}$$

From this example, we observe that as the number of coinciding ETs increases the variation in the input power becomes larger. Therefore, sensors which are located near an ET (and, thus, they mostly receive power from a single source) will receive a less time-varying input power than nodes located at further distances in a real network deployment (See Fig. 7.1). It is also interesting to observe that (7.8) is a monotonically increasing function with maximum value 1. The maximum value is rapidly reached when $m > 6$. As a result, we can infer that after a reasonable number of coinciding ETs (approximately $m > 6$) the received power will show similar properties than if we assume that the received power comes from the combination of *infinite* number of power sources. This will be later addressed in the section.

Obtaining a closed-form expression for the probability density function (pdf) of the received power at a given location is valuable in this study, as it can provide us more information than the expected value and its standard deviation. Unfortunately, as it is found in [3], there is no general expression for the pdf,

and its calculation results in non-intuitive and very specific formulas for each particular case. In this work, we derive the pdf for two particular cases of special interest, and then show how it can be numerically extended for multiple ETs.

Received Power as the Combination of Two ETs

We first consider the particular case of receiving energy from two ETs, denoted as ET_1 and ET_2. Without loss of generality, we assign these indexes as a function of the recevied power. Then, the sensor receives $P_1 = P$ from ET_1 and $P_2 = cP$, with $c \leq 1$, from ET_2. From (7.4), we can simplify the received power as:

$$p_R = P\left(1 + c + 2\sqrt{c}\cos(\Delta\phi)\right), \tag{7.9}$$

where $\Delta\phi = \phi_1 - \phi_2$ is an uniformly distributed random variable in $[-\pi, \pi)$, which refers to the phase difference between both RF waves in reception.

Therefore, the calculation of the cumulative distribution function (cdf) can be derived from:

$$F_{P_R}(p_R) = \Pr\left\{P_R < p_R\right\} = \Pr\left\{\frac{P_R/P - 1 - c}{2\sqrt{c}} < \cos\Delta\phi\right\}, \tag{7.10}$$

where if $\Delta\phi$ is uniformly distributed, the expression is reduced to:

$$F_{P_R}(p_R) = \frac{1}{\pi}\int_{\arccos\Delta\phi'(p_R)}^{\pi} d\Delta\phi, \tag{7.11}$$

where $\Delta\phi'(p_R) = (p_R/P - 1 - c)/2\sqrt{c}$. Finally, this integration yields into the following closed-form expression:

$$F_{P_R}(p_R) = \begin{cases} 0 & \text{if } p_R < P' \\ \frac{1}{2} + \frac{1}{\pi}\arcsin\left(\frac{p_R/P - 1 - c}{2\sqrt{c}}\right) & \text{if } P' \leq p_R \leq P'' \\ 1 & \text{if } p_R > P'' \end{cases}, \tag{7.12}$$

where $P' = P(1 + c - 2\sqrt{c})$ and $P'' = P(1 + c + 2\sqrt{c})$. Notice that the particular case of $c = 1$, the received power of the combination of two ETs, results in the arcsine distribution with normalized parameter $p_R/4P$.

Received Power as the Combination of Many ETs

We consider the case that the received power is the result of the combination of an arbitrarily large combination of ETs. Starting with (3), we find that both real and imaginary parts of the signal can be written as:

$$\Re\left(s_R\right) = \sum_{i=1}^{m} \sqrt{P_i}\cos(\phi_i);\ \Im\left(s_R\right) = \sum_{i=1}^{m} \sqrt{P_i}\sin(\phi_i), \tag{7.13}$$

where $\Re$ and $\Im$ refer to the real and imaginary operators. Since each phase shift, ϕ_i, is randomly selected, both real and imaginary part can be modeled according to the central limit theorem (CLT) as a Gaussian variable:

$$\Re\left(s_R\right),\ \Im\left(s_R\right) \sim \mathcal{N}\left(0, \sqrt{P_R/2}\right), \tag{7.14}$$

where P_R stands for the average received power.

Therefore, when both real and imaginary parts of a signal are Gaussian distributed, it is said that the distribution of the signal is complex Gaussian, $s \sim \mathcal{CN}\left(0, \sqrt{P_R}\right)$.

When a signal is complex Gaussian distributed with $s \sim \mathcal{CN}\left(0, \sqrt{P_R}\right)$, its amplitude, r, is given by the Rayleigh distribution [43]. Accordingly, the pdf of the signal amplitude is given by:

$$f_R = \frac{r}{(\sigma')^2} e^{-\frac{r^2}{2(\sigma')^2}}, \tag{7.15}$$

where $\sigma' = \sqrt{P_R}/\sqrt{2}$.

Likewise, the square or power of a signal that presents a Rayleigh distribution can be modeled with an exponential distribution with $\lambda = 1/P_R$ [43]:

$$f_{P_R}(p_R) = \frac{1}{P_R} e^{-p_R/P_R}. \tag{7.16}$$

In order to show the different distributions of the input power, we show in Fig. 7.5.a a numerical evaluation of the pdf of the received power when this is generated by 2, 3 and 4 ETs. These results are shown normalized over the average value of the received power, referred as input power ratio in the figure, and equal contribution from each ET. As it is observed, the particular case of 2

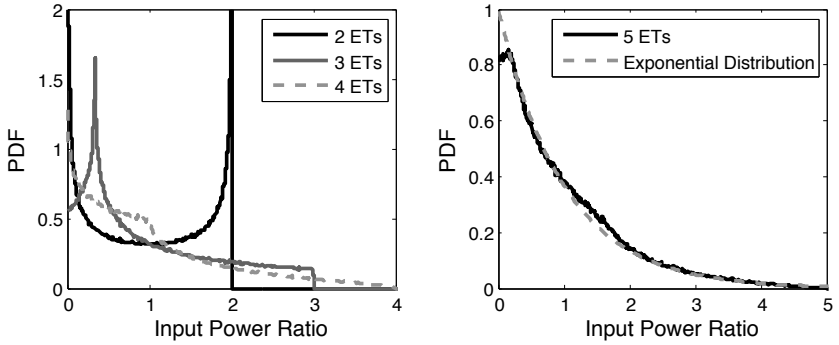

Figure 7.5: Distribution of the input power for $m = \{2, 3, 4, 5\}$ coinciding ETs.

ETs generates the U-shaped arcsine distribution centered in 1. Alternatively, it is also shown that when the number of ETs increase, the pdf approaches to the exponential distribution. In Fig. 7.5.b, the particular case of 5 ETs is compared to an ideal exponential distribution of $\lambda = 1$. As observed, the distribution of the received power is already very similar to the ideal distribution. We consider that, for a number of coinciding RF waves larger than 5, the exponential distribution with $\lambda = P_R$ is a good approximation of the received power at a given burst.

7.3.2 Model of the Energy Harvester

We describe the performance of an energy harvester through its efficiency, here referred as η. We observe that this efficiency is a function of the input power, as it is described in [106, 33, 13], and it is an increasing function of the input power, especially for low input power values.

We first consider the contribution of the duty cycle. We find that the duty cycle shifts the efficiency curve to lower input values. That is, the efficiently harvested power P_H can be expressed as:

$$P_H = \eta(P_R/D)P_R. \tag{7.17}$$

Notice that dividing the received power by the duty cycle can be expressed as a displacement of the curve of $-10\log(D)$ towards negative values in dB units.

Then we consider the contribution of the random phase by assuming a duty cycle $D = 1$. Due to the fact that DCRP intentionally generates both destructive

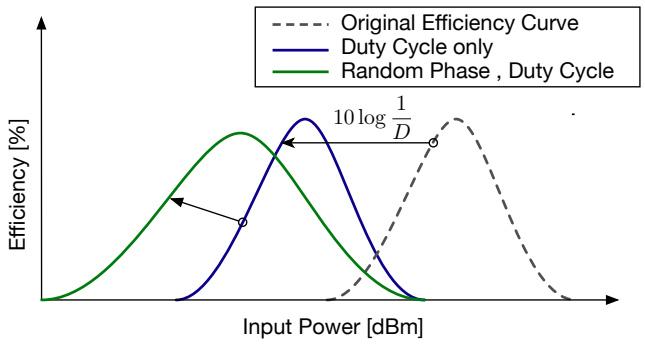

Figure 7.6: Contribution of the duty cycle and random phase to the eventual efficiency curve. The duty cycle shifts the efficiency curve to lower values of energy by $-10 \log D$ dB. The random phase equalizes the curve, thus broadening the range of admissible input powers.

and constructive interferences over time at the sensor node location, the efficiency of the energy harvester also presents a time-varying evolution. As a result, we pursue to find an *average efficiency* value, here referred as $\overline{\eta}$, such that the average harvested power, P_H, can be expressed as:

$$P_H = \mathbb{E}[\eta(p_R)p_R] = \overline{\eta} P_R. \tag{7.18}$$

Therefore, to calculate the average efficiency, we find that it can be obtained by:

$$\overline{\eta} = \frac{\int \eta(p_R) f_{P_R}(p_R)\, dp_R}{P_R}. \tag{7.19}$$

This integration results in an actual smoothing or equalization of the efficiency curve, which broadens the range of admissible input powers. To better understand the contributions of the duty cycle and the random phase, we show in Fig. 7.6 their contributions in tuning and equalizing the efficiency curve. As it is shown, the duty cycle shifts the efficiency curve down to lower values of input power by $-10 \log(D)$ dB, whereas the random phase broadens the range of admissible input powers.

In order to better understand the calculation of the temporal average input-to-output power conversion efficiency of DCRP, we analyze the particular case example of an energy harvester, such that its efficiency increases as a function of the input power. We find that this particular case example is of particular

importance provided that it gives an insight of the performance improvement of DCRP at the low input power range and it yields into a closed-form expression. In particular, we consider an energy harvester, which shows an input-to-output power conversion efficiency given by:

$$\eta(p_R) = kp_R^{\gamma} \tag{7.20}$$

where k and $\gamma > 0$ are constants [106, 33]. Then, if we assume that the energy is generated by a very large group of ETs (in practice, $m > 5$), and then the received power is exponentially distributed, (7.19) can be written as:

$$\overline{\eta} = \frac{\int_0^{\infty} kp_R^{\gamma+1} \frac{1}{P_R} exp^{-p_R/P_R}\, dp_R}{P_R} = kP_R^{\gamma}\Gamma(\gamma+2), \tag{7.21}$$

where Γ stands for the gamma function. We observe that if we compare the average efficiency to the efficiency that we would obtain if the sensor receives a constant amount of power, we find that:

$$\frac{\overline{\eta}}{\eta(P_R)} = \Gamma(\gamma+2) \tag{7.22}$$

which is always greater than 1. This means that the intentionally generated interferences of DCRP improve the efficiency at the low input power range in comparison to receiving power at a constant rate.

A realistic case-study, upon we base our further study, is addressed in the next section (see Fig. 7.7)

7.4 Node-level Experimental Evaluation

In this section we experimentally evaluate the performance of DCRP in the context of transmitting power from multiple ETs to a single energy harvesting sensor node.

7.4.1 Numerical Evaluation

We first evaluate DCRP considering the RF-to-DC conversion efficiency of the off-the-shelf energy harvester Powerharvester P1110 [33], from Powercast Corp.

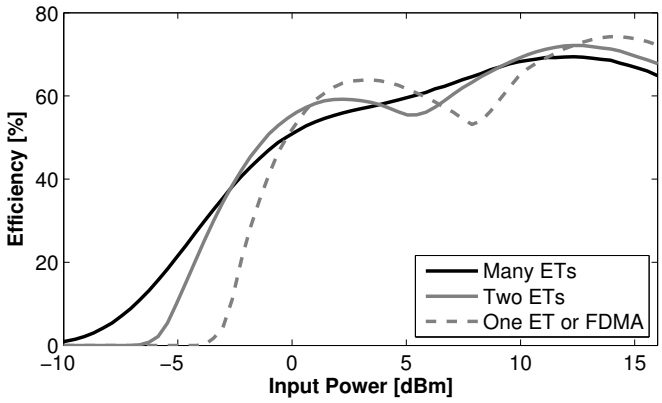

Figure 7.7: Efficiency curve as a function of the input power for the DCRP scheme with two and many ETs, compared to the reception of power from a single ET.

We show the efficiency curve as a function of the input RF power in Fig. 7.7 in gray dashed line. It can be observed that at the low input power range the efficiency grows with the input power, whereas it stays approximately constant at the large power range.

In order to show the performance of DCRP in this scenario, we evaluate (7.19) by considering both the exponential distribution (to consider the reception from many ETs) and the arcsine distribution (to consider the reception from two ETs). Provided that the contribution of the duty cycle is reduced to an effective displacement of the curve, the duty cycle of DCRP has been set to $D = 1$ during the numerical evaluation.

The results of these studies are shown in Fig. 7.7. It is shown that the use of DCRP has a remarkable positive impact upon the efficiency at low input powers. In particular, with only two ETs, the energy harvester is able to efficiently operate at lower input powers (from approximately -4 dBm to -6 dBm). In addition, the use of DCRP not only extends the minimum input power, but it also improves the efficiency. In fact, the efficiency at -3 dBm is increased from approximately 5% to 40%. However, the major benefits are obtained in the particular case of many ETs. This is mainly due to the fact that the input power is largely randomized with large energetic bursts, which can result in high efficiency in the actual harvested power. In this case, the minimum input power, which enables the conversion of power, is reduced down to approximately -10 dBm. As a final observation, DCRP equalizes the efficiency curve, thus providing a consistent

efficiency level as a function of the input power.

7.4.2 Experimental Evaluation

In this section, we validate the benefit of our approach through an experimental setup consisting of two ETs and one energy harvesting sensor.

Experimental Setup

To perform the experimental validation of a many-to-one wireless power transmission, we separately implement the transmitters and the receiver. On the transmitters side, we have employed two USRP Software Radio [118] devices and GNURadio open source software to create configurable duty-cycled signals, which emulate the operation of the ETs. The USRP devices can be synchronized in time, frequency and phase. In this experiment, we have configured the USRPs to generate sine signals at 915 MHz with random phase at each *on* duration of the duty cycle, as defined by the DCRP scheme. The period time for the experiment has been set to $T = 42$ ms, with a duty cycle of $D = 0.5$. To compare our approach, we have also configured the USRPs to implement an orthogonal method. Accordingly, these transmit FDMA signals in the 915 MHz ISM band. FDMA also implements a duty cycle of $D = 0.5$ (See Fig. 7.4), such that we evaluate the performance improvement due to the random combination of waves, rather than the effect of the duty cycle. Provided that the system performance is evaluated as a function of the input power at the receiver end, distributed beamforming is not implemented. The gain that these approaches offer is based on the constructive combination of RF waves over the RF medium. Hence, for a given received power, distributed beamforming shows no difference with respect to a single, constant transmission. The performance improvement of these approaches are found at the transmitter end, where an improvement of m, with m being the number of ETs can be achieved [94]. The output of USRPs is fed into 3 Watt MPA-0850 RF power amplifiers from RF Bay [62], which amplify the USRP signals and generate high power RF waves in a range that can be harvested by P1100 Powercast harvester (i.e., in the order of -10 dBm to 0 dBm at the receiver location).

At the receiver end, a P1100 Powercast energy harvester is connected to a receiving antenna. This is located at a close distance of the ETs and the re-

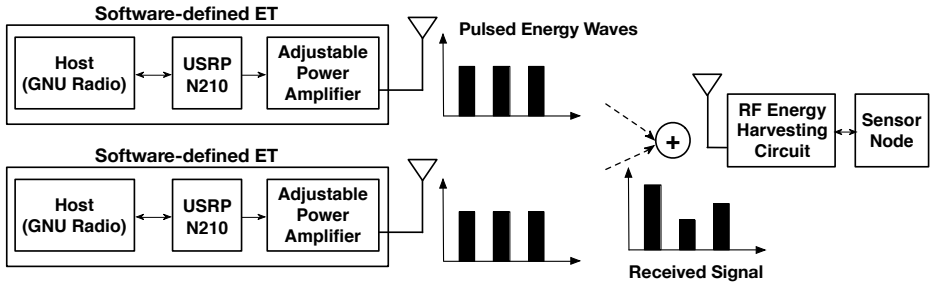

Figure 7.8: Experimental setup block diagram.

ceived power is adjusted by controlling the transmitted power at the ETs. At the output of the energy harvester, we have connected a 100 mF super-capacitor. To evaluate the performance of each energy multiplexing method for wireless RF power transmission, we have calculated the charging time that it takes to charge the capacitor from 0 V to 3.2 V. The charging time of the capacitor is a valid metric to evaluate the performance of the energy harvester, since it is inversely proportional to the output power of the energy harvester [125].

The block diagram of this experimental setup is shown in Fig. 7.8. As depicted, two ETs transmit RF waves, which combine over the wireless medium and arrive at the receiver end.

Experimental Results

We have first evaluated the input power at the energy harvesting sensor. An example of the received signal can be observed in Fig. 7.9. The figure shows the whole experiment timeline (top plot) and magnified view of input signal (second plot from top) in $W^{1/2}$ units. As predicted, the DCRP generates a random amplitude signal at the input of the energy harvester. In addition, the figure also shows the calculation of the input power, and the output power for the P1110 Powercast energy harvester. The positive impact of random amplitudes can be observed in the figure, since high power bursts are able to deliver output power and the other bursts are not efficiently converted.

As a second measurement, we compare in Fig. 7.10 the received signal at the energy harvester when using FDMA and DCRP, both transmitting with a duty cycle $D = 0.5$. The obtained results are compared to the ideal results, derived in Sec. II. The efficiency is estimated through an on-line mapping of the efficiency

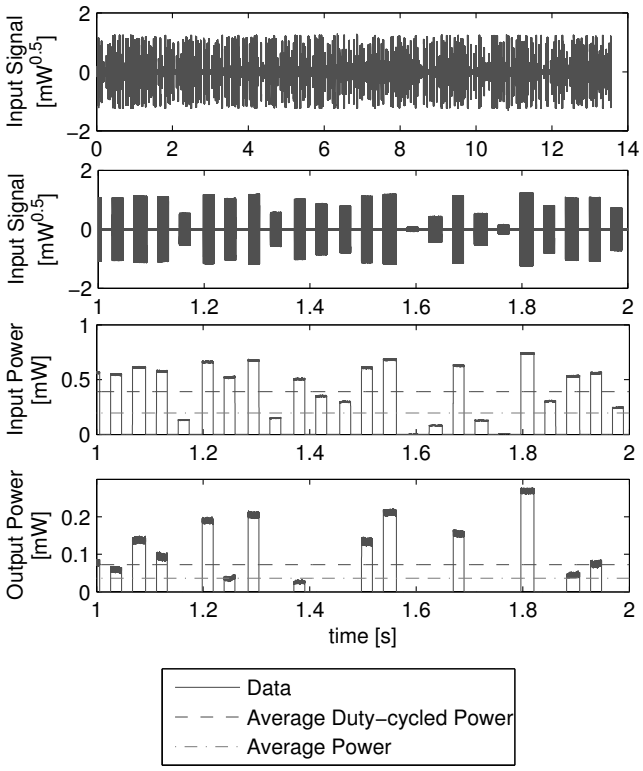

Figure 7.9: Reception of signal and its instantaneous power using DCRP. From top to bottom: input signal, a magnified view of the input signal, received instantaneous input power and efficiently harvested instantaneous power.

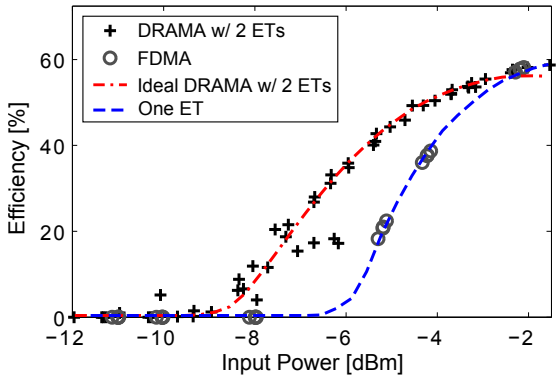

Figure 7.10: Comparison of the extrapolated efficiency curve as a function of the input power for the experimental evaluation of the DCRP scheme with two ETs to the orthogonal FDMA scheme.

curve of Powercast P1110 energy havester. As it is shown, the DCRP model coincides with the obtained results, whereas we observe that FDMA with two ETs achieve the same performance than using one ET, which transmits energy using a single frequency. This is because FDMA avoids the generation of interferences. Notice that there is a down-shift of -3 dBm for both cases, which is given by the use of a duty-cycled signal of $D = 50\%$.

Finally, we calculate the capacitor charging time. In Fig. 7.11, we show the charging voltage curve as a function of the time for DCRP and FDMA for the input RF powers of $P_R = \{-1,\ -5\}$ dBm. As it is observed, DCRP is able to charge the capacitor at a faster speed than FDMA. In addition, the time difference at -5 dBm is very significant. This is consistent with Fig. 7.7, since DCRP is able to improve the efficiency of the energy harvester efficiency at lower input powers.

In order to better compare these results, Fig. 7.12 shows the charging times as a function of the input power of the two energy multiplexing methods for wireless RF power transmission. We observe that DCRP is able to charge the energy storage capacitor at the sensor node at a faster speed. In fact, DCRP reduces the charging time by 23%. Alternatively, we observe that the energy harvester requires approximately from 5 to 6 dB less input RF power to charge the capacitor considering equal charging times, when comparing the DCRP method to FDMA. This reduction in the required input power is very important and results in increasing the power transmission distance. For example, an improvement of 6 dB in the path-loss behavior of a wireless power transmission equals to double

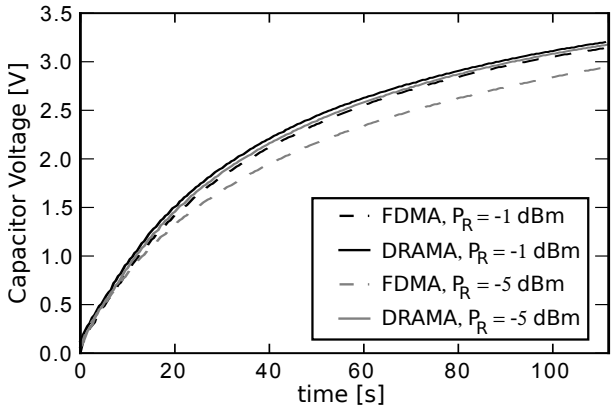

Figure 7.11: Comparison of the capacitor charging curve between DCRP and FDMA, for different values of input power.

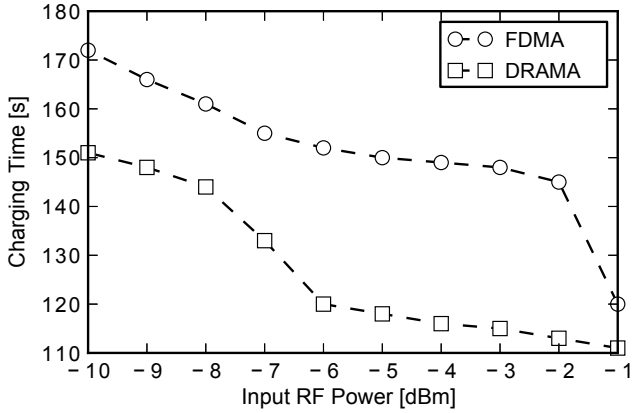

Figure 7.12: Comparison of the charging times as a function the input power for DCRP and FDMA.

the transmission distance in free-space conditions.

7.5 Network-level Evaluation

In this section, we evaluate the scenarios of many (ETs)-to-many (sensors) power transmission, and provide results for larger network sizes. The aim of this study is to model the effective energy that can be harvested at any possible location within the networking area. The many-to-many level simulation utilizes the experimental results which have been obtained in the previous sections and extrapolates the behavior in a networking area. We describe next the simulation setup and

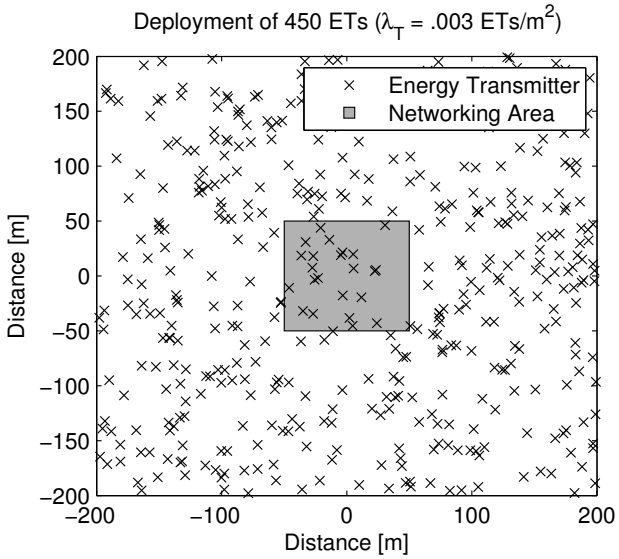

Figure 7.13: Deployment of ETs in the simulation framework. ETs are deployed over a larger area than the networking area of the sensors to avoid edge effects in the simulation.

present the simulation results.

7.5.1 Simulation Setup

We model the spatial distribution of the ETs according to a homogeneous Poisson point process in the two-dimensional plane. The probability of m ETs being inside an area A (not necessarily connected) is given by [75]:

$$\Pr\{m \text{ in } A\} = \frac{(\lambda_T A)^m}{m!} e^{\lambda_T A}, \quad m \geq 0 \tag{7.23}$$

where λ_T is the spatial density of ETs, in ETs per unit area. We have deployed the ETs over an area of 400x400 m^2, centered in $(0, 0)$. Recall that the average distance between neighboring ETs can be approximated by $\sqrt{1/\lambda_T}$.

We model the deployment area of sensor nodes as a 100x100 m^2 square area centered in $(0, 0)$. In this area, 400 uniformly distributed "sensors" or probe points are deployed. These probe points are entitled to model the energy that would be effectively harvested at any location of the networking area if a sensor is deployed there. Accordingly, the input power is sensed at each probe point and the input-to-output power conversion efficiency is computed.

The deployment area has been intentionally considered to be smaller than the area of deployment of the ETs. This avoids possible edge effects at the borders of the area under interest. We repeat each simulation 100 times. Fig. 7.13 shows an example of a deployment of ETs over the simulated area, for the particular case of $\lambda_T = .003$ ETs/m^2. We have referred the portion of area where the probe points, or "sensors", are deployed as networking area.

The ETs implement three energy multiplexing schemes for wireless RF power transmission. First, an ideal orthogonal method is considered that mitigates interferences between RF waves and guarantees perfect channel allocations. Accordingly, it ensures that the overall received power at the node locations equals to the sum of power of the considered ETs. Then, an ideal distributed beamforming approach is implemented. This guarantees that RF waves constructively combine at all node locations, maximizing the power transmission. This approach requires MISO set-ups (i.e., ETs equipped with multiple antennas and sensors with single antennas) with a minimum of k antennas at each ET, where k being the number of nodes, and node to ET data CSI feedback. Given that this optimized approach requires large hardware complexity and node to ET communication, we will consider this approach as an upper bound for our considered multple access method for wireless RF power transmission. Finally, DCRP is implemented. The three considered approaches assume a duty cycle of $D = 0.5$. The commercial site-general [2] channel model has been considered.

The simulation results are evaluated in terms of the percentage of powered area. This metric evaluates the extent of deployment area, wherein a sensor node is able to efficiently harvest at least the minimum power required for its operation. In this work, the minimum required efficiently harvested power has been set to $P_{H0} = 10$ μW, which is a reasonable target for low-power devices [121, 131]. In order to calculate the powered area, we approximate it to the number of probe points which are powered, since it is well known that if the number of probe points is large, and these are uniformly distributed in an area A, the probability that a probe point receives enough power converges to the following relation between powered area A_P, and the overall area A [143]:

$$\Pr\{P_{Hj} > P_{H0}\} \rightarrow \frac{A_P}{A}, \tag{7.24}$$

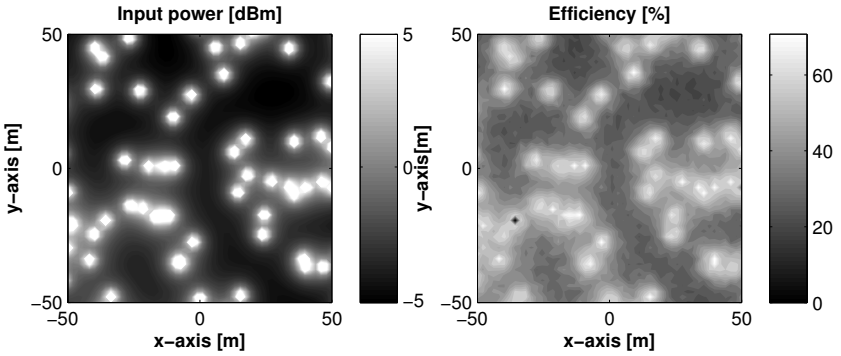

Figure 7.14: Network-level simulation. Input power and achieved efficiency at the probe point locations.

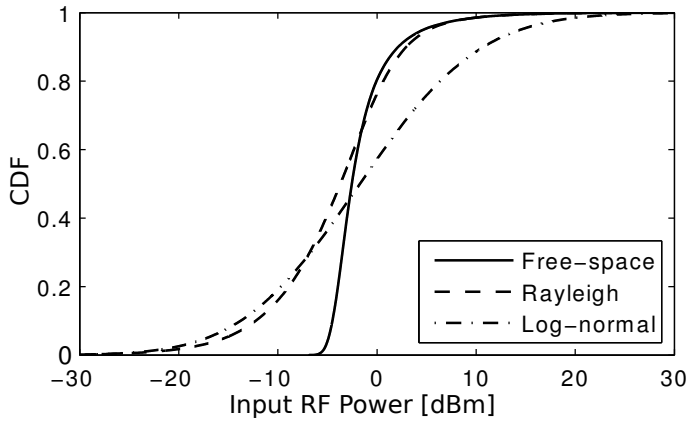

Figure 7.15: Cumulative distribution function (cdf) of the input RF power for different channel models.

where P_{Hj} refers to the power that a sensor node harvests at an arbitrary location.

7.5.2 Simulation Results

We first show in Fig. 7.14 a simulation example. This example shows the available input power at the 400 uniformly located probe points (left). We observe that the input power is distributed in a wide range, which covers from -5 dBm to more than 5 dBm. In addition, it also shows the efficiency of the energy harvested at a given location. As it is observed, the efficiency is largely correlated to the input power, being maximum in the neighboring of the ETs.

Then, we show in Fig. 7.15 the cdf of the input power at the probe points, for

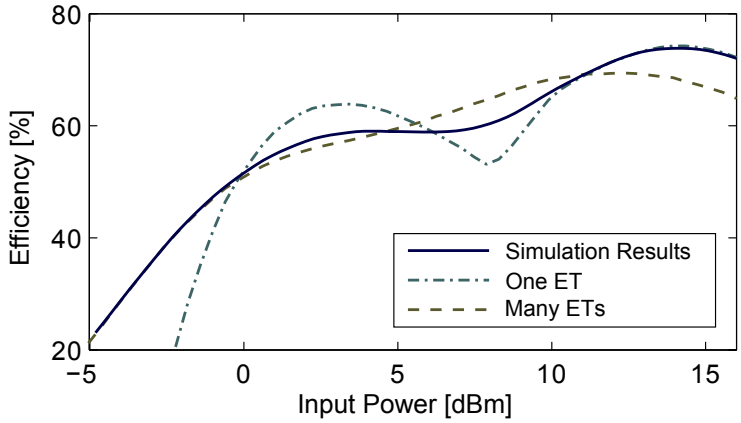

Figure 7.16: Simulated efficiency curve in a many-to-many topology as a function of the input power for the DCRP. It approaches the many ETs and single ET curves at low and high input powers, respectively.

different channel models, namely free-space, Rayleigh channel and log-distance path loss model with $\sigma = 9$ dB, which is a reasonable value for indoor RF propagation at the 915 MHz band [117]. To obtain these results, we have assumed a density of $\lambda_T = .005$ ET/m^2 (i.e., an average distance between ETs of approximately 14 m), and that each ET is transmitting a fixed power of $P_T = 3$ W and as it is observed, the input power present a very large deviation, as predicted from the α-stable distribution model [143]. This large variation motivates the design of the DCRP scheme, since the actual received power range in the deployment area is significantly wide.

We show in Fig. 7.16 the simulated efficiency curve that sensors find in the network. As observed, the efficiency of the energy harvesting front end approaches the numerically obtained curve for many ETs at low input powers. This is due to the fact that low input powers are obtained at probe points which are located at further distances from the ETs and thus, their received power is the combination of the action of many ETs. Further, we see that at moderate input powers, the obtained efficiency is located between the efficiency curves. The reason is that at moderate distances, the probe points receive power from just a few ETs. Finally, we observe that the probe points which receive large input powers receive this power from a single and very close ET. As a result, the efficiency approaches the *one ET* case, which at higher input power is slightly better than *many ETs* case.

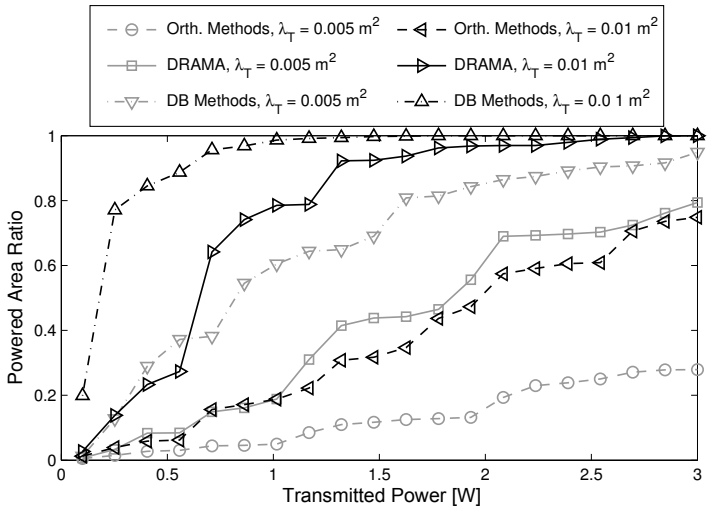

Figure 7.17: Comparison of the powered area as a function of the input power for the DCRP scheme to a orthogonal power transmission.

In Fig. 17, we show the ratio of area that receives a power larger than the threshold as a function of the transmitted power. The three considered energy multiplexing methods have been considered, namely a generic orthogonal method (referred as orth. methods), DCRP and distributed beamforming methods (referred as DB methods). As it is observed, orthogonal methods cannot entirely cover the networking area in our considered set-up. In particular, orthogonal methods achieve a ratio of approximately 0.8 for a $\lambda_T = 0.01$ m^{-2} (i.e., an approximated distance between ETs of 10 m) with an allocated power at the ETs of $P_T = 3$ W. Distributed beamforming methods show an outstanding performance in terms of powered ratio, rapidly approaching full coverage. It is observed that a ratio of powered area of 0.8 is achieved for either values $\lambda_T = 0.005$ m^{-2} and $P_T = 3$ W or $\lambda_T = 0.01$ m^{-2} and $P_T = 1$ W. Accordingly, the major benefit of distributed beam forming techniques is observed at larger values of λ_T, since it is able to constructively combine a larger amount of RF waves. Our proposed approach shows an intermediate performance, rapidly approaching distributed beamforming techniques as the density of deployed ETs increases. Accordingly, DCRP approximately offers the same system performance as orthogonal methods by requiring just the 50% of the resources employed in orthogonal methods, and stands as a feasible, cost-effective alternative to distributed beam forming.

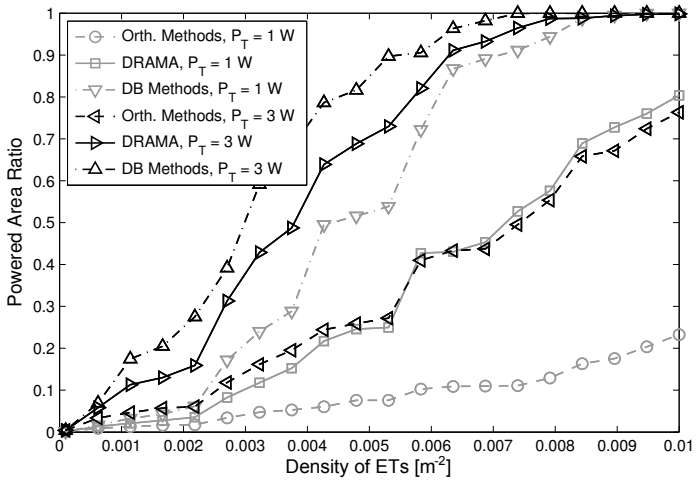

Figure 7.18: Comparison of the powered area as a function of the ET density for the DCRP scheme to an orthogonal power transmission.

Alternatively, we observe in Fig. 7.18 the ratio of area that receives sufficient power as a function of the density of ETs. In particular, we see that considering the DCRP with $P_T = 1$ W offers a similar performance than orthogonal methods with $P_T = 3$ W. In addition, we observe that the performance of DCRP with $P_T = 3$ W is lower and upper bounded by distributed beamforming approaches with transmitted powers $P_T = 1$ W and $P_T = 3$ W, respectively.

To better depict the dependence between the ET density, the transmitted power and the percentage of powered area, we show in Fig. 7.19 this relation for the three energy multiplexing approaches for wireless RF power transmission. As it is observed, the DCRP outperforms orthogonal methods and approaches the ideal operation of distributed beamforming methods, while requiring relaxed synchronization between ETs and single transmitting antennas.

Overall, we find that DCRP offers similar performance as CI methods and far better than classic orthogonal approaches.

DCRP yields significant benefits over orthogonal approaches, since it is possible to reduce both transmitted power and ET density, while still providing the same performance. This reduction of transmitted power and ET density is directly related with the deployment costs of the sensor network, its maintenance overhead and environmental impact.

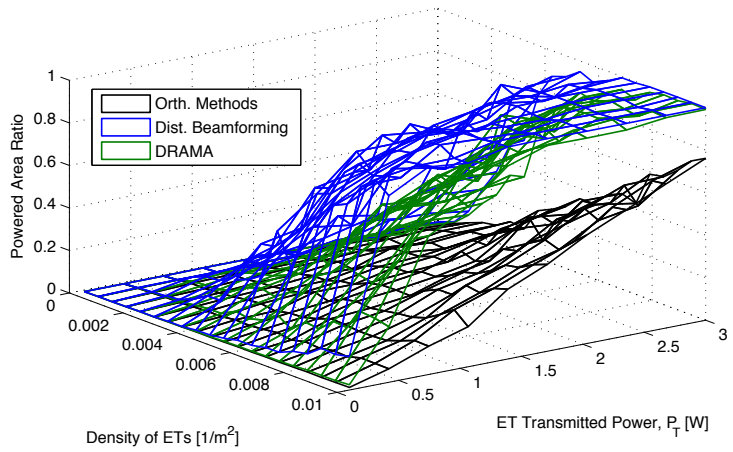

Figure 7.19: Comparison of the powered area as a function of the input power and ET density.

7.6 Summary and Conclusion

In this chapter, a duty-cycled random-phase energy multiplexing (DCRP) scheme for wireless RF power transmission is proposed. This scheme optimizes the wireless RF power transfer in a many (ETs)-to-many (sensors) transmission, and enables low-power wireless power transmission in a many-to-one configuration. The DCRP is compared to orthogonal energy multiplexing schemes for wireless RF power transmission, namely FDMA, through both real-testbed experiments and simulations. We demonstrate that, according to our results, the DCRP has two-fold benefits: first, it can potentially reduce the deployment costs of ETs of up to 50%, and second, it improves the efficiency of the power conversion at the node locations. The proposed approach shows 23% increase in the efficiency of the harvested energy in an experimental setup.

Chapter 8

Communications over Wireless RF Power Transmission

8.1 Introduction

Using the RF spectrum for both energy and data transfer may seriously affect network operations and performance, and require sophisticated hardware and devices that many systems cannot afford. For instance, transmitting energy and data on different frequencies [101] would require multiple or broadband access capabilities, since the frequency gap between energy and data communications cannot be very small [96]. Alternatively, when both energy and data share a single band, specialized MAC protocols are required [97]. In both cases, devices should feature two separate RF front-ends, for decoding the information and converting RF energy into DC [111]. Therefore, devising methods for energy provisioning without affecting data communications appears to be the challenge to tackle [48]. For instance, transmission of both point-to-point energy and data enables downlink communications from a base station (BS) to a node [82]. This is also beneficial in terms of hardware costs, since the signal receiver can be integrated in the energy harvester [149]. For uplink communications full duplex techniques have been proposed where the BS is able to simultaneously transmit energy and receive information on the same frequency [72]. However, enabling communication among network nodes while an ET is transmitting power still needs to be investigated [144].

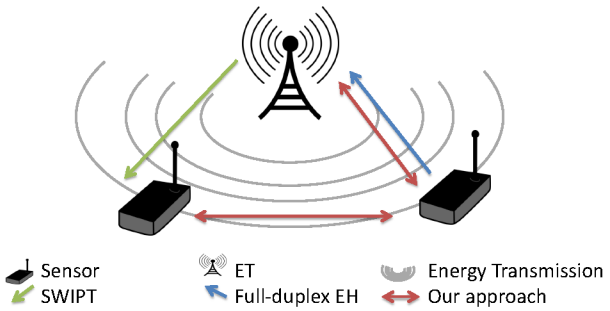

Figure 8.1: Contextualization between the proposed CoE and existing simultaneous data and energy transmission technologies.

In this chapter, we propose a new method for concurrent in band transmission of data and energy, where nodes exchange data among each other while being re-charged by ETs at the same time. The proposed method relates to other simultaneous data and energy transmission technologies as shown in Fig. 8.1. In particular, we compare our approach referred as Communications over wireless Energy (CoE) to SWIPT [82] and full-duplex EH [72].

In CoE, the combined signal at the antenna of the receiving node is characterized by a large bias component (generated by the transmission of energy) with small fluctuations (caused by the overlapping data). In order to enable successful data reception we decode the information by using the built-in energy detection properties of energy harvesters. This detection intermodulates both data and energy signals, amplifying the data signal through the action of the ET as a remote data signal amplifier. Then, a novel physical layer technique is designed to mitigate the data and energy phase misalignment.

The main contributions of this chapter are as follow.

- We present a communication model for data reception through energy harvesters, providing insights on the treatment of the signal through the action of the energy harvester.

- We validate this model by testbed-based experiments using off-the-shelf hardware, showing the simultaneous recharging of a node as it efficiently decodes data signals through its energy harvester.

- We develop a new physical layer technique to mitigate the obstacles that

our approach brings towards guaranteeing a successful point-to-point packet delivery.

The rest of the chapter is so organized. In Section 8.2 we describe the fundamentals of our Communications over wireless Energy (CoE) scheme. Section 8.3 presents a communication model for the energy harvester. In Section 8.4 we experimentally validate the proposed communication model. In Section 8.6 we describe a physical layer to enable reliable point-to-point communications. The corresponding link is evaluated in Section 8.7. Finally, Section 8.8 concludes the chapter.

8.2 Communications over Wireless Energy

This section defines our Communications over wireless Energy (CoE) scheme and describes the network topology that enables it.

8.2.1 Overview

We consider an RF wireless powered point-to-point link, made up of three components: An energy transmitter (ET), a transmitting node, and a receiving node. The purpose of the ET is to transmit power to the nodes. The nodes implement CoE to communicate between them.

The key idea of CoE is that of overlapping the simultaneous transmissions of data and energy in such a way that both transmissions can be successfully recovered at the receiving node. To do this, the transmitting node superimposes a low-power RF signal that modulates the envelope of the energy transmission, basically using the ET as a remote data signal amplifier (RDSA). The energy transmission is expectedly orders of magnitude larger than the power of the data transmission. To obviate this imbalance, the receiving node opportunistically utilizes the nonlinear properties of its energy harvester to intermodulate both transmissions, extract the data signal and retain the harvested energy.

This approach brings several benefits to the node. First, it reduces system complexity, as the node can be equipped with only one antenna and a single RF front-end for both data and energy reception. Second, the action of the ET as RDSA removes the need for an internal RF amplifier.Third, it enables

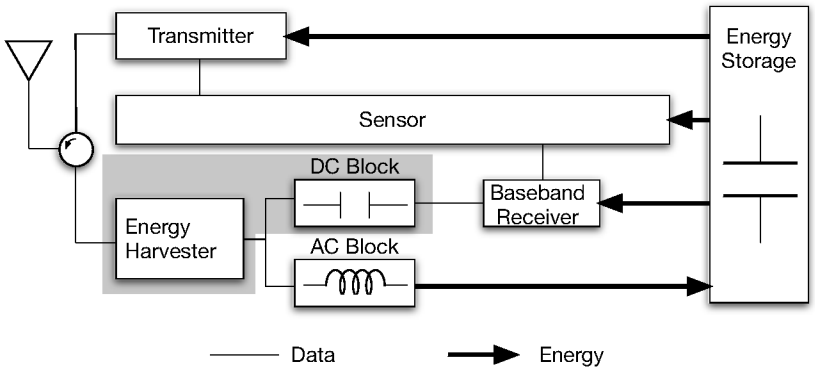

Figure 8.2: A CoE node.

low-power coherent signal reception without power hungry components (e.g., RF mixers). Finally, given that data and energy transmissions are simultaneous, the complexity of the MAC layer is reduced.

8.2.2 Design of a CoE transceiver

Designing a CoE device requires addressing two major challenges. First, the power required to implement CoE operation should be as low as possible, to enable energy neutral operations. Second, devices must be able to tolerate differences of orders of magnitude between the power of the simultaneous data and energy transmissions.

Fig. 8.2 shows the block diagram of a device with CoE. Since the transmitter and the energy harvester both use the same RF frequency, they are connected to the same antenna. The harvester is in charge of converting the RF energy into electric current to power the sensor, as well as of acting as an RF front-end for signal reception. (The communication data path in reception is showed in gray.)
Transmitter architecture. The design of the transmitter is not particularly challenging, and state-of-the-art wireless transmitters can be used to transmit data to the receiving sensor, since signal overlapping is performed at the antenna of the receiving node. Each transmitting node (i.e., the ET and a node) just generates an RF wave that is wirelessly propagated to the destination antenna.
Receiver architecture. Designing a CoE data receiver is challenging since the RF waves overlap at the receiving antenna. Therefore, this antenna must be able to separate the two transmissions, and do it with as little power as possible. To

address these challenges we use an energy harvester as both data and energy receiver. The idea is that of leveraging the energy transmission to amplify the data transmission, thus eliminating the need of power hungry signal amplifiers and performing a coherent RF baseband downconversion where oscillators are no longer required (Section 8.3.1).

8.3 Energy Harvesters as Data Receivers

In this section we describe a communication model for energy harvesters that are used as signal receivers for CoE, where the signal is recovered by sensing the output current of the energy harvester. The aim of this model is to help understanding why the energy harvester is suitable for data reception. Our model divides the action of an energy harvester as a signal receiver into conventional communication blocks and provides a high-level explanation of the reception process. The model is shown in Fig. 8.3.

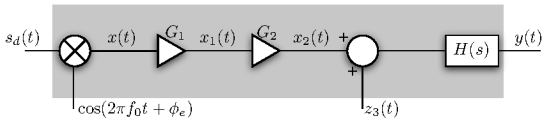

Figure 8.3: Communication model of a CoE energy harvester as a signal receiver.

It is made up of five components: A 1D homodyne receiver, two amplifier stages (G_1 and G_2), additive noise and an output low-pass filter.

8.3.1 Extracting the low-power overlapped information

The input power detection of an energy harvester used as a signal receiver for CoE implements the following two communication blocks.

- A 1D Homodyne receiver. The received RF signal is converted to baseband. Given that this unit is one-dimensional, only data arriving at the receiver in-phase with the energy transmission is received.
- An amplifying stage of gain $G_1 = 2\sqrt{\frac{P_e}{P_d}}$, where P_e and P_d are the received power from the energy and data transmissions, respectively.

The energy harvester operates as a power processing circuit that converts the available power received by the antenna into an electrical current, so that an energy storage unit can be recharged. Unlike signal processing circuits, power processing circuits maintain the relation between input and output power, determined by a certain efficiency. By assuming a fixed antenna impedance and a fixed output voltage, we observed that its output current is proportional to its input power. Therefore: $I_{out} = \beta V_{in}^2$, where β is a constant that depends on the electrical properties of the energy harvester (among others, its input-to-output power conversion efficiency), the input impedance of the circuit and the impedance matching. The RMS value of the generated voltage at the antenna V_{in} is such that $P_{in} = V_{in}^2/R_a$, with R_a being the antenna impedance.

At the receiving node, both energy and data signals are received simultaneously. First, the transmitted data signal arrives at the receiving end as:

$$s_d(t) = \sqrt{2P_d}\left[b_I(t)\cos\left(2\pi f_0 t + \phi_d\right) - b_Q \sin\left(2\pi f_0 t + \phi_d\right)\right] \tag{8.1}$$

where P_d is power received from the data signal, f_0 is the carrier frequency, and ϕ_d is the phase shift of the data at the receiving node. The phase and quadrature components of the baseband data stream, b_I and b_Q, are such that $E[B] = E[b_I + jb_Q] = 0$ and $E[|B|^2] = 1$, where $E[\cdot]$ is the statistical expectation. Then, the transmitted energy, characterized as a large power carrier wave, arrives at the receiver node as:

$$s_e(t) = \sqrt{2P_e}\cos(2\pi f_0 t + \phi_e), \tag{8.2}$$

where P_e is the received power from the energy signal and f_0 stands for the carrier frequency. Notice that the carrier frequency of both transmissions are the same.

The energy harvester performs power detection, which is transferred to the output in form of current. The input power can be calculated as:

$$x_1(t) = \left|s_d(t) + s_e(t) + z_1(t)\right|^2, \tag{8.3}$$

where $z_1(t)$ is the additive white Gaussian noise (AWGN) generated at the receiving antenna, with power P_{N1}. By substituting s_d and s_e from equations (8.1) and (8.2), respectively, neglecting the high-frequency terms (i.e., the terms at

frequency $2f_0$), and assuming $P_e \gg P_d$, we can approximate Equation (8.3) by:

$$x_1(t) = P_e + 2\sqrt{P_d P_e}\, \Re\left\{B(t)e^{\phi}\right\} + z_2(t), \tag{8.4}$$

where P_e is the data signal received power, B indicates the modulated information, ϕ is the phase shift between the energy and data transmissions, and $z_2(t)$ is the noise at the output of the energy harvester due to the antenna noise, defined as $z_2(t) = 2\sqrt{P_e P_{N1}}\, \Re\left\{z_1 e^{j\phi_e}\right\}$.

Counter-intuitively, decoding data during the transmission of energy shows significant benefits, as it performs a coherent reception and because the dual action of the ET as RDSA amplifies the data signal.

8.3.2 Power-to-current (P-I) gain

The detected signal is converted into small variations of the electrical current generated by the energy harvester. Even though, this conversion is ideally linear, it has been experimentally observed that the efficiency of the energy harvester is input-power dependent [27]. In general, we find that the output current is characterized by the power to current transconductance g, and it can be written as:

$$I_0 + x_2 = g(P_e + x_1(t)), \tag{8.5}$$

where I_0 is the constant component of the output current of the energy harvester and x_2 refers to its small signal fluctuations (Fig. 8.3). To derive the small signal gain, we approximate this function by its first order Taylor polynomial:

$$I_0 + x_2 \approx g(P_e) + \frac{\partial g}{\partial P}(P_e)x_1, \tag{8.6}$$

where $\frac{\partial g}{\partial P}(P_e)$ is the derivative of $g(\cdot)$ with respect to the input power evaluated in P_e. As a result, the P-I gain G_2 is:

$$G_2 = \frac{\partial g}{\partial P}(P_e). \tag{8.7}$$

Fig. 8.4 plots the gain G_2 (Equation (8.7)) for the Powerharvester P1100 from Powercast Co. [33].

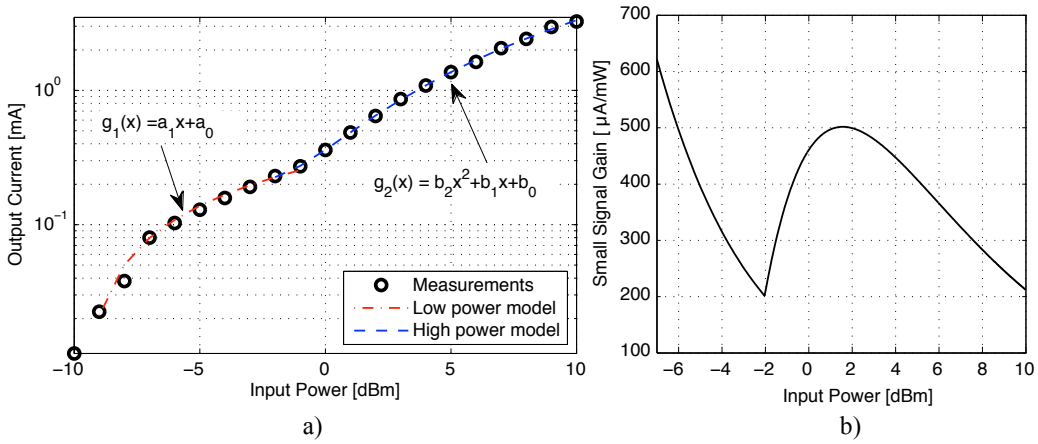

Figure 8.4: (a) Characterization of the output current of the Powerharvester P1100 [33]. (b) Calculation of its small signal gain G_2.

To obtain this curve, we have first measured its input power to output current relation (Fig. 8.4 (a)). The output DC current is modeled by a piece-wise function, with two distinguishable regions of operation. At input powers < -1dBm the output current, as a function of the input power (in dBm), can be modeled with the first order polynomial $g_1(x)$. At high input power it can be modeled by a second order polynomial $g_2(x)$:

$$g_1(x) = 2.935x + 0.2843 \text{ [mA/dBm]}. \tag{8.8}$$

$$g_2(x) = 1.912x^2 + 0.1058x + 0.3607 \text{ [mA/dBm]}. \tag{8.9}$$

We then calculate G_2 as the partial derivative of the obtained piece-wise function with respect to the input power (Fig. 8.4 (b)). Notice that this must be calculated in linear units, instead of dBm. We observe that the gain G_2 depends on the input power of the energy signal and it ranges from 200 μA/mW to 600 μA/mW.

8.3.3 Additive noise

As the noise that an energy harvester generates depends on the circuit topology, devices and design, it is not possible to provide a generic closed-form expression. As a consequence, the estimation of these values has to be performed either at circuit design time or by experimentation. Notice that current energy harvesters

do not target signal processing applications, and therefore, these are not optimized for low-noise. We expect that custom circuit design for CoE applications will lower the overall noise. According to our experiments (Section 8.4), we have measured a combined energy harvesting and measurement system noise characterized as AWGN with spectral density of -80 dBmA/Hz.

We refer as Z_3 to the overall induced noise of the system, this is given by:

$$Z_3 = Z_{EH} + G_2 Z_2, \tag{8.10}$$

where Z_{EH} is the internal noise, and $G_2 Z_2$ represents the contribution of the antenna noise after the P-I conversion stage.

8.3.4 Output filter

As the main purpose of energy harvesters is to regulate the output voltage, their circuits contain a relatively large output equivalent capacitance to provide a stable output. Unfortunately, this parallel capacitance at the output of the energy harvester limits the bandwidth of the output current, hence limiting the maximum achievable bit rate. To model this last output stage, we find that the effective output current of an energy harvester is low-pass filtered by:

$$H(s) = \frac{Z_0}{Z_0 + Z_{sense}}, \tag{8.11}$$

with Z_0 being the output impedance and Z_{sense} is the associated input impedance to the current sensing and energy storage unit. According to our experiments, the output impedance of a Powerharvester P1100 from Powercast Co. [33] is capacitive with capacitance $C_L = 5.5$ μF. Then, we have utilized a resistor as Z_{sense} to sense variations in the output current, which has ranged between 1 Ω and 100 Ω.

In this case, the output filter becomes a first order low-pass filter, given by:

$$H(s) = \frac{\tau}{s + \tau}, \tag{8.12}$$

where $\tau = R_{sense} C_L$. In our experiments, the cut-off frequency of the output ranges from 11.4 kHz (using $R_{sense} = 1$ Ω) to 1.14 MHz (when $R_{sense} = 100$ Ω).

8.3.5 Decoding the symbol

Once the signal is extracted, a baseband receiver must decode signal levels into a binary stream. We consider two main decoding alternatives.

Comparator-based decoding. By employing a comparator-based decoder, the received signal is compared against a given threshold, thus providing only two logic values. This is the most basic implementation of a signal receiver and shows significant advantages in power saving (offering a power consumption < 1 μW as reported in the literature [84]). However, these circuits suffer from low-performance, since no advanced signal processing techniques can be implemented.

ADC-based decoding. As a more advanced technique to recover information, the receiving sensor can implement analog-to-digital converters. This option requires a significantly larger amount of energy but enables the use of more advanced signal processing tools to improve signal quality. Power consumption in state-of-the-art micro power ADC in the order of a few tens of μW have been reported [137].

8.4 Proof of Concept

In this section we develop a CoE receiver using off-the-shelf hardware, and evaluate the model from Section 8.3 and its performance.

8.4.1 Implementation design and experimental set-up

Our experimental set-up is shown in Fig. 8.5.

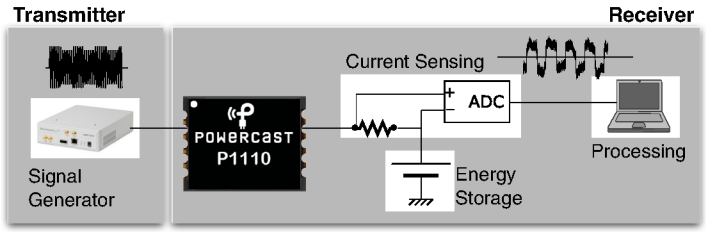

Figure 8.5: Experimental set-up.

Transmitter set-up. We used a signal generator that generates both energy and data transmissions at a fixed frequency of 915 MHz. The energy transmission is composed of a sine wave with power ranging from -1 dBm to 4 dBm. We have

also implemented a BPSK modulation at a rate of 1 kbps for data transmission. The power of the data signal is in the range from -68 dBm to -48 dBm.

Receiver set-up. We base our signal and energy receiver on off-the-shelf energy harvester Powerharvester P1100 from Powercast [33]. This circuit offers a reasonable performance in the desired frequency band, with efficiency rates above 50% for input powers ranging from -5 dBm to 20 dBm. The output current as a function of the input power is shown in Fig. 8.4 (a).

The output of the energy harvester has been connected to a super-capacitor operating as energy storage and management unit of the overall circuit. This unit is in charge of providing continuous operation over time, and its design presents several trade-offs [23]. Given that we are not constrained by the size of the circuits, in this work we have employed a capacity of 220 mF to ensure a steady output voltage during data reception.

A series resistor has been employed to sense the output current of the energy harvester. These resistors provide outstanding current sensing performance due to their linear properties. Given that the sensing gain is related to the resistance value, larger values provide a larger gain. However, resistors increase power losses and increase noise. Through experimentation, we have observed that values between 1 Ω to 100 Ω offer a reasonable tradeoff between sensing gain and power losses. In Fig. 8.6 we show the power losses associated with using different resistor at different input power levels, and compare it to the harvested power considering a Powerharvester P1100 [33]. In addition, we show the ideal operation of an energy harvester (i.e., output power equaling input power, dashed line).

Signal decoding. We have implemented a software-defined, computer based signal receiver. In particular, we have implemented a 16 bit analog-to-digital converter (ADC) with a sampling frequency of 10 kHz. The combination of the sensing resistor with the ADC provides a signal gain of $G_3 = 1310$ mV/mA units. We expect baseband signal decoders for sensors used for low-power applications to be of much lower performance and probably implementing comparator-based schemes. Once digitized, a matched filter is implemented and the optimum sampling time is computed. Finally, the decision threshold is computed to perform signal detection, so that the bit error rate (BER) is minimized. Accordingly, this last communication block converts the sensed voltages into a binary stream.

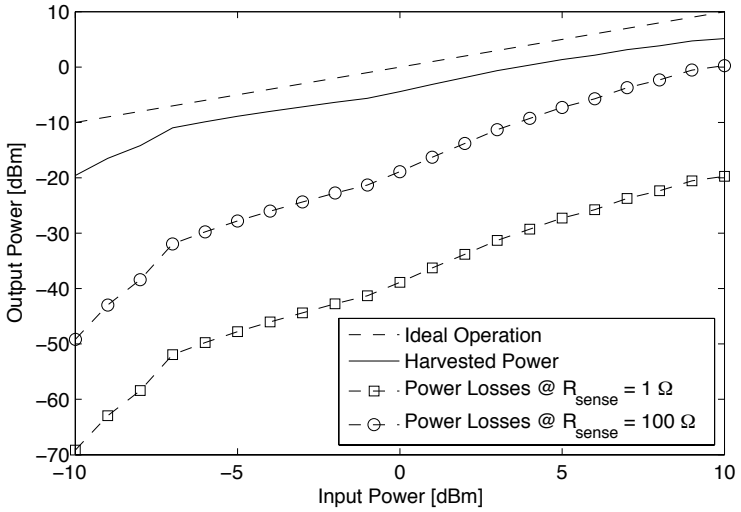

Figure 8.6: Power losses with different resistors vs. ideal operations.

8.4.2 Evaluation

To evaluate the validity and performance of this approach, we first perform proof-of-concept measurements. Then, we validate the communication model by observing the type of RF-to-baseband conversion and its gain. Finally, we evaluate the receiver performance as a function of the bit error rate (BER), by assuming a null phase shift between energy and data transmissions.

Proof of concept. We first validate the key idea that an energy harvester has built-in properties as a CoE signal receiver. Specifically, we measure the voltage drop at the current sensing resistor to detect the transmission of binary data. We set up a transmission of energy with a power of $P_e = 2$ dBm at a fixed frequency of 915 MHz. Overlapped to this RF wave, we transmit a periodic binary sequence, using a BPSK modulation with power $P_d = -49$ dBm and bit rate of 130 bps at the same center frequency of 915 MHz. This periodic binary sequence emulates actual data transmission.

Fig. 8.7 depicts the sensed voltage drop at the resistor.

The binary sequence can be recovered, showing two distinguishable voltage levels centered at 0 mV and with a voltage difference of approximately 8 mV (i.e., approximately 4 mV signal amplitude). This signal is compared to the expected sensed voltage according to the communication model (Section 8.4.2).

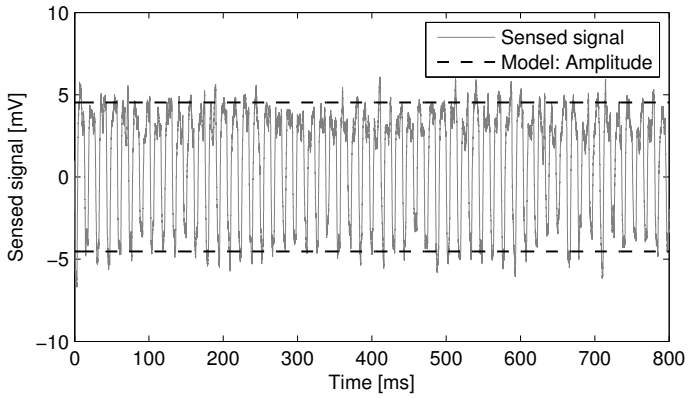

Figure 8.7: Recovered signal from an energy harvester used as data receiver.

In addition, we observe a certain ripple in the voltage levels of approximately 2 mV, which is a combination of the antenna, energy harvester and sensing noise. *Model validation.* In Fig. 8.8 we show the sensed peak-to-peak voltage at the input of the signal decoding unit.

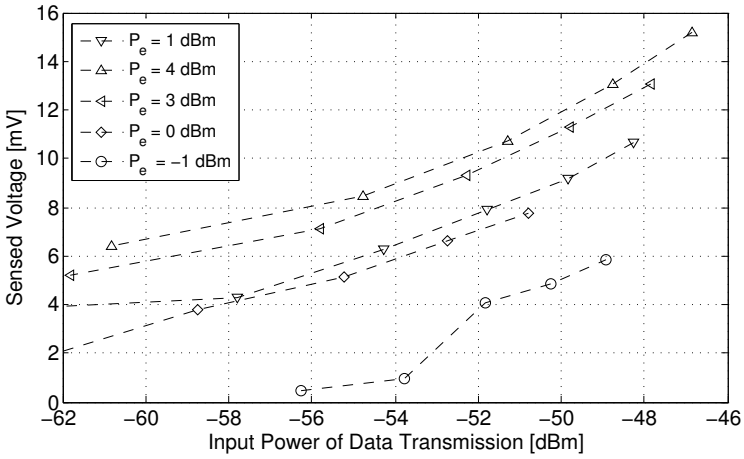

Figure 8.8: Peak-to-peak voltage difference at the input of the signal decoder as a function of the input power of both data and energy transmissions.

We observe the operation of the ET as RDSA, since the sensed voltage is effectively modulated by the received input power. In Fig. 8.9 we compare the sensed peak-to-peak voltage to the expected value according to our model. Our observation shows that the model is effective in predicting the sensed value with great accuracy in case for power $P_e = 1$ dBm. We also observe that as this power

grows, there appears a noticeable mismatch among the values. This is due to the fact that the small-signal approximation no longer applies for large values. Nonetheless, the value provided by the model is still within the same order of magnitude, thus still being useful for link budget calculations.

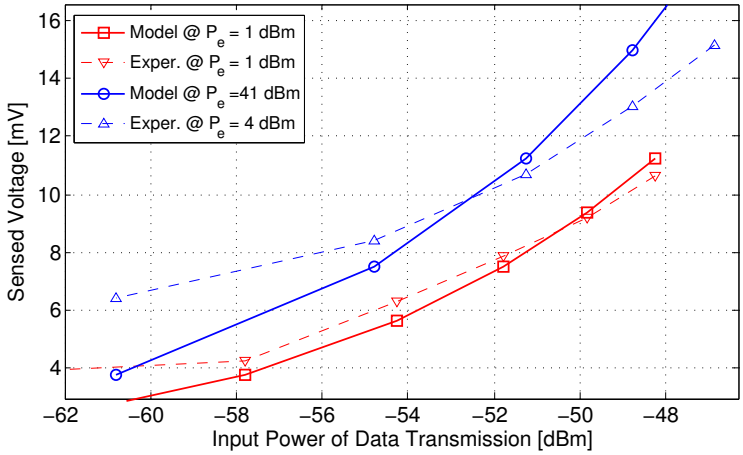

Figure 8.9: Model validation for the peak-to-peak voltage difference at the input of the signal decoder.

Calculation of the BER. We next evaluate the performance of the receiver for CoE. In particular, we measure the bit error rate (BER) observed when transmitting a raw binary sequence encoded in a BPSK modulation at a bit rate of 1 kbps. Given that a $BER < 10^{-2}$ can be considered enough in the context of device-to-device communications (when considering packet sizes of around 100 bits and implementing simple repetition coding [84]), we consider a $BER = 10^{-2}$ as our target. Additionally, we will refer as receiver sensitivity (in power units) as the minimum power that is required in order to obtain the targeted BER.

Fig. 8.10 shows the BER as a function of the power of the data transmission, for different values of power in the overlapped transmission of data and energy. In our experimental setup, we have obtained BERs confined around 10^{-3}. This has two main reasons: 1) The appearance of flicker noise in our current sensing platform, and 2) the lack of implemented delay-locked loop components to overcome temporal drifts. Implementing a signal amplification stage before the ADC unit can significantly improve the signal quality at the cost of higher power consumption. As shown by the figure, the intermodulation between energy and

data plays a key role in the performance of the device. Particularly, we observe that sensitivities of -53 dBm are required if the device is harvesting a power of $P_e = -1$ dBm, whereas this is reduced down to -65 dBm if the harvested power is increased just by 2 dB. The achieved performance using off-the-shelf hardware proves the feasibility of this approach and motivates further research in joint energy-data hardware design.

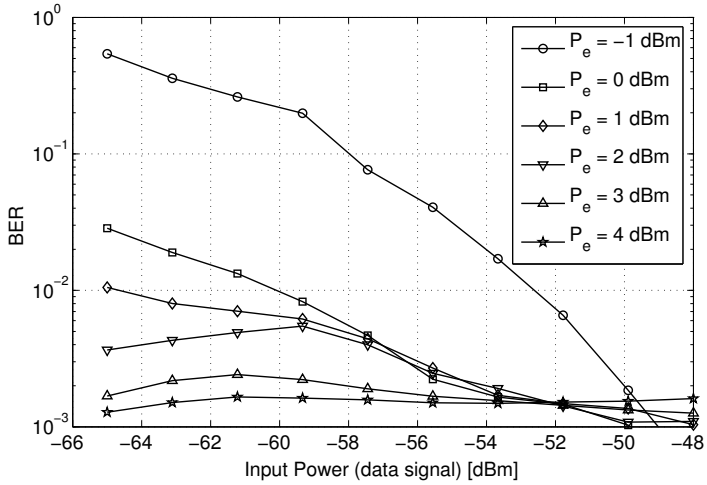

Figure 8.10: BER as a function of the input power of the data signal.

8.5 All-digital Design of a CoE Receiver

High-efficient energy harvesters integrate switch-mode DC-DC converters to optimize the operation of the rectifying stage [56, 34]. Their operation is based on harvesting an amount of energy and temporarily storing it in a low-leakage small capacitor. Once enough energy has been harvested, this is transferred in a form of a high amplitude, short time-scale energy pulse to the energy storage unit. Unfortunately, the non-linear packetization of the energy modifies the received waveform, hence making it difficult to integrate classical approaches for data reception in the energy harvester, such as the one presented in [149].

Here, we present an all-digital receiver architecture for low-bit-rate, ultra-low-power applications, where the digital signal used to control the switch-mode operation of the energy harvester is opportunistically employed to allow signal

reception through a digital counter. The key idea here is to leverage the period of the control signal to estimate the received information bit, by counting the number of times the current spikes are injected by the circuit.

8.5.1 Received signal

At the receiver end, an RF wave with incident average power P_H is sensed at the antenna. The average power is related to the required power to transmit a logical '1' and '0' as P_1 and P_0, respectively, by:

$$P_H = \frac{1}{2}(P_1 + P_0). \tag{8.13}$$

As a measure to relate the amount of energy that is being devoted to effectively modulate the information, we employ the modulation depth index, defined as:

$$h = \frac{P_1 - P_0}{P_1 + P_0}, \tag{8.14}$$

such that if $h = 1$ the transmission of a logical '0' is done through silence, whereas for $0 < h < 1$, the allocated power in P_0 accomplishes $P_1 > P_0 > 0$.

8.5.2 All-digital design

The considered energy harvester integrates two separated and generic stages for energy optimization [56]. First, a rectifying circuit is employed that can convert with very high efficiency the harvested power. Then, a DC-DC boost converter operating in discontinuous conduction mode (DCM) is considered to transfer the accumulated energy in a temporal capacitor towards the energy storage unit (i.e., a super-capacitor or battery). The control unit handles the operation of this converter. The configuration of the considered energy harvester topology is described in Fig. 8.11.

The aim of this dual-stage design is to optimize the transfer of energy by accurately matching the input impedance of the rectifying stage, which depends on its output load [100]. In particular, when connecting a rectifying stage for energy harvesting applications to an energy buffer, it shows a time-variable conversion efficiency, showing poor performance when the output capacitor voltage is either

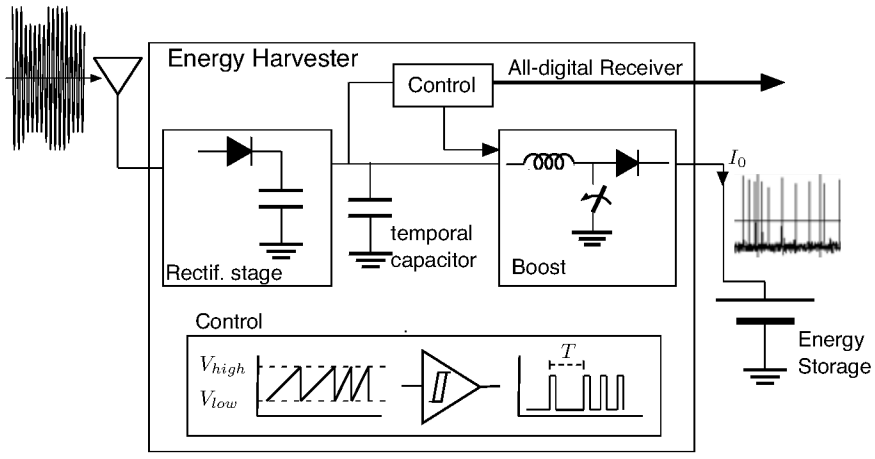

Figure 8.11: Internal operation of an energy harvester equipped with a DC-DC boost converter. The time between activations of the control unit is inversely related to the harvested power.

too low or too high [56]. For this, a small capacitor is connected to the output of the rectifier, which permits to rapidly skip the low-voltage operation regime (i.e., below V_{low} voltage level). When its output voltage surpasses a given threshold, V_{high}, the stored energy is high efficiently transferred to the output energy buffer through a DC-DC boost converter, leaving the voltage at the temporal capacitor at V_{low} voltage (the duration time of this action is referred as *on-time*). As such, we observe that the voltage of the temporal capacitor V_{cap} approximates a saw-tooth waveform [34], and the output current of the energy harvester is in form of short time-scale spikes. The operation of a dual-stage energy harvester is described in Fig. 8.11

We see that the period T of the saw-tooth waveform depends on the input power. In particular, the energy that is transferred each *on-time* is given by:

$$\Delta E = \frac{1}{2} C_{cap} \left(V_{high}^2 - V_{low}^2 \right), \tag{8.15}$$

where C_{cap} refers to the capacitance of the temporal capacitor. During the steady-state operation of the energy harvesting and neglecting the leakage current of the capacitor, the ΔE energy that is transferred to the output load equals to the energy that has been stored in the capacitor during the last period T. Both V_{high} and V_{low} are set as a design parameters to optimize the harvesting process, and we can assume that the energy during that time is harvested with optimal and

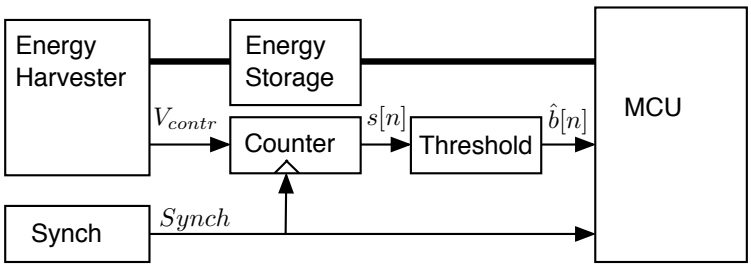

Figure 8.12: Block diagram of the integrated, all-digital receiver for SWIPT. It is based on counting the number of activations of the energy harvester control signal.

constant efficiency, η. Hence:

$$\Delta E = \eta P_i T \tag{8.16}$$

where P_i stands for the harvested power at a given time. By combining (8.15) and (8.16), we find that the period of the sawtooth depends on the input power as:

$$T = \frac{1}{2\eta P_i} C_{cap} \left(V_{high}^2 - V_{low}^2 \right). \tag{8.17}$$

We find that there exist 3 system parameters that can be tuned to optimize the operation of the energy harvester for both data and energy purposes, which are the selection of V_{high} and V_{low}, and the temporal capacitor C_{cap}. On the one hand, large values of C_{cap} or $V_{high} - V_{low}$ will increase the period time, hence reducing the eventual data-rate. On the contrary, reducing these values will increase the switching times and reduce the ΔE, hence potentially making the process less energy efficient.

The architecture of the all-digital receiver is shown in Fig. 8.12. It is composed of three separate units, namely a counter, a threshold comparator and a synchronization unit. The all-digital receiver leverages the control signal of the energy harvester that activates the DC-DC boost converter stage to estimate the power of the given symbol. To do this, the receiver simply counts the number of times that the control signal, V_{contr}, has been activated during the reception of a given bit, T_{bit}. The timing is provided by the synchronization unit through the *Synch* signal. Afterwards, the number of counts, $s[n]$, is compared to a threshold

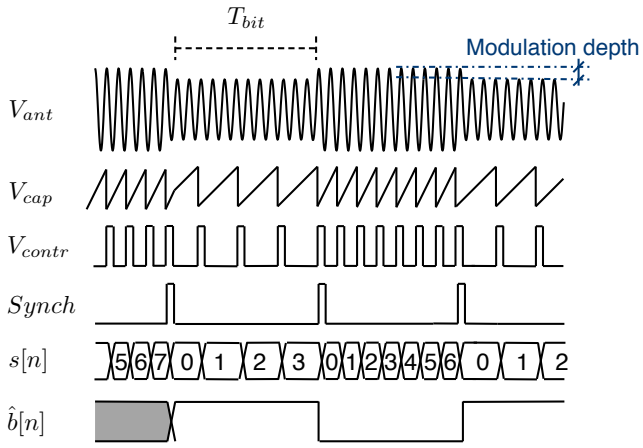

Figure 8.13: Internal operation waveforms of the all-digital receiver.

that decides whether the received symbol is a one or a zero. This last signal is referred as $\hat{b}[n]$. The synchronization unit is rendered key in the system functionality and it aims to determine the optimal sampling point. For this, similar digital-based approaches as in [91] may be implemented. However, this has been considered ideal in this work.

Fig. 8.13 describes the logical operation of the all-digital receiver. In the figure, we show the received signal at the antenna V_{ant}. This signal is harvested through the rectifying stage of the energy harvester and its power is transferred to the temporal capacitor. The control unit of the energy harvester activates the DC-DC boost converter through V_{contr}, which rapidly discharges the temporal capacitor and showing a saw-tooth signal in V_{cap}. This control signal V_{contr} is also used to estimate the power of the symbol in the all-digital receiver. In particular, the output of the counter unit, $s[n]$ shows the number of times that the control signal has been activated during a T_{bit} time. According to the depicted example, during the reception of a symbol '0', V_{contr} has been activated 3 times, whereas it has been activated 6 times to represent the symbol '1'.

Provided that the period of the control signal is independent of T_{bit}, the number of times that the control signal becomes active during T_{bit} is variable, even in a noise-free environment. In order to successfully receive information, we must guarantee that the number of control pulses during the reception of a '0', in the worst case, needs to be lower than the number of pulses during the reception of a '1' in the worst case. As such, T_{bit} is constrained such that the following condition

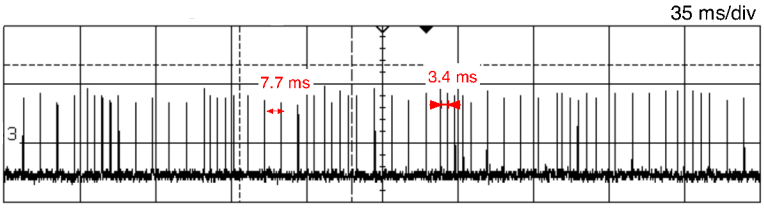

Figure 8.14: Experimentally sensed output current of the energy harvester when receiving an input signal with powers $P_0 = -9$ dBm and $P_1 = -6$ dBm.

is guaranteed:

$$\left\lceil \frac{T_{bit}}{T_0} \right\rceil < \left\lfloor \frac{T_{bit}}{T_1} \right\rfloor, \tag{8.18}$$

where T_0 and T_1 refer to the period of the control signal during the transmission of a logical '0' and a logical '1', respectively, and $\lceil \cdot \rceil$ and $\lfloor \cdot \rfloor$ refer to the ceil and floor functions, respectively. T_0 and T_1 can be obtained by combining equations (8.13), (8.14) and (8.17).

Given the simplicity of this approach, sensors can implement a software-based all-digital receiver that is run in a basic micro-controller connected to the harvesting circuit, thus reducing significant hardware size, complexity, cost and power consumption.

8.5.3 Proof-of-concept Implementation and Evaluation

In this section we demonstrate the feasibility of this approach and evaluate the performance of an all-digital data receiver.

Off-the-shelf Energy Harvester

We first characterize an off-the-shelf energy harvester to be used as a signal receiver. For this, we have considered the Powerharvester P2100 from Powercast Co [34]. This energy harvester implements a DC-DC boost converter to maximize the energy transfer. Due to the fact that it is an integrated circuit, we do not have access to its internal signaling. Accordingly, we have measured the output current of this circuit to determine the required signals, since the output current is only active when during the *on-time* of the DC-DC boost converter.

Fig. 8.14 shows the output current of the energy harvester, with $P_0 = -9$ dBm and $P_1 = -6$ dBm, $C_{cap} = 10$ μF and an output capacitor of 220 mF for energy

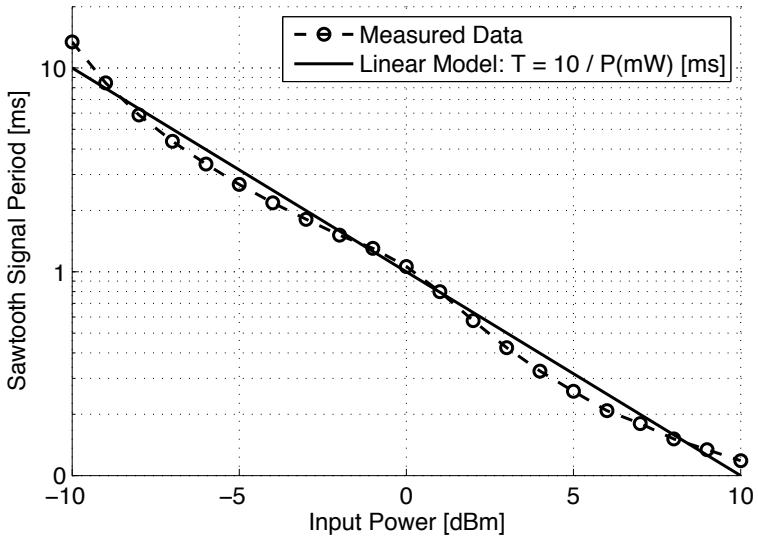

Figure 8.15: Input power dependence of the period of the control signal. Comparison between predicted model and actual operation.

storage. As it is shown, the variation of the input power effectively modulates the period of the generated spikes at the output current, showing a period of 7.7 ms and 3.4 ms for P_0 and P_1, respectively.

We then show in Fig. 8.15 the relation between the input power at the energy harvester and the period of the control signal (and, hence, the period of the current spikes). As it is shown, the predicted behavior of this period in (8.17) is consistent with the obtained results, showing that, in our experimental test-bed, the period can be approximated by: $T[\text{ms}] \approx 10/P[\text{mW}]$. The observed mismatch between curves is due to the dependence of the efficiency with the input power, as reported in [27].

Rate-Energy Trade-off

Given that the maximum allowed transmitting power is constrained by external regulation, a trade-off between achievable rate and transferred energy appears. That is, the transmission of the logical '1' is set to the maximum power, whereas the modulation depth will determine the allocated power of the logical '0'. Low values of modulation depth maximizes the energy transfer, since the average power P_H is larger. However, as the distance between symbols is reduced, the quantization errors of counting periods during T_{bit} requires longer T_{bit} times to

detect a significant difference at the output of the digital counter, $s[n]$. Notice that since we are considering an off-the-shelf energy harvester, the remainder parameters (i.e., V_{high}, V_{low} and C_{cap}) are fixed by the initial application and cannot be further optimized.

We have evaluated the maximum bit-rate that can be achieved by following this approach. For this, we have calculated the minimum T_{bit} that be utilized at given input powers P_1 and P_0, such that it is certain that the number of control actions detected during this the reception of a logical '0' is smaller than the number of actions of a logical '1'. To bound this bit rate, we have considered perfect bit-level synchronization and a noise-free environment, such that the derived bit-rate is constrained by the internal limitations of our approach.

We show in Fig. **??** the maximum achievable bit-rate as a function of the modulation depth index, for different values of P_1. These set of values aim to evaluate the maximum bit rate at a different distance between transmitter and receiver. As it can be observed, higher values of the index between, achieve higher bit-rates, reaching up to 422 bps with an index $h = 1$ and $P_1 = 10$ mW, that is the total harvested power equals to 5 mW. The effect of the period quantization shows a noticeable compression of the maximum achievable bitrate. Alternatively, we show that as this ratio increases, the maximum bit-rate rapidly drops. In particular, we observe that the bit-rate significantly drops for all values of input powers for modulation depth indices below $h < 0.1$.

8.6 Physical Layer Design

In this section, we devise a physical layer for CoE, which aims to guarantee that the transmitted information can be successfully decoded at the destination node. The main aim of this layer is to handle the phase shift misalignment between the received transmissions of data and energy through time-multiplexing techniques.

8.6.1 Time-multiplexing coherent reception

The properties as 1D homodyne receiver of an energy harvester enables coherent reception using power-saving, and even power generating, components. However, given that the phase shift between data and energy transmissions cannot be

controlled, there appears a distinct possibility that the modulated transmission cannot be received.

Implementing simple retransmissions of data packets can improve the eventual packet error rate (PER). We show in Fig. 8.16 the cumulative distribution function (CDF) of the packet error rate, when a data packet is being retransmitted assuming two different retransmission policies, namely reassigning a random phase shift and retransmitting the packet with a phase shift of $\pi/2$.

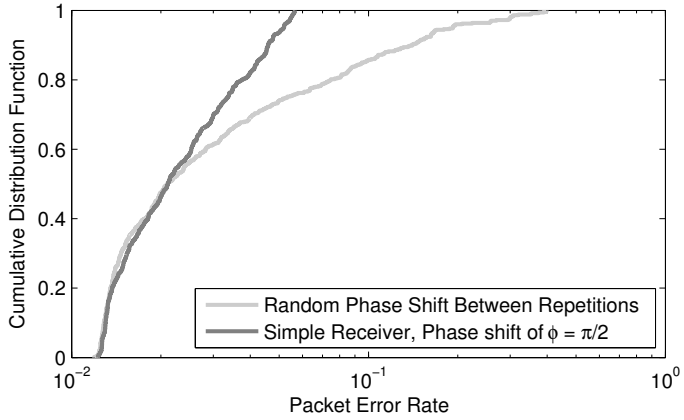

Figure 8.16: CDF of the PER for simple retransmissions of data packets.

Although this approach can achieve relatively low PER values, this solution renders inefficient in terms of energy consumption. For this, we implement a time-multiplexed coherent reception. To implement this concept, each symbol transmission is divided into two time epochs, namely e_I and e_Q. Both time epochs contain the same symbol, but with a phase shift of $\pi/2$ rad. In phasor notation, the transmitted symbol during the time epochs can be written as $s_I = b = b_I + jb_Q$ and $s_Q = -jb = b_Q - jb_I$. This approach lets the receiver to project the received symbol into two orthogonal axis. By assuming a generic phase shift between data and energy, ϕ, the received symbol at each epoch is given by:

$$\hat{s}_I = \Re\left\{s_I e^{\phi}\right\} = b_I \cos(\phi) - b_Q \sin(\phi) \tag{8.19}$$

$$\hat{s}_Q = \Re\left\{s_Q e^{\phi}\right\} = b_Q \cos(\phi) + b_I \sin(\phi). \tag{8.20}$$

Then, by estimating this phase misalignment, the transmitted symbol can be

successfully recovered. For this, the received symbol must be multiplied by the rotation matrix, $\hat{b} = \mathbf{R}\hat{s}$, the rotation matrix is defined as:

$$\mathbf{R} = \begin{bmatrix} \cos(\hat{\phi}) & -\sin(\hat{\phi}) \\ \sin(\hat{\phi}) & \cos(\hat{\phi}) \end{bmatrix} \tag{8.21}$$

where $\hat{\phi}$ refers to the estimated phase shift. An error in the phase estimation $\epsilon = \hat{\phi} - \phi$ will eventually impact upon the received symbol by:

$$\hat{b} = \begin{bmatrix} b_I \cos(\epsilon) - b_Q \sin(\epsilon) \\ b_Q \cos(\epsilon) + b_I \sin(\epsilon) \end{bmatrix} \tag{8.22}$$

We next show the separated implementation of the physical layer at both the transmitting and receiving ends.

8.6.2 Transmitter

Fig. 8.17 illustrates the block diagram of the operation of the transmitter node implementing time-multiplexed coherent transmission.

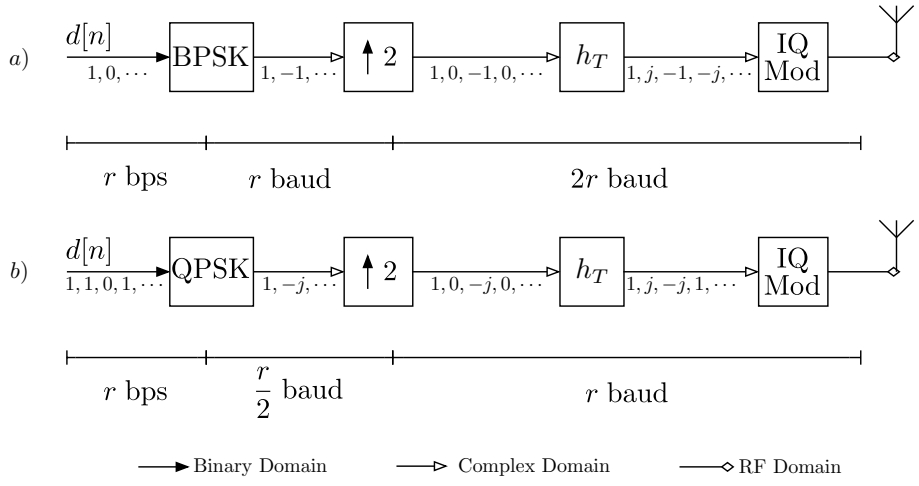

Figure 8.17: PHY-Layer of the transmitter. (a) BPSK modulation and (b) QPSK modulation.

The transmitter encodes the bit stream $d[n]$ at a rate of r bits per second into either a BPSK (Fig. 8.17 (a)) or a QPSK (Fig. 8.17 (b)) signal at a rate of r or $r/2$ symbols per second, respectively. Then, the signal is interpolated by two,

such that samples are placed between zeros. Afterwards, the signal is convoluted with the interpolator filter h_T, defined as:

$$h_T = \begin{bmatrix} 1 \\ -j \end{bmatrix}. \tag{8.23}$$

Finally, the signal is IQ modulated and transferred to the antenna. By employing this physical layer, we time multiplex the two dimensions of a coherence transmission (i.e., the I-Q components). Using one or the other modulation will depend on the receiving capabilities of the destination node.

8.6.3 Receiver

A block diagram of the operations of the receiver node is shown in Fig. 8.18.

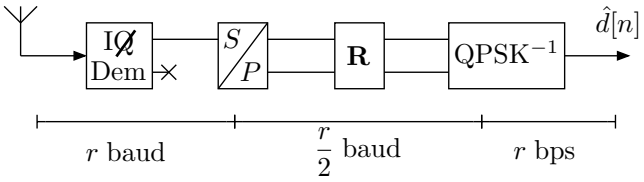

Figure 8.18: PHY-Layer of the receiver for both BPSK and QPSK modulations (QPSK case).

The received signal first passes through a 1D homodyne demodulator, represented as the I~~Q~~ dem block.. This unit represents the action of the energy harvester as a signal receiver, which is able to only collect the projection of the data signal over the phase of the energy signal). Provided that the Q component is transmitted through time-multiplexing, the I component is passed through a 1-input-2-output serial-parallel to emulate the reception of both components. This signal is then multiplied by the aforementioned matrix $\mathbf{R}$ which is used to correct the phase shift between the energy and data signals.

8.6.4 Packet framing and data-energy phase-shift estimation

A physical layer header is considered in the transmission of each data packet. This header must include a known binary sequence used to perform the estima-

tion of the channel state information (CSI) at the receiver (i.e., the matrix $\mathbf{R}$). In particular, the data-energy phase shift is estimated by calculating the scalar product between the known sequence and the received signal.

8.7 Physical Layer Evaluation

We emulate the proposed physical layer for data and energy phase misalignment mitigation using MATLAB software and evaluate its performance. For this, we first evaluate the BER as a function of the ratio between the energy per bit and the noise level, E_b/N_0. This is a standard metric that allows us to better compare the performance of our approach against conventional receivers.

To derive the BER calculations, we evaluate the model, i.e., equations from (8.19) to (8.22) with modulations BPSK and QPSK, considering both comparator or ADC based receivers. To derive generic results, we have considered generic AWGN antenna noise (the internal noise of the receiver has not been considered).

8.7.1 Comparator-based receiver

Given that simple communication schemes based on energy detection can only recover non-coherent amplitude shift keying (ASK) modulations, we compare in Fig. 8.19 the BER as a function of the E_b/N_0 with a preamble of 4, 8 and 16 bits and compare the obtained results to the BER of theoretical non-coherent ASK [74]. In addition, we also show the obtained BER if the proposed physical layer is not implemented and the theoretical BER for coherent ASK [74].

It is first observed that CoE requires a physical layer to operate well. Then, we find that CoE outperforms in terms of BER non-coherent detection for values of E_b/N_0 below 10.5 dB. In addition, we find that CoE improves the sensitivity of our system (fixing a threshold of $BER < 10^{-2}$) by 0.6 dB. Finally, we observe that the obtained BER is lower bounded by the theoretical coherent ASK reception.

8.7.2 ADC-based receiver

Analog-to-digital converters can offer higher accuracy and performance during the signal detection process at the cost of higher power consumption. By using this

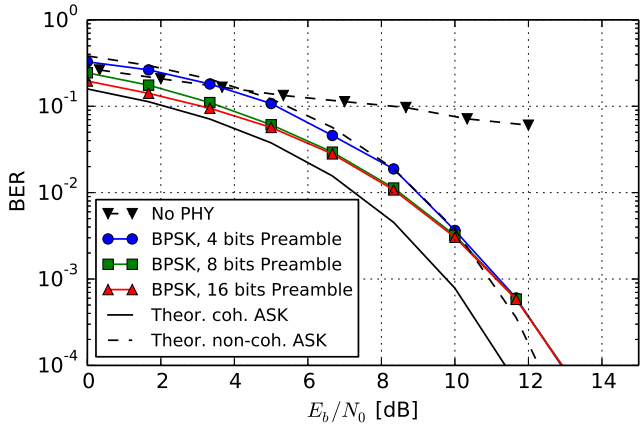

Figure 8.19: Comparison of the obtained BER between a comparator-based receiver for CoE and classical communication schemes.

approach, we can leverage signal processing techniques and to use CSI estimation techniques to correct the phase shift between the data and the energy signal. We find that on the one hand, we can transmit information using QPSK modulations (i.e., we can double the achievable throughput of a sensor node), as well as to approach the theoretical limit in BER as a function of the E_b/N_0 ratio.

We show in Fig. 8.20 the obtained BER as a function of the E_b/N_0 ratio for BPSK and QPSK modulations. In the figure, we compare the performance as a function of the number of quantization bits employed in the ADC. In addition, we show the theoretical bound for BPSK and QPSK, as well as the coherent ASK bound in the BER.

We observe that the BPSK modulation is more robust to a low number of quantization bits than QPSK. We also note that this curve approaches the theoretical bound for coherent ASK when the number of quantization bits becomes sufficiently large. That is, there is a loss of 3 dB compared to ideal BPSK due to the fact that each symbol is transmitted twice using the time-multiplexed I and Q components. However, given that this approach enables low-power coherent detection through the energy detection mechanism of an energy harvester, this performance is still remarkable and better than non-coherent energy detection mechanisms.

Alternatively, we see that QPSK shows less resilience to a low number quantization bits. Nonetheless, we observe that the set of QPSK curves approaches the theoretical bound for BPSK and QPSK when the number of quantization bits

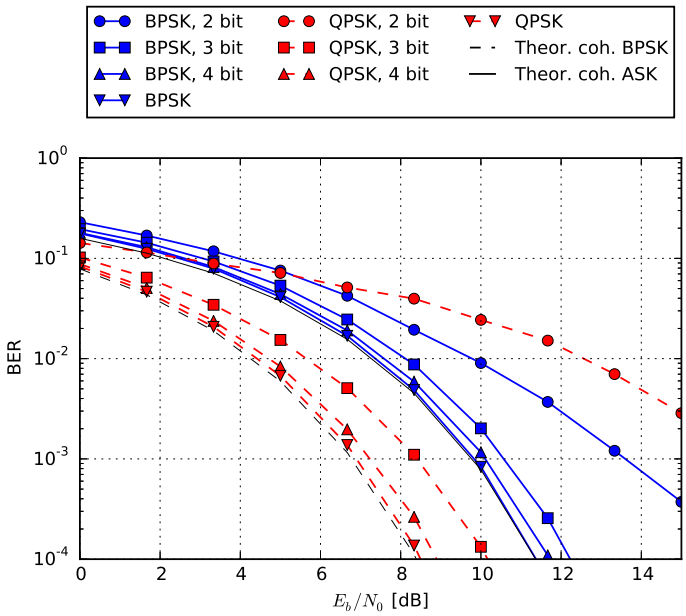

Figure 8.20: Comparison of the obtained BER between a comparator-based receiver for CoE and classical communication schemes.

becomes sufficiently large. That is, the proposed physical layer overcomes the phase misalignment between data and energy transmissions, and permits a near optimal operation if an ADC-based CoE receiver is implemented.

8.8 Summary and Conclusion

This chapter introduces Communications over wireless Energy (CoE) as a method to enable simultaneous energy and data transfer for the wireless networked systems such as Internet of Things. We show that transmission of in-time, in-band data and energy permits uninterrupted transmission of energy, as well as a reduction of system design redundancy. To accomplish the successful reception of data, energy transmitters (ETs) have shown a key role to enhance the signal quality at the receiver, which decodes the information through its energy harvester. To validate this approach, we have modeled and implemented a proof-of-concept receiver, which has been validated through extensive experimentation. A physical layer is proposed to mitigate the energy and data phase misalignment. We provided quantitative results to demonstrate the viability of our joint energy and

data transfer approach, offering sensitivity below -60 dBm with off-the-shelf energy harvesters. Our results open the door to the design of future joint energy and data RF harvesters.

Chapter 9

Conclusions and Future Work

Energy Harvesting has been considered as the key-enabling-technology of the Internet of Things and promises to change the way the considered devices make use of the energy. Through this technique, the considered sensors have a time-unlimited access to a scarce source of energy, which relaxes the need for large energy storage units and manual re-charging. Unfortunately, the available energy is not controllable, and often not even predictable, hence showing significant variations in the expected harvested energy in terms of both space and time. In this sense, spatial energy shadowing causes that certain areas of the network may render disconnected from normal operation, whereas temporal fadings may temporarily inhibit sensing operations, temporarily interrupt the network operation or to cause excessive traffic delays.

This thesis has studied the access of energy at the sensors and has considered dual approach to guarantee a successful network operation. First, the impact of energy harvesting has been studied at both sensor node and network levels. This has permitted the understanding of the dynamics of the entire system and oriented the design of future networks by providing guidelines that help reducing the temporarily interruption of the nodes and the eventual network. The derived knowledge of this first part has allowed the research on the second part. Here, it has been studied how to generate controllable, synthetic energy fields with the help of Energy Transmitters (ETs). This has allowed us to guarantee the deliver of wireless power to all those sensor nodes that may render inactive due to the lack of alternative sources in its close environment.

As a first step towards analyzing the performance of the IoT powered by en-

ergy harvesting, chapter 3 has introduced the basic principles and definitions. Accordingly, a general-purpose energy-source-agnostic definition of the ambient energy by defining the energy field, and it has provided an implementation-independent system model, through the energy path function. This has enabled a generic framework to model arbitrary sources of energy and to characterize the access that sensors do with it. As the main outcome, a Markov-based model defined with negative-energy packets has been proposed that inverts the energy queue to provide a one-to-one mapping of the queue with communication queues. This has provided a high level of duality between both worlds. To evaluate the system performance Energy-erlang, a statistical unit for energy harvesting resources has been presented.

The derived models have been considered in chapter 4 to study the bounds for throughput capacity of energy-harvesting-enabled wireless sensor networks. These bounds set an important guideline for feasibility and deployability during the design process of a network powered by energy harvesting. It has been shown that such bound can be defined by $\tilde{\Theta}\left(f\left(n^{-\alpha/2}\right)n^{(\alpha-1/2)}\right)$, where n refer to the number of nodes and f is the energy path function. It has been shown that such expression coincides with the bounds in power constrained networks when the energy conversion is ideal. Non-ideal factors during the energy acquisition and buffering can alter the scalability of such networks, making them less resilient to node failure (the throughput capacity scales as $\tilde{\Theta}\left(n^{(2\alpha-1)/2}\right)$ if employing battery-less sensors) or even non-scalable (it scales as $\tilde{\Theta}(1)$ if sensors are overdimensioned). This chapter has overviewed the main factors which affect the proper scalability of these networks and motivates a joint network deployment and sensor co-design in order to guarantee a successful operation of energy harvesting powered wireless sensor networks.

The scalability analysis has proven that increasing the number of nodes help improving the performance of wireless communications when nodes are powered by ambient energy sources. To derive this conclusion, the harvested energy has been considered ideal, showing a flat behavior in both time and space domains. Chapter 5 has explored the spatio-temporal character of the energy harvesting sources, and its impact on the sensor node performance. To do this, the negative-energy queue model has been implemented and the system performance has been evaluated as a function of the defined Energy-Erlang unit. On the one hand,

temporal variations and the compression of energy has shown a trade-off between eitherincreasing the capacity of the energy storage or implementing multi-source and self-tunable energy harvesters. On the other hand, the correlation of the energy state, as a function of the spatial correlation among nodes has shown design trade-offs that will affect the upper layers in the network design.

Overall, energy harvesting is posed as a feasible key enabling technology. The first part of this thesis has described this process and provided energy-source-agnostic guidelines for the design of both sensors and networks. Here, the interrelation between the different system design layers have been shown. Among others, it is shown that optimal routing in non-ideal sensor nodes has fixed distance between hops, regardless of the considered deployed node density. As such, joint design of the sensor nodes and the network protocol stack has shown mandatory to optimize the end network performance.

In these lines, improving the harested energy rates by combining multiple sources or adapting the energy harvester circuit has shown a large potential. This thesis has overviewed their benefits and presented a first order model to capture the essence of generic multi-source and self-tunable energy harvesters. Developing accurate models for these energy harvesting platforms, as well as considering these novel models in the analysis will have a realistic impact and determine the joint design of the sensor nodes and the deployed network. To further improve the energy harvesting rates, we advocate for developing algorithms to track the spectral power density in self-tunable energy harvesting. In this context, optimizing the sensing time, estimatint the energy burst length or developing energy models to optimize the frequency band switching are some of the research topics that need to be addressed. For this, cognitive-radio inspired approaches can be implemented.

The second alternative to cope with spatial unavailability of energy is covered in the latter part of this thesis. Wireless RF power transmission has shown its potential as a feasible, energy efficient, manner to power the deployed nodes. Given that the propagation distance of the energy is rather limited. We have opted for the simultaneous transmission of power from multiple energy transmitters (ETs) to cover arbitrariliy large networking areas. The first question that has been addressed in these directions has been presented in Chapter 6 and is as follows: *In order to guarantee sufficient power at the deployed nodes, is it better to increase*

the number of ETs, to increase their transmitted power or to increase their system complexity? The main findings of our work have shown that this power metric is bounded, in its worst case, by $O(s^{1-\alpha/2})$, where α refers to the propagation path-loss exponent. By implementing optimal power transmission schemes, this bound scales up to approximately s times faster in ideal transmission channels, whereas this improvement becomes less noticeable at higher values of the path-loss exponent. In summary, two main conclusions are derived. First, increasing the number of deployed ETs reduce the aggregated transmitted power. Then, researching and developing sophisticated interference-aware schemes for near-ideal channel conditions poser large benefits, while these do not show a clear performance improvement against simple approaches when the channel degrades.

Coordinating the multiple transmissions of power has shown a potential gain of s with respect to orthogonal methods, especially in near-ideal conditions and line-of-sight environments. Unfortunately, these approaches generally require expensive hardware and complex optimization software that needs to be runing on real time. Chapter 7 has provided a method to schedule transmissions of energy such that channel orthogonality is achieved in long term. This guarantees that there are no spots in the networking area where transmissions destructively combine. The transmission of energy is performed in a duty cycled manner, and with an allocated randonm phase. This generates a time-varying power profile at the sensors, which has proven to be converted with significantly higher efficiency than simple orthogonal methods. In particular, we have shown that this method offers a performance improvement of an additional equivalent gain of 5 dB at the receiver input power.

Employing the wireless medium with transfers of power, however, restrain the communication capabilities of the deployed nodes. Chapter 8 has presented a communication scheme, referred as communications over wireless energy (CoE) that enables simultaneous downlink wireless transmission of power and inter-node data communication. This approach permits uninterrupted transmission of energy, as well as a reduction of system design redundancy. To accomplish the successful reception of data, energy transmitters (ETs) have non-intuitively shown a key role to enhance the signal quality at the receiver, which decodes the information through its energy harvester. A proof-of-concept receiver has been implemented to validate this approach, offering a sensitivity below -60 dBm with

off-the-shelf energy harvesters.

Operating multiple ETs as a method to synthesize an arbitrary energy field over the networking area has been demonstrated as a scalable solution to power and re-charge the deployed wireless sensor nodes. It has been shown that defining sophisticated multiple access methods for energy multiplexing can provide a significant gain. Accordingly, an opportunistic method has been designed that leverages inter-ET interferences to provide a 5 dB gain. Finally, a method to compatibilize the simultaneous transmission of ET-to-sensor energy and sensor-to-sensor information has been proposed.

This thesis has opened the door to the research in the field of communications over wireless energy. This research field remains unexplored. The demonstrated uniqueness of the underlying physical channel imposes opposed viewpoints at the entire protocol stack. Examples of the open research problems cover, at the PHY-layer, sensors can optimize the communication channel by leveraging the transmissions of power as remote data signal amplifiers (RDSA). Optimal power allocation for CoE needs to be investigated. MAC protocols for CoE need to guarantee active transmissions of energy, as a first step in the communication. As such, these not only cannot aim at finding idle channels, but need to find channels, which are being occupied by an active transmission of energy. Nodes which are being actively recharged have higher signal sensitivity due to the effect of the RDSA. Route optimization not only needs to consider the remaining energy of the nodes, but also their instantaneous recharging power. Finally, provided that only the projection of the data over the transmission of energy can be recovered at the receiving end, only half of the information can be successully receiver at any point of the network. This fact can be used to implement built-in security during the communication.

In summary, this thesis explores the manners to circunvent the lack of spatio-temporal availability of environmental energy. The focus is set in two main approaches, namely design guidelines through analysis of the energy harvesting sources and manually operated wireless RF power tranmission. Key performance metrics have been defined in each scenario and their scalability as a function of both number of nodes and energy transmitters has been evaluated. These results establish a general framework which may serve designers as a guide to implement autonomous wireless sensor networks with perpetual operation.

Appendix A

List of Publications

A.1 Derived Publications from this Work

- Cid-Fuentes, R. G., Naderi, M. Y., Doost-Mohammady, R., Chowdhury, K. R., Cabellos-Aparicio, A. and Alarcón E., "*A Duty-cycled Random-phase Energy Multiplexing Scheme for Wireless RF Power Transmission*," Submitted for Publication.

- Cid-Fuentes, R.G., Cabellos-Aparicio, A., Alarcón, E., "*Scalability of Network Capacity in Wireless Sensor Networks Powered by Energy Harvesting,*" Submitted for Publication.

- Cid-Fuentes, R. G., Naderi, M. Y., Basagni, S., Chowdhury, K. R., Cabellos-Aparicio, A. and Alarcón E., "*An All-digital Receiver for Low Power, Low Bit-rate Applications using Simultaneous Wireless Information and Power Transmission,*", in Proceedings of the the IEEE International Symposium on Circuits and Systems (ISCAS), 2016

- Cid-Fuentes, R. G., Naderi, M. Y., Basagni, S., Chowdhury, K. R., Cabellos-Aparicio, A. and Alarcón E., "*On signaling power: Communications over Wireless Energy,*" in Proceedings of the IEEE International Conference on Computer Communications (INFOCOM), 2015.

- Cid-Fuentes, R. G., Naderi, M. Y., Doost-Mohammady, R., Chowdhury, K. R., Cabellos-Aparicio, A. and Alarcón E., "*Leveraging deliberately generated*

interferences for multi-sensor wireless RF power transmission," in Proceedings of the IEEE Global Communications Conference (GLOBECOM) 2015.

- Cid-Fuentes, R. G., Cabellos-Aparicio, A. and Alarcón, E., "*Scalability of Network Capacity in Nanonetworks Powered by Energy Harvesting*," in Proceedings of the Second Annual International Conference on Nanoscale Computing and Communication (NANOCOM'15), pp. 19:1-19:6, September 2015.

- Cid-Fuentes, R. G., Cabellos-Aparicio, A. and Alarcón, E., "*Area Model and Dimensioning Guidelines of Multi-source Energy Harvesting for Nanonetworks*," IEEE Internet of Things Journal, vol.PP, no.99, pp.1,1

- Cid-Fuentes, R. G., Cabellos-Aparicio, A., Alarcón, E., "*Energy Buffer Dimensioning Through Energy-Erlangs in Spatio-Temporal-Correlated Energy-Harvesting-Enabled Wireless Sensor Networks*," IEEE Journal on Emerging and Selected Topics in Circuits and Systems (JETCAS), vol.4, no.3, pp.301,312, Sept. 2014.

- Cid-Fuentes, R.G., Cabellos-Aparicio, A., Alarcón, E., "*Circuit area optimization in energy temporal sparse scenarios for multiple harvester powered systems*," Proceedings of the IEEE International Symposium on Circuits and Systems (ISCAS), vol., no., pp.2486,2489, 1-5 June 2014.

- Cid-Fuentes, R. G., Cabellos-Aparicio, A. and Alarcón, E., "*Energy Harvesting Enabled Wireless Sensor Networks: Energy Model and Battery Dimensioning*," in Proc. of the International Conference on Body Area Networks (BODYNETS), Oslo, September 2012.

A.2 Other Publications

- Naderi, M. Y., Cid-Fuentes, R. G., Basagni, S., Cabellos-Aparicio, A., Alarcón E., Chowdhury, K. R., "*HYDRA: Harvesting Energy from Direct RF and Ambient Sources*", Submitted for Publication.

- Cid-Fuentes, R.G., Jornet, J.M., Akyildiz, I.F., Alarcón, E., "*A receiver architecture for pulse-based electromagnetic nanonetworks in the Terahertz*

Band," IEEE International Conference on Communications (ICC), vol., no., pp.4937,4942, 10-15 June 2012.

- Cid-Fuentes, R. G., Martinez, H., Poveda, A., Alarcón, E., "*Electronically tunable switch-mode high-efficiency adaptive band-pass filters for energy harvesting applications*," IEEE International Symposium on Circuits and Systems (ISCAS), vol., no., pp.684,687, 20-23 May 2012.

References

[1] "Understanding the FCC regulations for low-power, non-licensed transmitters," Office of Engineering and Technology Federal Communications Commission, Tech. Rep., 1993.

[2] "P.1238-8: Propagation data and prediction methods for the planning of indoor radiocommunication systems and radio local area networks in the frequency range 300 MHz to 100 GHz," ITU-R, Tech. Rep., 2012.

[3] A. Abdi, H. Hashemi, and S. Nader-Esfahani, "On the PDF of the sum of random vectors," *IEEE Transactions on Communications*, vol. 48, no. 1, pp. 7–12, Jan. 2000.

[4] I. F. Akyildiz, W. Su, Y. Sankarasubramaniam, and E. Cayirci, "Wireless sensor networks: a survey," *Computer Networks (Elsevier) Journal*, vol. 38, no. 4, pp. 393–422, Mar. 2002.

[5] R. Amirtharajah and A. P. Chandrakasan, "Self-powered signal processing using vibration-based power generation," *IEEE Journal of Solid-State Circuits*, vol. 33, no. 5, pp. 687–695, May 1998.

[6] M. H. Anisi, G. Abdul-Salaam, M. Y. I. Idris, A. W. A. Wahab, and I. Ahmedy, "Energy harvesting and battery power based routing in wireless sensor networks," *Wireless Networks*, pp. 1–18, 2015.

[7] A. Arafa and S. Ulukus, "Optimal policies for wireless networks with energy harvesting transmitters and receivers: Effects of decoding costs," *Journal of Selected Areas in Communications*, vol. 33(12), pp. 2611–2625, Dec. 2015.

[8] S. Bandyopadhyay and A. Chandrakasan, "Platform architecture for solar, thermal, and vibration energy combining with mppt and single inductor,"

IEEE Journal of Solid-State Circuits, vol. 47, no. 9, pp. 2199–2215, Sep. 2012.

[9] S. Basagni, M. Y. Naderi, C. Petrioli, and D. Spenza, "Wireless sensor networks with energy harvesting," in *Mobile Ad Hoc Networking: The Cutting Edge Directions,*, I. Press, J. Wiley, and Sons, Eds., Piscataway, NJ and Hoboken, NJ, 2010, ch. 20, pp. 1–36.

[10] S. Beeby, M. Tudor, and N. White, "Energy harvesting vibration sources for microsystems applications," *Measurement Science and Technology*, vol. 17, no. 12, pp. R175–R195, Dec. 2006. [Online]. Available: http://eprints.soton.ac.uk/263645/

[11] J. O. Berger, V. D. Oliveira, and B. Sanso, "Objective Bayesian analysis of spatially correlated data," *JOURNAL OF THE AMERICAN STATISTICAL ASSOCIATION*, vol. 96, pp. 1361–1374, 2000.

[12] D. Bertsekas and R. Gallager, *Data Networks*. Prentice Hall, 1992.

[13] A. Boaventura, D. Belo, R. Fernandes, A. Collado, A. Georgiadis, and N. Borges Carvalho, "Boosting the efficiency: Unconventional waveform design for efficient wireless power transfer," *IEEE Microwave Magazine*, vol. 16, no. 3, pp. 87–96, Apr. 2015.

[14] A. Boaventura, A. Collado, A. Georgiadis, and N. Borges Carvalho, "Spatial power combining of multi-sine signals for wireless power transmission applications," *IEEE Transactions on Microwave Theory and Techniques*, vol. 62, no. 4, pp. 1022–1030, Apr. 2014.

[15] D. Bouchouicha, F. Dupont, M. Latrach, and L.Ventura, "Ambient RF energy harvesting," in *Proc. of the International Conference on Renewable Energies and Power Quality (ICREPQ10)*, 2010.

[16] D. Cabric, A. Tkachenko, and R. Brodersen, "Spectrum sensing measurements of pilot, energy, and collaborative detection," in *IEEE Military Communications Conference,*, Oct. 2006, pp. 1–7.

[17] P. Castiglione, O. Simeone, E. Erkip, and T. Zemen, "Energy Management Policies for Energy-Neutral Source-Channel Coding," *Communications, IEEE Transactions on*, vol. 60, no. 9, pp. 2668–2678, 2012.

[18] R. Catanuto, S. Toumpis, and G. Morabito, "Opti{c,m}al: Optical/optimal routing in massively dense wireless networks," in *INFOCOM 2007. 26th IEEE International Conference on Computer Communications. IEEE*, May 2007, pp. 1010–1018.

[19] S. Chalasani and J. Conrad, "A survey of energy harvesting sources for embedded systems," in *IEEE Southeastcon*, Apr. 2008, pp. 442–447.

[20] Z. Chen, B. Xia, and H. Liu, "Wireless information and power transfer in two-way amplify-and-forward relaying channels," in *Proc. of the IEEE GlobalSIP*, Dec. 2014, pp. 168–172.

[21] R. G. Cid-Fuentes, A. Cabellos, and E. Alarcon, "Energy harvesting enabled wireless sensor networks: Energy model and battery dimensioning," in *in proc. of the 7th International Conference on Body Area Networks (BODYNETS)*, Sep. 2012.

[22] R. G. Cid-Fuentes, A. Cabellos-Aparicio, and E. Alarcón, "Circuit area optimization in energy temporal sparse scenarios for multiple harvester powered systems," in *Proc. of the IEEE International Symposium on Circuits and Systems (ISCAS)*, Jun. 2014, pp. 2486–2489.

[23] R. G. Cid-Fuentes, A. Cabellos-Aparicio, and E. Alarcon, "Energy buffer dimensioning through Energy-Erlangs in spatio-temporal-correlated energy-harvesting-enabled wireless sensor network," *IEEE Journal on Emerging and Selected Topics in Circuits and Systems*, vol. 4, no. 3, pp. 301 – 312, Sep. 2014.

[24] R. G. Cid-Fuentes, M. Y. Naderi, S. Basagni, K. R. Chowdhury, E. Alarcon, and A. Cabellos-Aparicio, "An all-digital receiver for low power, low bit-rate applications using simultaneous wireless information and power transmission," in *Proc. of the IEEE ISCAS*, May 2016.

[25] ——, "On signaling power: Communications over wireless energy," in *Proc. of the IEEE INFOCOM*, Apr. 2016.

[26] ——, "On the scalability of energy in wireless RF powered internet of things," 2016.

[27] R. G. Cid-Fuentes, M. Y. Naderi, R. Doost-Mohammady, K. R. Chowdhury, E. Alarcon, and A. Cabellos-Aparicio, "Leveraging deliberately generated interferences for multi-sensor wireless RF power transmission," in *Proc. of the IEEE GLOBECOM*, Dec. 2015.

[28] ——, "A duty-cycled random-phase energy multiplexing scheme for wireless RF power transmission," *Submitted for publication*, 2016.

[29] R. G. Cid-Fuentes, S. Abadal, A. Cabellos-Aparicio, and E. Alarcon, "Scalability of network capacity in nanonetworks powered by energy harvesting," in *Proc. on Nanoscale Computing and Communication*, ser. NANOCOM' 15. New York, NY, USA: ACM, 2015, pp. 19:1–19:6.

[30] R. G. Cid-Fuentes, H. Martinez, A. Poveda, and E. Alarcon, "Electronically tunable switch-mode high-efficiency adaptive band-pass filters for energy harvesting applications," in *Proc. of the IEEE International Symposium on Circuits and Systems (ISCAS)*, May 2012, pp. 684–687.

[31] R. Cid-Fuentes, A. Cabellos, and E. Alarcon, "Area model and dimensioning guidelines of multi-source energy harvesting for nano-micro interface," *IEEE Internet of Things Journal*, vol. PP, no. 99, pp. 1–1, 2015.

[32] P. J. Cornwell, J. Goethal, J. Kowko, and M. Damianakis, "Enhancing power harvesting using a tuned auxiliary structure," *Journal of Intelligent Material Systems and Structures*, vol. 16, no. 10, pp. 825–834, 2005. [Online]. Available: http://jim.sagepub.com/content/16/10/825.abstract

[33] P. Corporation, "P1110 - 915 MHz RF Powerharvester Receiver." [Online]. Available: http://www.powercastco.com/PDF/P1110-datasheet.pdf

[34] ——, "P2110 - 915 MHz RF Powerharvester Receiver." [Online]. Available: http://www.powercastco.com/PDF/P2110-datasheet.pdf

[35] ——, "TX91501 user's manual." [Online]. Available: http://www.powercastco.com/PDF/TX91501-manual.pdf

[36] R. Doost, K. Chowdhury, and M. Di Felice, "Routing and link layer protocol design for sensor networks with wireless energy transfer," in *Proc. of the IEEE GLOBECOM*, Dec. 2010, pp. 1–5.

[37] A. Driemel, S. Har-Peled, and B. Raichel, "On the expected complexity of voronoi diagrams on terrains," in *Proc. of the 2012 symposuim on Computational Geometry*, 2012, pp. 101–110.

[38] C. Eichhorn, R. Tchagsim, N. Wilhelm, and P. Woias, "A smart and self-sufficient frequency tunable vibration energy harvester," *Journal of Micromechanics and Microengineering*, vol. 21, no. 10, p. 104003, 2011.

[39] M. Erol-Kantarci and H. Mouftah, "DRIFT: Differentiated RF power transmission for wireless sensor network deployment in the smart grid," in *Proc. of the IEEE Globecom Workshops*, Dec. 2012, pp. 1491–1495.

[40] ——, "Mission-aware placement of RF-based power transmitters in wireless sensor networks," in *IEEE Symposium on Computers and Communications (ISCC)*, Jul. 2012, pp. 000 012–000 017.

[41] Z. A. Eu, H.-P. Tan, and W. K. Seah, "Opportunistic routing in wireless sensor networks powered by ambient energy harvesting," *Computer Networks*, vol. 54, no. 17, pp. 2943–2966, 2010. [Online]. Available: http://www.sciencedirect.com/science/article/pii/S1389128610001581

[42] ——, "Design and performance analysis of MAC schemes for Wireless Sensor Networks Powered by Ambient Energy Harvesting," *Ad Hoc Networks*, vol. 9, no. 3, pp. 300–323, 2011. [Online]. Available: http://dx.doi.org/10.1016/j.adhoc.2010.07.014

[43] C. Forbes, M. Evans, N. Hastings, and B. Peacock, *Statistical distributions*. Wiley, 2010.

[44] M. Gorlatova, P. Kinget, I. Kymissis, D. Rubenstein, X. Wang, and G. Zussman, "Energy-harvesting active networked tags (EnHANTs) for ubiquitous

object networking," *IEEE Wireless Communications*, vol. 17, no. 6, Dec. 2010.

[45] M. Gorlatova, A. Wallwater, and G. Zussman, "Networking low-power energy harvesting devices: Measurements and algorithms," in *Proc. of the IEEE INFOCOM*, Apr. 2011, pp. 1602–1610.

[46] ——, "Networking low-power energy harvesting devices: Measurements and algorithms," *IEEE Transactions on Mobile Computing*, vol. 12, no. 9, pp. 1853–1865, 2013.

[47] M. Grossglauser and D. Tse, "Mobility increases the capacity of ad-hoc wireless networks," *IEEE/ACM Transactions on Networking*, vol. 10, no. 4, pp. 477–486, Aug. 2002.

[48] P. Grover and A. Sahai, "Shannon meets tesla: Wireless information and power transfer," in *Proc. of the IEEE ISIT*, Jun. 2010, pp. 2363–2367.

[49] N. Guilar, T. Kleeburg, A. Chen, D. Yankelevich, and R. Amirtharajah, "Integrated solar energy harvesting and storage," *IEEE Transactions on Very Large Scale Integration (VLSI) Systems,*, vol. 17, no. 5, pp. 627–637, May 2009.

[50] P. Gupta and P. Kumar, "The capacity of wireless networks," *IEEE Transactions on Information Theory*, vol. 46, no. 2, pp. 388–404, Mar. 2000.

[51] J. Hagerty, F. Helmbrecht, W. McCalpin, R. Zane, and Z. Popovic, "Recycling ambient microwave energy with broad-band rectenna arrays," *IEEE Transactions on Microwave Theory and Techniques*, vol. 52, no. 3, pp. 1014–1024, Mar. 2004.

[52] A. Hajati, S. Bathurst, H. Lee, and S. Kim, "Design and fabrication of a nonlinear resonator for ultra wide-bandwidth energy harvesting applications," in *Proc. of the IEEE International Conference on Micro Electro Mechanical Systems (MEMS)*, Jan. 2011, pp. 1301–1304.

[53] D. Hasenfratz, A. Meier, C. Moser, J.-J. Chen, and L. Thiele, "Analysis, comparison, and optimization of routing protocols for energy harvesting

wireless sensor networks," in *Sensor Networks, Ubiquitous, and Trustworthy Computing (SUTC), 2010 IEEE International Conference on*, Jun. 2010, pp. 19–26.

[54] L.-M. He, "Time synchronization based on spanning tree for wireless sensor networks," in *Proc. of the 4th International Conference on Wireless Communications, Networking and Mobile Computing*, Oct. 2008, pp. 1–4.

[55] S. He, J. Chen, F. Jiang, D. K. Yau, G. Xing, and Y. Sun, "Energy provisioning in wireless rechargeable sensor networks," *IEEE Transactions on Mobile Computing*, vol. 12, no. 10, pp. 1931–1942, 2013.

[56] P.-H. Hsieh, C.-H. Chou, and T. Chiang, "An RF energy harvester with 44.1% PCE at input available power of -12 dBm," *IEEE Transactions on Circuits and Systems I: Regular Papers*, vol. 62, no. 6, pp. 1528–1537, Jun. 2015.

[57] J. Hsu, S. Zahedi, A. Kansal, M. Srivastava, and V. Raghunathan, "Adaptive duty cycling for energy harvesting systems," in *Proc. of the International Symposion on Low Power Electronics and Design (ISLPED'06)*, Oct. 2006, pp. 180–185.

[58] C. Huang, R. Zhang, and S. Cui, "Optimal power allocation for outage probability minimization in fading channels with energy harvesting constraints," *IEEE Transactions on Wireless Communications*, vol. 13, no. 2, pp. 1074–1087, 2014.

[59] K. Huang, "Spatial throughput of mobile Ad Hoc networks powered by energy harvesting," *IEEE Transactions on Information Theory*, vol. 59, no. 11, pp. 7597–7612, 2013.

[60] K. Huang, M. Kountouris, and V. O. K. Li, "Renewable Powered Cellular Networks: Energy Field Modeling and Network Coverage," *IEEE Transactions on Wireless Communications*, vol. 14, no. 8, pp. 4234–4247, 2015. [Online]. Available: http://ieeexplore.ieee.org/lpdocs/epic03/wrapper.htm?arnumber=7073654

[61] F. Iannello, O. Simeone, and U. Spagnolini, "Medium access control protocols for wireless sensor networks with energy harvesting," pp. 1381–1389, 2012.

[62] R. B. Inc., "MPA-0850, 750-950MHz 5 W RF Power Amplifier." [Online]. Available: http://rfbayinc.com/

[63] V. Jelicic, M. Magno, D. Brunelli, V. Bilas, and L. Benini, "Benefits of wake-up radio in energy-efficient multimodal surveillance wireless sensor network," *IEEE Sensors Journal*, vol. 14, no. 9, pp. 3210–3220, Sep. 2014.

[64] J. Jeong and D. Culler, "Predicting the long-term behavior of a micro-solar power system," *ACM Transactions on Embedded Computer Systems*, vol. 11, no. 2, pp. 35:1–35:38, Jul. 2012.

[65] X. Jiang, J. Polastre, and D. Culler, "Perpetual environmentally powered sensor networks," in *Fourth International Symposium on Information Processing in Sensor Networks (IPSN)*, Apr. 2005, pp. 463–468.

[66] ——, "Perpetual environmentally powered sensor networks," in *Proc. of the International Symposium on Information Processing in Sensor Networks*, Apr. 2005, pp. 463–468.

[67] S. Jo, M. Kim, and Y. Kim, "Passive-self-tunable vibrational energy harvester," in *International Solid-State Sensors, Actuators and Microsystems Conference (TRANSDUCERS),*, Jun. 2011, pp. 691–694.

[68] R. H. Jones and A. V. Vecchia, "Fitting continuous ARMA models to unequally spaced spatial data," *Journal of the American Statistical Association*, vol. 88, no. 423, pp. pp.947–954, 1993. [Online]. Available: http://www.jstor.org/stable/2290786

[69] J. M. Jornet and I. F. Akyildiz, "Graphene-based nano-antennas for electromagnetic nanocommunications in the terahertz band," in *Proc. of EUCAP 2010, Fourth European Conference on Antennas and Propagation*, Apr. 2010.

[70] J. Jornet and I. Akyildiz, "Joint energy harvesting and communication analysis for perpetual wireless nanosensor networks in the terahertz band," *IEEE Transactions on Nanotechnology*, vol. 11, no. 3, pp. 570–580, May 2012.

[71] S. Kamath, U. Niesen, and P. Gupta, "The capacity per unit energy of large wireless networks," in *IEEE International Symposium on Information Theory Proceedings (ISIT)*, Aug. 2011, pp. 1618–1622.

[72] X. Kang, C. K. Ho, and S. Sun, "Full-duplex wireless-powered communication network with energy causality," *IEEE Transactions on Wireless Communications*, vol. PP, Jun. 2015.

[73] A. Kansal, J. Hsu, S. Zahedi, and M. B. Srivastava, "Power management in energy harvesting sensor networks," *ACM Trans. Embed. Comput. Syst.*, vol. 6, no. 4, pp. 32–38, Sep. 2007.

[74] Y. Kim, S.-W. Tam, G.-S. Byun, H. Wu, L. Nan, G. Reinman, J. Cong, and M.-C. Chang, "Analysis of noncoherent ASK modulation-based RF-interconnect for memory interface," *IEEE Journal on Emerging and Selected Topics in Circuits and Systems*, vol. 2, no. 2, pp. 200–209, Jun. 2012.

[75] J. Kingman, *Poisson Processes*, O. U. Press, Ed. Oxford UK, 1993.

[76] S. Kosunalp, "MAC Protocols for Energy Harvesting Wireless Sensor Networks : Survey," *ETRI Journal*, vol. 37, no. 4, pp. 804–812, 2015. [Online]. Available: http://etrij.etri.re.kr/etrij/journal/article/article.do?volume=37{&}issue=4{&}page=804

[77] C. Krishna, "Managing battery and supercapacitor resources for real-time sporadic workloads," *IEEE Embedded Systems Letters*, vol. 3, pp. 32–36, 2011.

[78] D. Lee and K. Chugg, "A pragmatic approach to cooperative communication," in *Proc. of the IEEE Military Communications Conference (MILCOM)*, Oct. 2006, pp. 1–7.

[79] S. Lee, K. Huang, and R. Zhang, "Cognitive energy harvesting and transmission from a network perspective," in *Proc. of the IEEE International Conference on Communication Systems (ICCS)*, Nov. 2012, pp. 225–229.

[80] S. Lee, L. Liu, and R. Zhang, "Collaborative wireless energy and information transfer in interference channel," *IEEE Transactions on Wireless Communications*, vol. 14, no. 1, pp. 545–557, Jan. 2015.

[81] S. Li, J. Yuan, and H. Lipson, "Ambient wind energy harvesting using cross-flow fluttering," *Journal of Applied Physics*, vol. 109, p. 0126104, 2011.

[82] L. Liu, R. Zhang, and K. C. Chua, "Wireless information transfer with opportunistic energy harvesting," *IEEE Transactions on Wireless Communications*, vol. 12, no. 1, pp. 288 – 300, Jan. 2013.

[83] R. S. Liu, K. W. Fan, Z. Zheng, and P. Sinha, "Perpetual and fair data collection for environmental energy harvesting sensor networks," *IEEE/ACM Transactions on Networking*, vol. 19, no. 4, pp. 947–960, 2011.

[84] V. Liu, A. Parks, V. Talla, S. Gollakota, D. Wetherall, and J. R. Smith, "Ambient backscatter: Wireless communication out of thin air," *SIGCOMM Computer Communication Reviews*, vol. 43, no. 4, pp. 39–50, Aug. 2013.

[85] Y. Liu, K. L. Ren, H. F. Hofmann, and Q. Zhang, "Investigation of electrostrictive polymers for energy harvesting," *IEEE Transactions on Ultrasonics, Ferroelectrics, and Frequency Control*, vol. 52, no. 12, pp. 2411–2417, Dec. 2005.

[86] C. Lu, V. Raghunathan, and K. Roy, "Efficient design of micro-scale energy harvesting systems," *IEEE Journal on Emerging and Selected Topics in Circuits and Systems*, vol. 1, no. 3, pp. 254–266, Sep. 2011.

[87] J. Mannermaa, K. Kalliomaki, T. Mansten, and S. Turunen, "Timing performance of various GPS receivers," in *Proc. of the Joint Meeting of the European Frequency and Time Forum and the IEEE International Frequency Control Symposium*, vol. 1, 1999, pp. 287–290vol.1.

[88] B. Medepally, N. Mehta, and C. Murthy, "Implications of energy profile and storage on energy harvesting sensor link performance," in *IEEE Global Telecommunications Conference (GLOBECOM)*, 2009, pp. 1–6.

[89] J. Medhi, *Stochastic Models in Queueing Theory*, A. Press, Ed. Elsevier Science, 2003.

[90] S. Meninger, J. O. Mur-Miranda, R. Amirtharajah, A. P. Chandrakasan, and J. H. Lang, "Vibration-to-electric energy conversion," *IEEE Transactions on Very Large Scale Integration (VLSI) Systems*, vol. 9, no. 1, pp. 64–76, 2001.

[91] P. Mercier, M. Bhardwaj, D. Daly, and A. Chandrakasan, "A low-voltage energy-sampling IR-UWB digital baseband employing quadratic correlation," *IEEE Journal of Solid-State Circuits*, vol. 45, no. 6, pp. 1209–1219, Jun. 2010.

[92] R. Mills and G. Prescott, "A comparison of various radiometer detection models," *IEEE Transactions on Aerospace and Electronic Systems*, vol. 32, no. 1, pp. 467–473, Jan. 1996.

[93] P. Mitcheson, T. Green, E. Yeatman, and A. Holmes, "Architectures for vibration-driven micropower generators," *Journal of Microelectromechanical Systems*, vol. 13, no. 3, pp. 429–440, Jun. 2004.

[94] R. Mudumbai, D. Brown, U. Madhow, and H. Poor, "Distributed transmit beamforming: challenges and recent progress," *IEEE Communications Magazine*, vol. 47, no. 2, pp. 102–110, Feb. 2009.

[95] G. Murillo, M. Leeb, C. Xub, G. Abadal, and Z. L. Wang, "Hybrid resonant energy harvester integrating zno nws with MEMS for enabling zero-power wireless sensor nodes," *Nano Communication Networks*, vol. 2, no. 4, p. 235241, 2011.

[96] M. Y. Naderi, K. R. Chowdhury, S. Basagni, W. Heinzelman, S. De, and S. Jana, "Surviving wireless energy interference in RF-harvesting sensor networks: An empirical study," in *IEEE SECON Workshop on Energy Harvesting Communications*, Jun. 2014.

[97] M. Naderi, P. Nintanavongsa, and K. Chowdhury, "RF-MAC: A medium access control protocol for re-chargeable sensor networks powered by wireless energy harvesting," *Wireless Communications, IEEE Transactions on*, vol. 13, no. 7, pp. 3926–3937, Jul. 2014.

[98] R. Negi and A. Rajeswaran, "Capacity of power constrained ad-hoc networks," in *INFOCOM 2004.*, vol. 1, Mar. 2004, pp. 4 vol. (xxxv+2866).

[99] D. Ng, E. Lo, and R. Schober, "Wireless information and power transfer: Energy efficiency optimization in OFDMA systems," *IEEE Transactions on Wireless Communications,*, vol. 12, no. 12, pp. 6352–6370, Dec. 2013.

[100] P. Nintanavongsa, U. Muncuk, D. Lewis, and K. Chowdhury, "Design optimization and implementation for RF energy harvesting circuits," *IEEE Journal on Emerging and Selected Topics in Circuits and Systems (JETCAS)*, vol. 2, no. 1, pp. 24–33, Mar. 2012.

[101] H. Nishimoto, Y. Kawahara, and T. Asami, "Prototype implementation of ambient RF energy harvesting wireless sensor networks," in *IEEE Sensors*, Nov. 2010, pp. 1282–1287.

[102] O. Ozel, K. Tutuncuoglu, J. Yang, S. Ulukus, and A. Yener, "Transmission with energy harvesting nodes in fading wireless channels: Optimal policies," *Journal of Selected Areas in Communications*, vol. 29, pp. 1732–1743, Sep. 2011.

[103] O. Ozel and S. Ulukus, "AWGN channel under time-varying amplitude constraints with causal information at the transmitter," in *Conference Record - Asilomar Conference on Signals, Systems and Computers*, 2011, pp. 373–377.

[104] ——, "Achieving AWGN capacity under stochastic energy harvesting," *IEEE Transactions on Information Theory*, vol. 58, no. 10, pp. 6471–6483, 2012.

[105] G. Papotto, F. Carrara, and G. Palmisano, "A 90-nm CMOS threshold-compensated RF energy harvester," *IEEE Journal of Solid-State Circuits*, vol. 46, no. 9, pp. 1985–1997, Sep. 2011.

[106] ——, "A 90-nm CMOS threshold-compensated RF energy harvester," *IEEE Journal of Solid-State Circuits*, vol. 46, no. 9, pp. 1985–1997, Sep. 2011.

[107] C. Park and P. Chou, "Ambimax: Autonomous energy harvesting platform for multi-supply wireless sensor nodes," in *Sensor and Ad Hoc Communications and Networks, 2006. SECON '06. 2006 3rd Annual IEEE Communications Society on*, vol. 1, 2006, pp. 168–177.

[108] ——, "Ambimax: Autonomous energy harvesting platform for multi-supply wireless sensor nodes," in *Proc. of the 3rd Annual IEEE Communications Society on Sensor and Ad Hoc Communications and Networks (SECON)*, vol. 1, 2006, pp. 168–177.

[109] J. Park and B. Clerckx, "Joint wireless information and energy transfer in a two-user MIMO interference channel," *IEEE Transactions on Wireless Communications*, vol. 12, no. 8, pp. 4210–4221, Aug. 2013.

[110] ——, "Joint wireless information and energy transfer in a k-user MIMO interference channel," *IEEE Transactions on Wireless Communications*, vol. 13, no. 10, pp. 5781–5796, Oct. 2014.

[111] A. N. Parks, A. Liu, S. Gollakota, and J. R. Smith, "Turbocharging ambient backscatter communication," in *Proc. of the ACM Conference on SIGCOMM*, New York, NY, USA, 2014, pp. 619–630.

[112] D. Pech, M. Brunet, H. Durou, P. Huang, V. Mochalin, Y. Gogotsi, P.-L. Taberna, and P. Simon, "Ultrahigh-power micrometre-sized supercapacitors based on onion-like carbon," *Nature Nano*, vol. 5, no. 9, pp. 651–654, Sep. 2010.

[113] Z. Popovic, E. Falkenstein, D. Costinett, and R. Zane, "Low-power far-field wireless powering for wireless sensors," *Proceedings of the IEEE*, vol. 101, no. 6, pp. 1397–1409, Jun. 2013.

[114] V. Raghunathan, A. Kansal, J. Hsu, J. Friedman, and M. Srivastava, "Design considerations for solar energy harvesting wireless embedded systems," in *Proc. of the International Symposium on Information Processing in Sensor Networks*, Apr. 2005, pp. 457–462.

[115] R. Rajesh, V. Sharma, and P. Viswanath, "Information capacity of energy harvesting sensor nodes," in *Proc. of the IEEE International Symposium on Information Theory*, 31 2011-aug. 5 2011, pp. 2363–2367.

[116] Y. K. Ramadass and A. P. Chandrakasan, "An efficient piezoelectric energy harvesting interface circuit using a bias-flip rectifier and shared inductor," *IEEE Journal of Solid-State Circuits*, vol. 45, no. 1, pp. 189–204, Jan. 2010.

[117] T. S. Rappaport, *Wireless communications principles and practices*. Prentice-Hall, 2002.

[118] E. Research, "N210 Universal Software Radio Peripheral (USRP)." [Online]. Available: http://ettus.com/

[119] V. Rodoplu and T. Meng, "Bits-per-joule capacity of energy-limited wireless networks," *IEEE Transactions on Wireless Communications,*, vol. 6, no. 3, pp. 857–865, Mar. 2007.

[120] S. Roundy, P. K. Wright, and K. S. Pister, "Micro-electric vibration-to-electricity converters," *Proceedings of ASME International Mechanical Engineering Congress & Exposition*, pp. 1–10, 2002.

[121] S. Roy, V. Jandhyala, J. Smith, D. Wetherall, B. Otis, R. Chakraborty, M. Buettner, D. Yeager, Y.-C. Ko, and A. Sample, "RFID: From supply chains to sensor nets," *Proceedings of the IEEE*, vol. 98, no. 9, pp. 1583–1592, Sep. 2010.

[122] A. Sample and J. Smith, "Experimental results with two wireless power transfer systems," in *IEEE Radio and Wireless Symposium,*, Jan. 2009, pp. 16–18.

[123] A. Seyedi and B. Sikdar, "Modeling and analysis of energy harvesting nodes in wireless sensor networks," in *46th Annual Allerton Conference on Communication, Control, and Computing*, Sep. 2008, pp. 67–71.

[124] N. Shenck and J. Paradiso, "Energy scavenging with shoe-mounted piezoelectrics," *Micro, IEEE*, vol. 21, no. 3, pp. 30–42, 2001.

[125] B. J. H. Sheng Xu and Z. L. Wang, "Piezoelectric-nanowire-enabled power source for driving wireless microelectronics," *Nature Communications*, vol. 1, p. 93, Oct. 2010.

[126] W.-Y. Shin, S.-W. Jeon, N. Devroye, M. Vu, S.-Y. Chung, Y. Lee, and V. Tarokh, "Improved capacity scaling in wireless networks with infrastructure," *IEEE Transactions on Information Theory,*, vol. 57, no. 8, pp. 5088–5102, Aug. 2011.

[127] H. a. Sodano, G. E. Simmers, R. Dereux, and D. J. Inman, "Recharging Batteries using Energy Harvested from Thermal Gradients," *Journal of Intelligent Material Systems and Structures*, vol. 18, no. 1, pp. 3–10, 2006.

[128] S. Sudevalayam and P. Kulkarni, "Energy harvesting sensor nodes: Survey and implications," *IEEE Communications Surveys Tutorials*, vol. 13, no. 3, pp. 443 –461, 2011.

[129] B. Sundararaman, U. Buy, and A. D. Kshemkalyani, "Clock synchronization for wireless sensor networks: a survey," *Ad Hoc Networks*, vol. 3, p. 281323, 2005.

[130] A. Susu, A. Acquaviva, D. Atienza, and G. De Micheli, "Stochastic modeling and analysis for environmentally powered wireless sensor nodes," in *6th International Symposium on Modeling and Optimization in Mobile, Ad Hoc, and Wireless Networks and Workshops*, April 2008, pp. 125–134.

[131] W. I. S.-P. E. Systems, "Wispes w24th." [Online]. Available: http://www.wispes.com/?wpsc-product=wispes-w24th

[132] J. Taneja, J. Jeong, and D. Culler, "Design, modeling, and capacity planning for micro-solar power sensor networks," in *Information Processing in Sensor Networks, 2008. IPSN '08. International Conference on*, 2008, pp. 407–418.

[133] E. O. Torres and G. A. Rincón-Mora, "A 0.7-um bicmos electrostatic energy-harvesting system IC," *IEEE Journal of Solid-State Circuits*, vol. 45, pp. 483–496, 2010.

[134] K. Tutuncuoglu, O. Ozel, A. Yener, and S. Ulukus, "Binary energy harvesting channel with finite energy storage," in *IEEE International Symposium on Information Theory - Proceedings*, 2013, pp. 1591–1595.

[135] S. Ulukus, A. Yener, E. Erkip, O. Simeone, M. Zorzi, P. Grover, and K. Huang, "Energy Harvesting Wireless Communications: A Review of Recent Advances," pp. 360–381, 2015.

[136] J. Ventura and K. R. Chowdhury, "Markov modeling of energy harvesting body sensor networks," in *Proc. of IEEE PIMRC, Toronto*, September 2011.

[137] N. Verma and A. Chandrakasan, "An ultra low energy 12-bit rate-resolution scalable sar adc for wireless sensor nodes," *IEEE Journal of Solid-State Circuits*, vol. 42, no. 6, pp. 1196–1205, June 2007.

[138] H. Visser and R. Vullers, "RF energy harvesting and transport for wireless sensor network applications: Principles and requirements," *Proceedings of the IEEE*, vol. 101, no. 6, pp. 1410–1423, June 2013.

[139] M. C. Vuran, O. B. Akan, and I. F. Akyildiz, "Spatio-temporal correlation: theory and applications for wireless sensor networks," *Computer Networks Journal (Elsevier)*, vol. 45, pp. 245–259, 2004.

[140] R. Want, "An introduction to RFID technology," *IEEE Pervasive Computing*, vol. 5, no. 1, pp. 25–33, Jan 2006.

[141] A. S. Weddell, M. Magno, G. V. Merrett, D. Brunelli, B. M. Al-Hashimi, and L. Benini, "A survey of multi-source energy harvesting systems," in *Proc. of the Design, Automation Test in Europe Conference Exhibition (DATE)*, 2013, pp. 905–908.

[142] M. Weimer, T. Paing, and R. Zane, "Remote area wind energy harvesting for low-power autonomous sensors," in *Power Electronics Specialists Conference, 2006. PESC '06. 37th IEEE*, 2006, pp. 1–5.

[143] M. Win, P. Pinto, and L. Shepp, "A mathematical theory of network interference and its applications," *Proceedings of the IEEE*, vol. 97, no. 2, pp. 205–230, Feb 2009.

[144] L. Xiao, P. Wang, D. Niyato, D. Kim, and Z. Han, "Wireless networks with rf energy harvesting: A contemporary survey," *IEEE Communications Surveys Tutorials*, vol. PP, no. 99, pp. 1–1, 2015.

[145] L. Xie, Y. Shi, Y. Hou, and A. Lou, "Wireless power transfer and applications to sensor networks," *IEEE Wireless Communications*, vol. 20, no. 4, pp. 140–145, August 2013.

[146] G. Yang, C. K. Ho, and Y. L. Guan, "Dynamic resource allocation for multiple-antenna wireless power transfer," *IEEE Transactions on Signal Processing*, vol. 62, no. 14, pp. 3565–3577, July 2014.

[147] R. Zhang and C. K. Ho, "MIMO broadcasting for simultaneous wireless information and power transfer," *IEEE Transactions on Wireless Communications*, vol. 12, no. 5, pp. 1989–2001, May 2013.

[148] S. Zhang and A. Seyedi, "Analysis and design of energy harvesting wireless sensor networks with linear topology," in *IEEE International Conference on Communications*, June 2011, pp. 1–5.

[149] X. Zhou, R. Zhang, and C. K. Ho, "Wireless information and power transfer: architecture design and rate-energy tradeoff," *IEEE Transactions on Communications*, vol. 61, no. 11, pp. 4757 – 4767, November 2013.